

# Changes in chemical and physical properties of South African caking coals during pyrolysis

**R White**  
**21667373**

Dissertation submitted in partial fulfillment of the requirements for the degree *Magister Scientiae* in *Chemistry* at the Potchefstroom Campus of the North-West University

Supervisor: Prof CA Strydom

Co-supervisor: Prof JR Bunt

May 2015



# Acknowledgements

The author wishes to acknowledge the following people for their contribution to this project:

- I want to dedicate this work to My Heavenly Father. Through His grace alone I received wisdom, strength, perseverance and courage to complete this study.
- My supervisors, Prof CA Strydom and Prof JR Bunt, for their expert guidance and insight during this investigation.
- Sasol and the NWU for their financial support regarding this investigation.
- Dr. Louwrens Tiedt at NWU, Laboratory of Electron Microscopy, for his assistance with the SEM images.
- Mr Gregory Okolo for his assistance during the CO<sub>2</sub> BET surface area experiments.
- Mr Zach Sehume and Ms Jackie Collins for their motivation and assistance.
- My loving family for their moral support throughout my studies. Without their motivation all hope would have been lost.
- Mr Kalla Rautenbach, for his love and inspiration. Thank you for always lifting my spirit during the difficult times throughout this study.
- This work is based on the research supported by the South African Research Chairs Initiative of the Department of Science and Technology and National Research Foundation of South Africa.

Any opinion, finding or conclusion or recommendation expressed in this material is that of the author(s) and the NRF does not accept any liability in this regard.

# Abstract

The plasticity of coal during pyrolysis is of significant importance, since it affects the reactivity, porosity, particle size and the density of the char and thus also the behaviour of the char during further utilisation processes. The main focus of this study was to characterize the chemical and physical changes which the thermally treated coal undergoes, in order to better understand the pyrolysis process of caking and non-caking South African coals. The pyrolysis behaviour of three South African coals with different caking indices was investigated. The coal samples included; (1) Highveld (TWD), a medium rank C coal with a free swelling index (FSI) of 0, (2) Grootegeluk (GG), also a medium rank C coal, with a FSI of 6.5, and (3) Tshikondeni (TSH), a medium rank B coal with the highest FSI of 9. The three coal samples were classified as vitrinite-rich coals consisting of mainly aliphatic structures. Thermogravimetric experiments were used to determine the different temperatures relating to specific percentages of mass loss using set conditions. The pyrolysis process was stopped at various percentages of mass loss (thus at various stages of the reactions) to characterize the chemical structural changes that occurred at the specific mass loss percentages.

The results obtained from characterization analyses indicated that the three coals differ in chemical composition and thus were expected to behave differently during pyrolysis. The coal samples consist of different amounts of macerals and minerals according to X-ray Fluorescence (XRF) and X-ray Diffraction (XRD) analyses. The Diffuse Reflectance Infrared Fourier Transform Spectroscopy (DRIFT) results indicated that some of the functional groups within the coal samples evolved with the increase in temperature. The highly caking coal (TSH) exhibited the highest aromaticity and ring condensation. The surface areas were determined by CO<sub>2</sub> adsorption and an increase in surface area was observed with an increase in temperature. The surface area of the GG and TSH coal-derived char samples decreased at some stage, which is an indication of thermoplastic behaviour and subsequent swelling of the coal samples. Scanning electron microscopy (SEM) images confirm the plastic stage of caking coals at specific temperatures and volatile matter release via the multiple bubble mechanism. All these results are given and discussed extensively in this dissertation.

*Keywords:* South African coal, caking coals, pyrolysis

# Opsomming

Die plastisiteit van steenkool gedurende pirolise is van uiterse belang, omdat dit die reaktiwiteit, porositeit, partikel grootte asook die digtheid van die sintel affekteer. Dit het dus 'n effek op verdere steenkoolomsettingsprosesse. Die hoof fokus van hierdie studie was om die chemiese en fisiese veranderinge waardeur die termies behandelde steenkool gaan, te karakteriseer, om sodoende die pirolise proses van verskeie bitumeneuse Suid-Afrikaanse steenkool beter te verstaan. Die gedrag tydens pirolise van drie Suid-Afrikaanse steenkoolmonsters, met verskeie vry swellingsindekse (FSI), is ondersoek; (1) Hoëveld (TWD), 'n medium rang C steenkool met 'n vry swellingsindeks van 0, (2) Grootegeluk (GG), ook 'n medium rang C steenkool met 'n vry swellingsindeks van 6.5, en (3) Tshikondeni (TSH), 'n medium rang B steenkool met die hoogste vry swellingsindeks van 9. Die drie steenkoolmonsters is geklassifiseer as vitriniet-ryke steenkool wat hoofsaaklik uit alifatiese strukture bestaan. Termogravimetrieë eksperimente is gebruik om die verskillende temperature te bepaal wat ooreenstemmend is met die spesifieke persentasies massa verlies onder vasgestelde toestande. Die pirolise proses is gestop by die verskeie persentasies massa verlies (dus by die verskeie fases van die reaksie) om die chemiese strukturele veranderinge wat plaasvind te karakteriseer.

Die resultate verkry vanaf die karakteriserings analises het aangedui dat die drie steenkoolmonsters verskillende chemiese komposisies bevat en word daar dus verwag dat die steenkool verskillend gaan reageer tydens die piroliseproses. Die steenkoolmonsters het, volgens X-straal fluoressensie (XRF) en X-straal diffraksie (XRD) analises, uit verskillende hoeveelhede minerale bestaan. Die Diffuse Reflektansie Infrarooi Fourier Transform spektroskopie (DRIFT) resultate het aangedui dat sommige funksionele groepe, teenwoordig in die steenkoolmonsters, vrygestel word met 'n toename in die temperatuur. Die TSH steenkool het die hoogste aromatisiteit en aromatiese ring kondensasie getoon. Die oppervlakarea is bepaal deur CO<sub>2</sub> adsorpsie en 'n toename in die oppervlakarea is waargeneem met 'n toename in die temperatuur. 'n Afname in die oppervlakarea van die GG en die TSH steenkool- en sintelmonsters kan op 'n sekere stadium waargeneem word, wat 'n aanduiding van termoplastiese- en swelgedrag is. SEM foto's het die plastiese fase van die GG en die TSH steenkoolmonsters by spesifieke temperature bevestig. Die vrystelling van vlugtige produkte deur middel van die borrelmeganisme kan ook waargeneem word in die SEM foto's. Al die resultate word volledig bespreek.

Sleutelwoorde: Suid-Afrikaanse steenkool, swelling, pirolise.

# Table of Contents

Acknowledgements .....	i
Abstract .....	ii
Opsomming.....	iii
List of Figures.....	viii
List of Tables.....	x
Abbreviations .....	xi
<b>Chapter 1: Introduction</b> .....	<b>1</b>
1.1 Problem statement and substantiation.....	1
1.2 Hypothesis .....	2
1.3 Research aim and objectives.....	2
1.4 Chapter overview of dissertation.....	3
<b>Chapter 2: Literature Review</b> .....	<b>5</b>
2.1 Coalification.....	5
2.2 Coal resources in South Africa .....	7
2.3 Caking and plasticity of coal .....	8
2.4 Pyrolysis of coal .....	10
2.5 Mechanism of pyrolysis .....	10
2.6 Pyrolysis of caking coal .....	12
2.7 Products of pyrolysis .....	13
2.8 Summary of previous studies done on pyrolysis of caking coal .....	14

<b>Chapter 3: Background On Experimental Technique .....</b>	<b>17</b>
3.1 Proximate analysis .....	17
3.2 Ultimate analysis .....	18
3.3 Thermogravimetric (TG) analysis.....	18
3.4 X-ray Fluorescence .....	21
3.5 X-ray Diffraction (XRD).....	23
3.6 Diffuse Reflectance Infrared Fourier Transform Spectroscopy (DRIFT).....	25
3.7 CO <sub>2</sub> BET surface analysis .....	26
3.8 Scanning electron microscopy (SEM).....	26
<b>Chapter 4: Experimental Procedure.....</b>	<b>28</b>
4.1 Experimental plan.....	28
4.2 Coal samples.....	30
4.3 Sample preparation .....	30
4.4 Thermogravimetry-Mass Spectrometry (TG-MS).....	32
4.5 Thermogravimetric (TG) analysis.....	33
4.6 Mass Spectrometer (MS).....	33
4.7 Char preparation in the tube furnace .....	34
4.8 Proximate and ultimate analyses .....	35
4.9 X-ray Fluorescence (XRF).....	36
4.10 X-ray Diffraction (XRD).....	36
4.11 Diffuse Reflectance Infrared Fourier Transform Spectroscopy (DRIFT).....	37
4.12 CO <sub>2</sub> BET surface analysis.....	38

4.13 Scanning electron microscopy (SEM) .....	39
<b>Chapter 5: Results And Discussion On The Chemical Changes Of South African Caking And Non-Caking Coals .....</b>	<b>40</b>
5.1 Conventional analyses .....	40
5.2 Thermogravimetric and mass spectrometric analyses results .....	51
5.3 Mass Spectrometry results .....	54
5.4 X-ray Fluorescence (XRF) results.....	60
5.5 X-ray Diffraction (XRD) results.....	63
5.6 Diffuse Reflectance Infrared Fourier Transform Spectroscopy (DRIFT) results.....	67
5.7 Summary .....	73
<b>Chapter 6: Results And Discussion On The Physical Changes Of South African Caking And Non-Caking Coals .....</b>	<b>76</b>
6.1 CO <sub>2</sub> adsorption analysis results.....	76
6.2 Scanning electron microscopy (SEM) results.....	82
6.3 Summary .....	87
<b>Chapter 7: Conclusions And Recommendations .....</b>	<b>88</b>
7.1 Characteristic properties.....	88
7.2 Thermogravimetric analysis .....	89
7.3 Mass Spectrometry.....	90
7.4 DRIFT .....	90
7.5 CO <sub>2</sub> BET Surface area .....	91
7.6 Scanning electron microscopy .....	91
7.7 Summary of the differences between caking and non-caking coals .....	91

7.8 Recommendations.....	93
<b>Bibliography</b> .....	95
Appendix A .....	104
Appendix B .....	106
Appendix C .....	108
Appendix D .....	110



# List of Figures

Figure 1.1	Outline of the dissertation
Figure 2.1	The Van Krevelen diagram
Figure 2.2	A map of the South African coalfields
Figure 2.3	Devolatilization of coal during pyrolysis
Figure 2.4	The pyrolysis of caking coals
Figure 3.1	Components of the TGA
Figure 3.2	A typical TGA thermal curve
Figure 3.3	A first derivative curve (DTG)
Figure 3.4	A schematic diagram of the components within the MS
Figure 3.5	Diagram of XRF spectrograph
Figure 3.6	Typical XRF graph
Figure 3.7	Principle of XRD analysis
Figure 3.8	Principle of DRIFT spectroscopy
Figure 3.9	Schematic diagram of a typical SEM
Figure 4.1	Diagram of experimental work and analysis
Figure 4.2	The cone and quarter method
Figure 4.3	Rotary riffle splitter dividing coal into six identical fractions
Figure 4.4	TG-MS experimental set-up
Figure 4.5	Lenton tube furnace used to prepare the char samples
Figure 4.6	Vertex FTIR spectrometer with DRIFT sample holder
Figure 4.7	The Micrometrics ASAP analyser used for CO <sub>2</sub> surface analyses
Figure 5.1	Carbon contents for Highveld (m.f.b.)

Figure 5.2	Carbon contents for Grootegeluk (m.f.b.)
Figure 5.3	Carbon contents for Tshikondeni (m.f.b.)
Figure 5.4	Aromaticity factors for the three coal samples
Figure 5.5	Thermogravimetric weight loss curves for the raw coal samples
Figure 5.6	DTG curves of the three raw coal samples
Figure 5.7	Mass spectra of H <sub>2</sub> (m/z = 2) evolution
Figure 5.8	Mass spectra of CH <sub>3</sub> <sup>+</sup> (m/z = 15) evolution
Figure 5.9	Mass spectra of H <sub>2</sub> O (m/z =18) evolution
Figure 5.10	DRIFT spectra for three raw coal samples
Figure 5.11	DRIFT spectra of TWD raw coal and coal-derived char samples
Figure 5.12	DRIFT spectra of GG coal and coal-derived char samples
Figure 5.13	DRIFT spectra for TSH coal and coal-derived char samples
Figure 5.14	Aromatic/Aliphatic CH peak area ratio of the three coal samples
Figure 5.15	CH aromatic / C=C peak area ratio for the three coal samples
Figure 6.1	CO <sub>2</sub> BET surface areas for the three coals during pyrolysis
Figure 6.2	BET CO <sub>2</sub> adsorption isotherms for TWD
Figure 6.3	BET CO <sub>2</sub> adsorption isotherms for GG
Figure 6.4	BET CO <sub>2</sub> adsorption isotherms for TSH

# List of Tables

Table 4.1	Experimental conditions for the pyrolysis process
Table 4.2	Temperatures at which specific mass loss observed from TGA
Table 4.3	Analytical procedures and test methods
Table 5.1	Conventional analysis results for the three raw coals
Table 5.2	Conventional analysis results of Highveld coal samples
Table 5.3	Conventional analysis results of Grootegeluk samples
Table 5.4	Conventional analysis results of Tshikondeni samples
Table 5.5	Aromaticity factors of the coal and coal-derived char samples
Table 5.6	Parameters from DTG curves
Table 5.7	XRF analysis results of the coal samples
Table 5.8	XRD analysis results for raw coal and coal-derived char samples
Table 6.1	CO <sub>2</sub> physical parameters for coal and coal-derived char samples
Table 6.2	SEM images for the TWD coal and coal-derived char samples
Table 6.3	SEM images for the GG coal and coal-derived char samples
Table 6.4	SEM images for the TSH coal and coal-derived char samples
Table 7.1	Comparison of the three South African coals
Table 7.2	Temperatures correlating to different mass loss percentages

# Abbreviations

Abbreviation	Description
d.b.	dry basis
ASTM	American Society for Testing Materials
BET	Brunauer-Emmett-Teller
C <sub>db</sub>	Carbon on a dry basis
CPD	Chemical Percolation Devolatilization
DR	Dubinin-Radushkevich
DRIFT	Diffuse Reflectance Infrared Fourier Transform Spectroscopy
DTG	Differential thermogravimetric/thermogravimetry
DVC	Depolymerization Vaporization and Cross-linking model
$f_a$	aromaticity factor
FC	Fixed Carbon
FG	Functional Group model
FSI	Free Swelling Index
FTIR	Fourier transform infrared spectroscopy
GG	Grootegeeluk coal sample
H <sub>al</sub>	aliphatic Hydrogen
H <sub>ar</sub>	aromatic Hydrogen
ISO	International Organization for Standardization
LOIF	Loss on ignition free basis
m.f.b.	moisture free basis
MS	Mass Spectrometry
SEM	Scanning Electron Microscopy
SR	Secondary Reactions model

---

<b>TGA</b>	Thermogravimetric Analyser
<b>TSH</b>	Tshikondeni coal sample
<b>TWD</b>	Highveld coal sample
<b>V<sub>db</sub></b>	Volatile Matter on a dry basis
<b>VM</b>	Volatile Matter
<b>vol.%</b>	Volume percentage
<b>wt.%</b>	Weight percentage
<b>XRD</b>	X-ray Diffraction
<b>XRF</b>	X-ray Fluorescence

---

# Chapter 1

## Introduction

*An introduction and the purpose for investigating the pyrolysis behaviour of South African caking coals are provided in this chapter. The problem statement and substantiation for this study are discussed, where the importance of caking coals and the significance of the pyrolysis process are explained. A formulation of the hypothesis is then provided, followed by the research aims and objectives. This chapter is then concluded with the outline of the study and the chapter overview of the dissertation.*

### 1.1 Problem statement and substantiation

Coal is currently South Africa's primary energy source by providing approximately 79% of the country's total energy needs. South Africa exports the good quality coal, while using the lower grade coals with high mineral matter content in power stations for electricity generation [Falcon and Van der Riet, 2007; Malumbazo, 2011]. South African coal reserves consist of approximately 2% anthracite and over 95% bituminous coal [Kershaw and Taylor, 1992]. Almost 70% of South Africa's coal is located in the Waterberg, Witbank and Highveld coalfields. Some of these major coalfields are reaching exhaustion according to Jeffrey [2005], while the coal quality of the other coalfields is causing problems with the mining procedures. Therefore, these major coalfields are investigating new extraction technologies to utilize lower grade coals, high ash content coals, and coals with caking behaviour [Jeffrey, 2005].

Due to the low cost and abundance of coal in South Africa, coal will remain the major source of energy despite renewable energy sources, nuclear energy and natural gas [Jeffrey, 2005]. The higher grade coal sources are estimated to survive up to 2050 [Jeffrey, 2005], but by utilizing new technologies and understanding the pyrolysis of lower grade and caking coals, the industrial process can be adjusted to fit the properties of caking coals and assure good quality pyrolysis products.

The caking of coal describes the agglomeration, plasticity and softening of coal particles with increasing temperature, without any implication on the nature of the solid residue that forms [Maloney *et al.*, 1982]. The plasticity of coal during pyrolysis is of significant importance, since it

affects the reactivity, porosity, particle size and the density of the char, and thus also the behaviour of the char during further utilization processes [Sheng and Azevedo, 2000].

The caking properties of bituminous coals will influence the process efficiency and may cause operational problems, such as build-up pressure of the oven walls due to the swelling, as well as obstruction of gas flow through the agglomerates [Maloney *et al.*, 1982; Yu *et al.*, 2003; Fu *et al.*, 2007]. It is therefore crucial to investigate the behaviour of caking coals during pyrolysis.

Pyrolysis of coal, also described as devolatilization, is an important industrial process as it is the initial step of gasification, hydrogenation and combustion [Arenillas *et al.*, 2003]. The products derived from pyrolysis include: cokes, chars, tars and gaseous compounds. These products are necessary for further industrial processes [Alonso *et al.*, 1999]. The behaviour of coal during pyrolysis is dependent on the operating conditions, i.e. the temperature, particle size, heating rate, pressure, as well as on the characteristics of the raw coal, i.e. the coal type, rank and maceral composition [Hambly, 1998; Alonso *et al.*, 1999]. Pyrolysis of caking coal is crucial for coal utilization where new advanced technologies must be developed [Yu *et al.*, 2007]. It is crucial to understand the behaviour of coal during pyrolysis, since it has a significant effect on the conversion processes.

Limited research has been done on South African caking coals and their behaviour during pyrolysis. The main focus of this study will be to characterize the chemical and physical changes which the thermally treated coal undergoes in order to better understand the pyrolysis process of caking and non-caking South African coals.

### **1.2 Hypothesis**

By characterizing the changes in chemical and physical structural properties of caking coals during pyrolysis, the behaviour in terms of structural changes of South African caking coals can be described. Different types of caking coals may behave differently during pyrolysis and their chemical compositions and physical structural changes may be used as an indication of these differences.

### **1.3 Research aim and objectives**

The aim of this study is to determine the behaviour of South African caking coals during pyrolysis and to compare that to a non-caking coal. Physical and chemical characteristics at different decomposition percentages of the caking coals during pyrolysis will be determined.

The chemical structural changes, determined as changes in chemical functional groups at the various temperatures, gases evolved at the various temperatures and other chemical structural changes will be identified.

The following objectives are stipulated:

- Characterize three South African coal samples with different swelling indices.
- Determine temperatures where the coals have reacted at different percentages on a mass loss basis. The mass loss percentages include: 20, 40, 60, 80 and 100%. The 100% mass loss represents the mass loss percentage which occurred at 900°C.
- Analyse the changes in chemical and physical properties during pyrolysis, using conventional and advanced analytical techniques.
- Explain the pyrolysis behaviour of each coal individually to determine where the significant changes occur.
- Compare the pyrolysis behaviour of the three coals in order to distinguish between caking and non-caking coals.

### **1.4 Chapter overview of dissertation**

This dissertation is divided into seven chapters and an outline of the chapters is provided in Figure 1.1. The first chapter provides a brief overview of the significance of the investigation into the pyrolysis behaviour of South African caking coals. The formulation of the problem statement, hypothesis as well as the aims and objectives are included. Chapter 2 contains a literature review on coal, South African coal resources, caking and plasticity of coal as well as on the pyrolysis of caking coals. The current state of the research on the pyrolysis of caking coals is addressed. In Chapter 3, a review on background relating to the experimental techniques used during this study is discussed.



Chapter 1	<ul style="list-style-type: none"><li>•Introduction</li><li>•background and motivation for the study</li></ul>
Chapter 2	<ul style="list-style-type: none"><li>•Literature review</li><li>•Literature survey including the research in the field of caking coals and pyrolysis</li></ul>
Chapter 3	<ul style="list-style-type: none"><li>•Background on the analytical techniques</li><li>•Discussion on the significance of the chemical and physical analyses that will be conducted</li></ul>
Chapter 4	<ul style="list-style-type: none"><li>•Experimental procedure</li><li>•Sample preparation and the information on the instruments that will be used for the analysis</li></ul>
Chapter 5	<ul style="list-style-type: none"><li>•Results and discussion of the changes occurring in the chemical properties.</li></ul>
Chapter 6	<ul style="list-style-type: none"><li>•Results and discussion of the changes occurring in the physical properties</li></ul>
Chapter 7	<ul style="list-style-type: none"><li>•Conclusions and recommendations</li></ul>

**Figure 1.1: Outline of the dissertation.**

Experimental conditions and instrument specifications regarding experimental procedures are included in Chapter 4. Chapters 5 and 6 provide the results and discussion on the chemical and physical properties, respectively. These results are aimed at giving insight into the chemical structural changes occurring within the coals and the effect of pyrolysis on the composition of the coal samples. Finally, in Chapter 7, the conclusions are made on the differences between caking and non-caking coals and their behaviour during pyrolysis. Recommendations for future work regarding caking coals and pyrolysis are summarized in Chapter 7.

# Chapter 2

## Literature Review

*In this review the background of South African caking coals will be summarized. Firstly, the coalification process will be discussed, explaining the formation and structure of coal. The geological occurrence of coal in South Africa will then be reviewed as well as the importance of coal as an energy source. The review continues by providing a detailed background on the caking and plastic behaviour of coal during heat treatment. Information about the mechanism of pyrolysis on coal samples as well as on caking coals and the products of pyrolysis will also be provided. Finally, the current state of the research on the pyrolysis of caking coals will be addressed.*

### 2.1 Coalification

Coal is formed from fossilized plant material resulting in heterogeneous organic sedimentary rock [Falcon and Snyman, 1986; Green, 1987; Van Niekerk *et al.*, 2009]. This occurs when plant material is compacted, transformed through chemical reactions and metamorphosed by heat, pressure and time. The processes of coal formation and coalification are described in detail in literature [Meyers, 1982; Speight, 1994; Schobert, 2013]. The Van Krevelen diagram is used to describe the changes occurring in the elemental composition of coal during coalification. Coal is generally classified by rank when the carbon to hydrogen atomic ratios and the carbon to oxygen atomic ratios are compared [Heald *et al.*, 2010]. The major ranks are termed as lignite, sub-bituminous, bituminous and anthracite [Yu *et al.*, 2007]. A typical Van Krevelen diagram is presented in Figure 2.1.

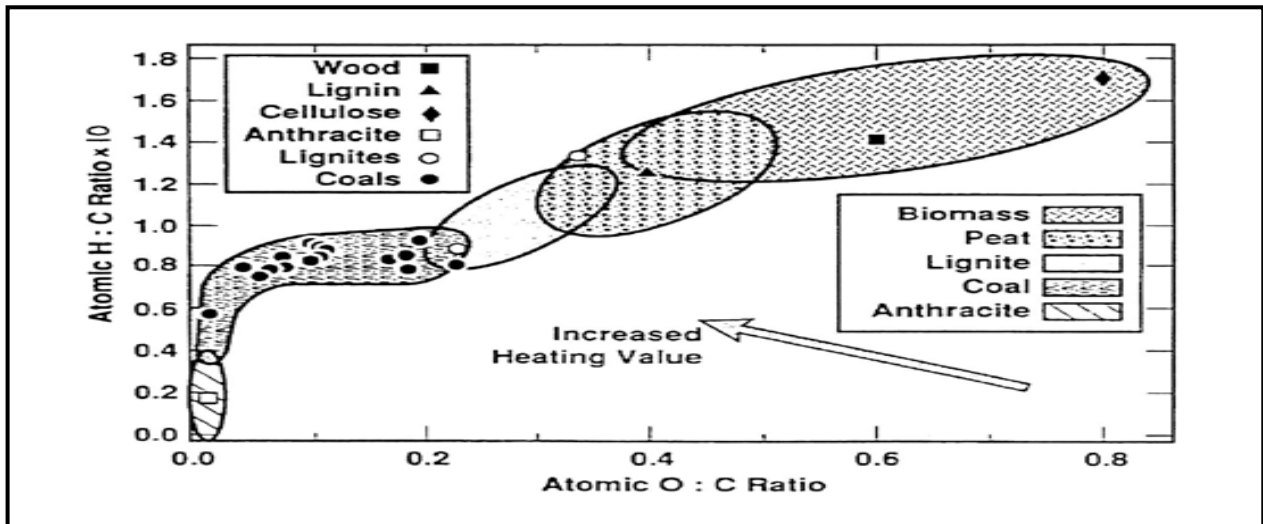


Figure 2.1: The Van Krevelen diagram [Hustad and Barrio, 2000].

The aromaticity of carbon and aromatic ring condensation increase with the increase in coal rank [Gavalas, 1982]. The important differences in coal properties between coal ranks can be summarised in three main concepts. Firstly, with higher rank coal, lower oxygen and moisture levels are present due to the loss of carbonyl, hydroxyl and carboxyl groups. Secondly, the aromaticity increases while volatile matter decreases with increasing coal rank. This is as result of the removal of alicyclic and aliphatic groups. Thirdly, anthracite can be characterized by an increase in reflectance and a rapid decrease of hydrogen content [Borrego *et al.*, 2000]. Coal of various ranks will behave differently under heat treatment because of the differences in the chemical structure [Smoot and Pratt, 1979].

Organic and inorganic materials are present within the heterogeneous structure of coal. The organic material consists mainly of liptinite, vitrinite and inertinite, also referred to as the complex macerals [Yu *et al.*, 2007]. Benfell [2001] reported that when particles contain different maceral components they will behave differently in terms of the swelling behaviour, char structure, ash composition, amount of volatile matter released and in the reactivity. The inorganic material of coal, also known as the mineral matter, can be grouped in three types of mineral classifications present within the coal; (1) mineral salts, which are dissolved in the water and precipitated in the pores, (2) inherent mineral matter, which is part of the structure of coal, and (3) inorganic compounds bound to the organic material [Ward, 2002]. During heat treatment some of these minerals present in the coal structure may have a catalytic effect on the reactions which occur. This catalytic effect will depend on the concentration of the minerals,

the nature in which the minerals occur within the coal sample, as well as the distribution of the minerals within the coal structure [Samaras *et al.*, 1996].

Coal is a very complex energy source, making the research into the chemical and structural properties essential for optimum coal utilization technologies [Komaki *et al.*, 2005].

## **2.2 Coal resources in South Africa**

Coal is currently South Africa's primary energy source by providing approximately 79% of the country's total energy needs. South Africa exports the good quality coal, while using the lower grade coals with high mineral matter content in power stations for electricity generation. The metallurgical industry, the petrochemical industry, and coal for domestic use are alternative applications for this lower grade coal in South Africa [Falcon and Van der Riet, 2007; Malumbazo, 2011].

Coal will remain the major source of energy in South Africa, despite alternative sources such as natural gas, nuclear energy and renewable energy sources, due to the low cost and the abundance of coal resources in South Africa. South African coal reserves consist of approximately 2% anthracite and over 95% bituminous coal [Kershaw and Taylor, 1992]. Almost 70% of South Africa's coal is located in the Waterberg, Witbank and Highveld coalfields. Some of these major coalfields are reaching exhaustion according to Jeffrey [2005], while the coal quality of the other coalfields is causing problems with the mining procedures. Therefore, new extraction technologies must be investigated in order to utilize lower grade coals, high ash content coals, and coals with caking behaviour [Jeffrey, 2005]. The South African coalfields are presented in Figure 2.2.

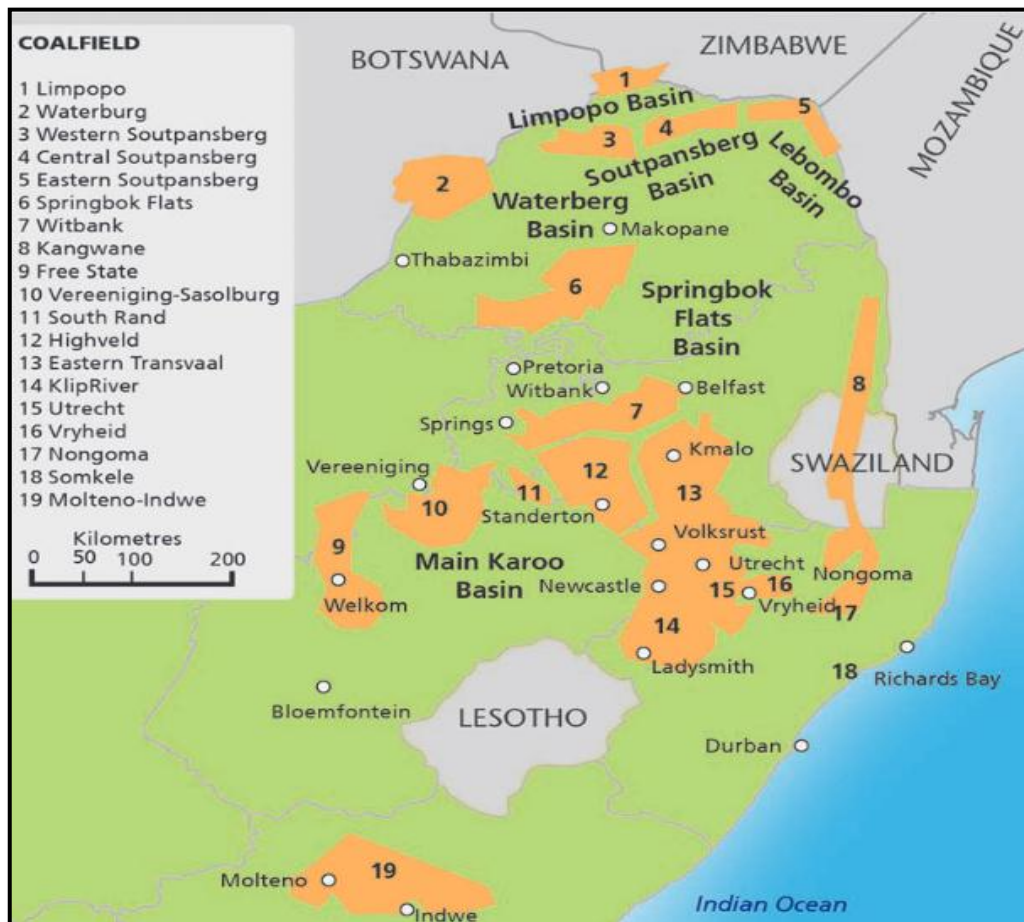


Figure 2.2: A map of the South African coalfields [Maskew Miller Longman, 2013].

It is reported that South African coal has a low vitrinite and high inertinite content, although the inertinite is variable. There is a distinctive variation of inorganic and organic matter in South African coal. Semi-reactive inertinite is also present in some South African coals. South African coals formed in both low water level areas as well as in swamp areas [Falcon, 1986].

### 2.3 Caking and plasticity of coal

The caking of coal describes the agglomeration and softening of coal particles with increasing temperature, without any implication on the nature of the solid residue that forms [Maloney *et al.*, 1982]. When a strong, coherent solid forms, known as metallurgical coke, the process is referred to as the coking of coal. The main difference between caking and coking coals can be summarized: all coking coals are caking coals, but not all caking coals are coking coals [Scaroni *et al.*, 2005; Speight, 2005].

The thermoplastic properties of coal refer to the softening, melting, swelling and re-solidifying of bituminous coals when heated in the absence of air. These swelling and caking properties of

coal occur within a distinctive temperature range under pyrolysis conditions and have been described numerous times in literature [Fischer, 1925; Serio *et al.*, 1987; Painter *et al.*, 1990; Takagi *et al.*, 2004; Yu *et al.*, 2004; Yoshizawa 2006; Minkina *et al.*, 2010; Coetzee *et al.*, 2014]. Plasticity of coal has been investigated by many researchers and can be interpreted by the metaplast theory, i.e., coal → metaplast → coke/char [Elliot, 1981; Serio *et al.*, 1987; Solomon *et al.*, 1992; Yu *et al.*, 2007]. These physical changes of coal originate from chemical reactions and transformations. It is therefore crucial to investigate the chemical and physical evolution along with the swelling mechanism in order to understand the behaviour of coal during pyrolysis.

The swelling of a coal particle can be described using the multi-bubble mechanism [Yu *et al.*, 2004]. With an increase in temperature, the plastic stage forms the metaplast, and as a result the pore openings within the caking coal are blocked. The volatile matter will be trapped inside the particles and bubbles will form as a consequence. When these bubbles form in the metaplast, the volatile matter will diffuse into bubbles instead of escaping from the surface of the particle. The bubbles rupture and release the volatile matter when they reach the surface of the coal particle. This growth of bubbles causes the swelling phenomena of coal particles under heat treatment [Habermehl *et al.* 1981; Gao *et al.* 1997; Yu *et al.*, 2004].

The plastic stage is a highly viscous liquid and is dependent on the coal rank, surrounding gas, particle size, heating rate and pressure [Kugo, 1953]. Higher ranking coals soften and swell at higher temperatures than lower ranking coals. Thus, with an increase in coal rank, the phases within the plastic range shifts to higher temperatures, this results in a larger plastic range in the low ranking coals [Barriocanal *et al.*, 2003]. Another important parameter for the plastic range is the conditions of heating. When the heating rate is fixed, increased fluidity can be achieved by increasing the pressure or the mass of a sample [Gavalas, 1982].

The plastic range within the bituminous coal sources has an effect on the formation of the char and thus will also influence coal conversion processes [Sheng and Azevedo, 2000]. Some of the operational problems caused by caking coals include the build-up of pressure inside the ovens as result of the swelling behaviour. Obstruction of the gas flow may also occur due to the agglomerates which form during the swelling of coal particles [Maloney *et al.*, 1982; Yu *et al.*, 2003; Fu *et al.*, 2007]. It is therefore crucial to investigate the behaviour of caking coals during pyrolysis.

## 2.4 Pyrolysis of coal

Pyrolysis of coal, is described as devolatilization, is an important industrial process as it is the initial step of gasification, hydrogenation and combustion [Arenillas *et al.*, 2003]. Pyrolysis may account for approximately 70% weight loss of the coal sample and depends on the organic composition of the parent coal [Serio *et al.*, 1987; Solomon 1993]. The pyrolysis process affects the swelling and agglomeration of the coal as well as the structure and reactivity of the char [Serio *et al.*, 1987; Solomon 1988; Solomon 1993]. The behaviour of coal during pyrolysis is dependent on the operating conditions, i.e. the temperature, particle size, heating rate, pressure and oxygen levels, as well as on the characteristics of the raw coal, i.e. the coal type, rank and maceral composition [Hambly, 1998; Alonso *et al.*, 1999].

Pyrolysis of caking coal is crucial for coal utilization where new advanced technologies must be developed [Yu *et al.*, 2007]. It is therefore important to understand the behaviour of coal during pyrolysis, since it has a significant effect on the conversion processes.

## 2.5 Mechanism of coal pyrolysis

Pyrolysis is the thermal decomposition of coal when heated in an oxygen deprived atmosphere. Volatile matter and tars are driven out of the particle and a solid residue, referred to as char, remains [Hambly, 1998].

During pyrolysis a multitude of simultaneous and consecutive reactions occur. The sum of all these reactions is represented in the experimental results of pyrolysis [Arenillas *et al.*, 2003]. Some of these reactions include the decomposition of functional groups, which lead to the formation of gaseous species and tar from macromolecular networks [Ulloa *et al.*, 2004]. Hydroaromatic structures, alkyl bridges, alkyl chains, aromatic nuclei and oxygen groups are some of the functional groups of the coal structure that are responsible for the reactivity of the coal [Gavalas, 1982]. In Figure 2.3 the hypothetical behaviour of coal during pyrolysis is illustrated.

Multiple models and mechanisms have been used in order to explain the pyrolysis behaviour of coals and caking coals, including the chemical percolation devolatilization (CPD) model, functional group model (FG), the hydrocarbon cracking model and the equilibrium model [Gavalas 1982; Howard 1981; Saxena 1990; Solomon 1992; Fletcher *et al.*, 1992].

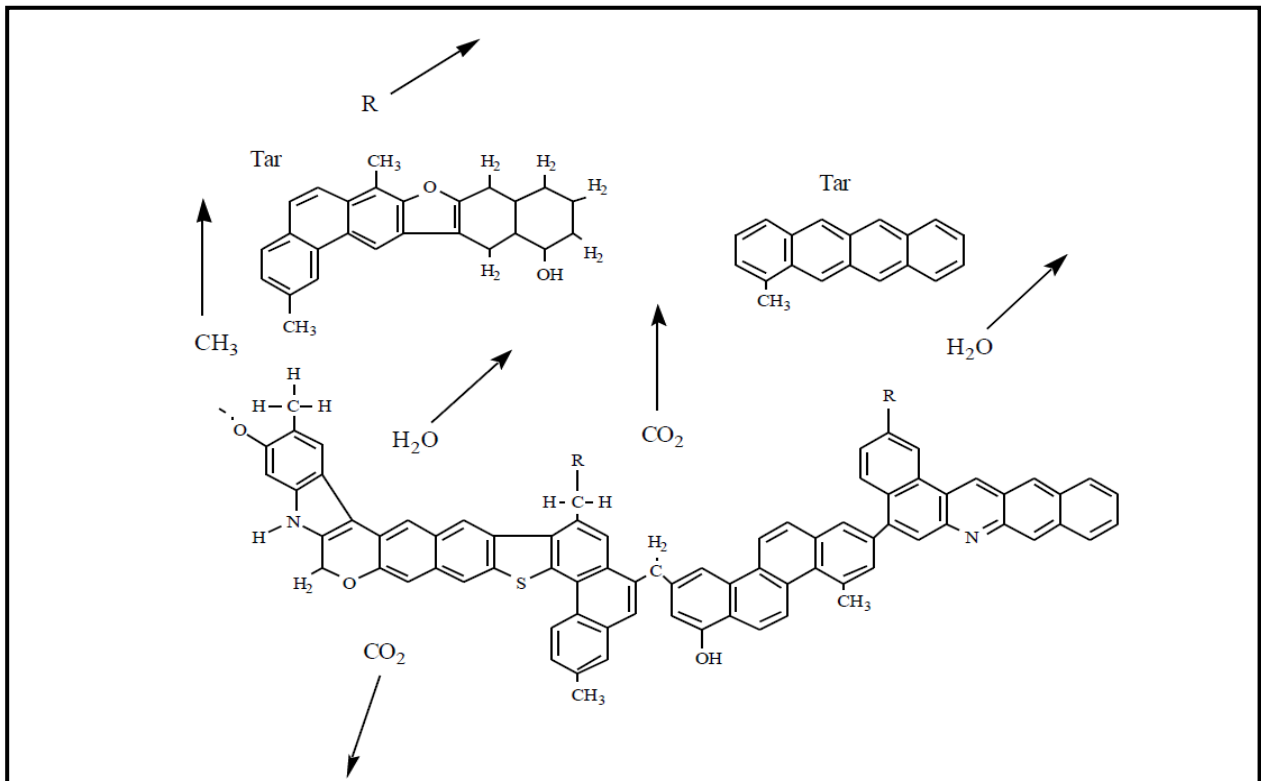


**Figure 2.3: Devolatilization of coal during pyrolysis [Solomon *et al.*, 1988].**

The functional group (FG) model is used to describe the changes in the composition of the functional groups within the char and tar due to the evolution of gaseous compounds [Gavalas 1982; Solomon *et al.* 1987]. An overall model for the behaviour of coal samples during heat treatment can be proposed by describing the thermal decomposition behaviour of functional groups common to all the coal samples. The FG model is considered a successful method in order to determine and monitor the progress and extent of pyrolysis, since the pyrolysis temperature and coal rank have no influence on the relation between functional groups and their behaviour during pyrolysis.

The depolymerisation, vaporization, and cross-linking (DVC) model is used to describe the cross-linking density and distribution of molecular weight in the char, as well as the transport properties, molecular weight and yield of the tar. This model is also integrated with the FG model (FG-DVC) in order to eliminate ultimate tar yield as a parameter.

The secondary reactions (SR) model, described by Serio *et al.* [1987], is used to describe the formation of light gaseous compounds due to the cracking of olefins and paraffins via a hydrocarbon cracking model. The SR model also includes an equilibrium model for the carbon-, hydrogen- and oxygen-containing compounds present at high temperatures.



The pore structure and viscosity are the two major physical properties of interest when coal is heated, because they determine the rate of mass transport which affects the yield of the volatile matter. The pore size distribution of the char is determined by the thermoplastic properties of caking coals. During pyrolysis, the swelling of coal particles varies significantly, and therefore the char residues formed have different physical structures [Yu *et al.*, 2007].

## 2.6 Pyrolysis of caking coal

The pyrolysis process for caking coals, illustrated in Figure 2.4, can be divided into three stages as proposed by Chermin and van Krevelen [1957]. The metaplast consists of the primary gas and liquid compounds as result of the decomposition of the macromolecular structure of coal. The fluidity of coal under heat treatment is the result of this metaplast [Yu *et al.*, 2007]. Under specific temperatures, the metaplast may act as a plasticizer. This suggests that the temperature where the metaplast has maximum concentration relates to the temperature of maximum plasticity [Van Krevelen *et al.* 1956]. The formation of the char in stage I is due to bond breaking that competes with bond stabilization. Hydrogen bonding is reduced during stage I, which may cause the coal particles to melt.

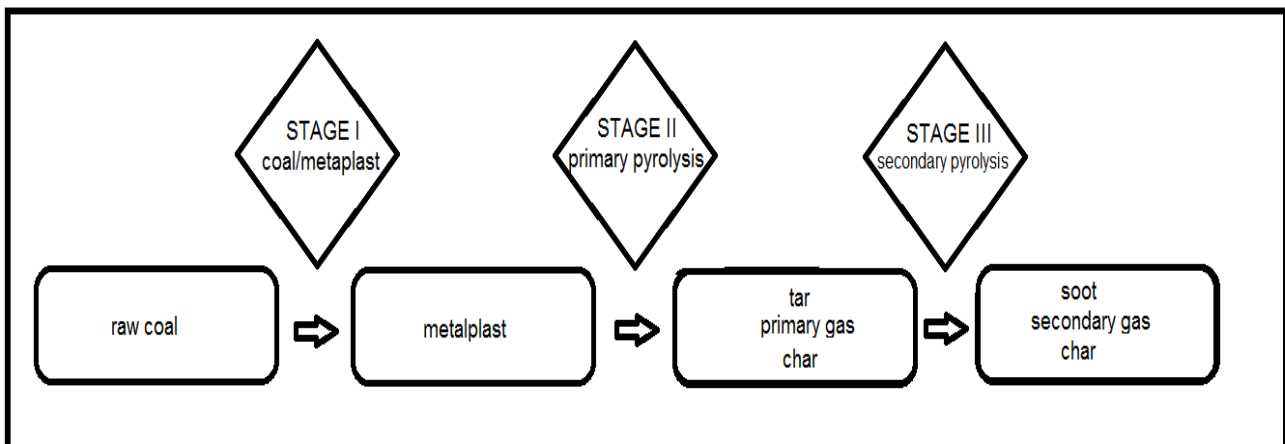


**Figure 2.4:** The pyrolysis of caking coals.

Primary pyrolysis is represented by stage II, where evolution of tar and gases occur due to further bond breaking. Tar represents the low-molecular-weight component of the metaplast. Serio *et al.* [1987] observed an increase in the aromatic hydrogen during the primary pyrolysis stage. During the evolution of tar molecules, hydrogen is converted to aromatics by removing the hydrogen from hydroaromatic structures. The primary pyrolysis stage is dominated by the evolution of tar, aliphatic gaseous compounds and the decrease in aliphatic hydrogen ( $H_{(al)}$ ). A

loss in the plasticity and signs of swelling can be observed with the loss in  $H_{(al)}$ . Additional events during the primary pyrolysis stage include the evolution of aliphatic gases,  $CO_2$ , some  $CH_4$  and  $H_2O$ , due to the decomposition of the functional groups. This evolution may lead to re-polymerization reactions.

The high-molecular-weight components within the metaplast re-attach, by cross-linking reactions, to the char structure. These cross-link reactions within the char structure continue in stage III, secondary pyrolysis, for further ring condensation, while mainly  $CO$  and  $H_2$  are evolved from the char. Recent studies have indicated that these cross-link reactions have a direct relation to the fluidity of a coal sample [Solomon *et al.*, 1988; Solomon *et al.*, 1993]. A decrease in aromatic hydrogen ( $H_{(ar)}$ ) can be observed as result of ring condensation as well as the evolution of  $H_2$ . Soot, secondary gases and coke are formed through the cracking of the tars and primary gases [Serio *et al.*, 1987]. Traces of methane,  $HCN$ ,  $CO$  and  $H_2$  may be observed at the secondary pyrolysis, mainly due to ring nitrogen components, ether links and ring condensation reactions present within the char sample.

## 2.7 Products of pyrolysis

The products derived from pyrolysis include: cokes, chars, tars and gaseous compounds. These products are necessary for further coal conversion processes [Alonso *et al.*, 1999].

### • 2.7.1 Char

The pyrolysis of bituminous coals produces char which can be defined as the product of the coal macromolecule when reorganized in the absence of oxygen [Hambly, 1998]. The char structure is highly heterogeneous between particles and also within the individual char particle, making it a very complex structure. The chemical properties of the char depend on the properties of the raw coal, while the structure strongly depends on the thermal conditions such as heating rate, temperature and pressure [Gavalas, 1982; Yu *et al.*, 2007; Campbell *et al.*, 2010]. According to Berkowitz [1985], the structure of the char is associated with the swelling of the particle during the plastic stage. The particle size of the char, its porosity and the thickness of the walls are determined by the extent of swelling during heat treatment. Thus, the more swelling occurs, the more porous the structure of the char will be [Berkowitz, 1985]. The presence of micropores in the char structure is also an indication of the thermoplasticity and secondary pyrolysis of the coal sample [Tsai and Scaroni, 1987].

- **2.7.2 Coke**

Carbonisation of coking coal results in a solid fuel with a porous structure known as coke. The major uses for coke include industrial as well as domestic applications; to produce a smokeless fuel, for use in blast furnaces, and to produce combustible gas [Hambly, 1998].

- **2.7.3 Tar**

Tar is a mixture of different compounds with varying molecular weights and is a viscous liquid or solid at room temperature [Gavalas, 1982]. The characteristics of tars vary with different temperatures and coal rank [Yu *et al.*, 2007].

- **2.7.4 Gaseous compounds**

Gaseous compounds are also products of pyrolysis and are the result of the decomposition of functional groups at high temperatures. Thus, under pyrolysis conditions, coals consisting of various functional groups will behave differently [Yu *et al.*, 2007].

## **2.8 Summary of previous studies done on pyrolysis of caking coals**

Serio *et al.* [1987] investigated different models in order to predict the behaviour of coal during pyrolysis. Various chemical parameters for the coal and char samples were investigated in order to predict the following: (a) the evolution rate, amount and the composition of volatile matter and gaseous compounds, (b) the yield and composition of the tar, and (c) the reactivity and viscosity of the metaplast phase.

Tsai and Scaroni [1987] investigated pulverized coal particles and the effect of the chemical composition on their transformation during pyrolysis. A bituminous coal sample, from the Kentucky Hazard No. 5 Seam, was crushed to smaller than 150  $\mu\text{m}$  and sieved in order to divide the sample into different size fractions. The change in microporosity during pyrolysis was determined by  $\text{CO}_2$  surface area analysis. The majority surface area was only generated during stage III of pyrolysis, i.e. during secondary pyrolysis. It was also found that the micropores developed after the re-solidification of the chars. This formation of micropores relates to the thermoplasticity, which reduces the formation of micropores, as well as to the secondary pyrolysis, which leads to an increase in microporosity. With regards to the macerals composition, the inertinite present reduces thermoplastic properties of the coal and the resultant char is a thick-walled cenosphere.

Maloney *et al.* [1982] investigated three highly caking coals with size fractions ranging from 425  $\mu\text{m}$  to 63  $\mu\text{m}$ . It was reported that an increase in the surface area indicates a loss in the fluidity of the coal sample. Therefore, a decrease in surface area was observed in the temperature region where contraction of the coal sample occurs.

Three bituminous coals were studied by Alonso *et al.* [1999] in order to determine the pyrolysis behaviour at specific temperatures. These chars were prepared at relatively high temperatures of 1000 to 1300°C. These high temperatures represent the temperatures of the coal particles within pulverized fuel boilers. The obtained results indicated the following: (a) Caking behaviour was observed for the chars obtained from high volatile bituminous coal. This phenomenon can be explained by cross-linking reactions during the early pyrolysis with hydroxylic oxygen. (b) The low volatile bituminous coal showed a drop in reactivity from the low temperature to the high temperature chars. This was explained by the mobility of the polyaromatic systems and the decrease in concentration of the active sites. (c) Different chars were also produced from the inertinite-rich coal sample. The char produced at the higher temperature was anisotropic, which was due to the plastic stage through which the coal sample passed during heat treatment.

Yu *et al.* [2004] developed the multibubble mechanism in order to explain the swelling of pulverized coal during pyrolysis. Different char structures were reported and the conclusion was drawn that, at slower heating rates, cenospheric chars will evolve, and at higher heating rates, the evolution of foam structure chars will occur.

Minkina *et al.* [2010] studied lumps (20 to 40 mm) of bituminous coals and compared the char structures after devolatilization to examine the formation mechanism of the different char types. The study included six bituminous coals with various amounts of volatile matter ranging from 18 to 38%. Three coals were caking coals and the other three non-caking coals. Devolatilization experiments were conducted under nitrogen at different temperatures from 300 to 800°C. They concluded that lumps of caking coal swell uniformly to produce a char that has a highly porous core within a less porous shell. The non-caking coals showed swelling and shrinking to a small extent. The char showed porous bands with cracks and the higher the volatile matter content, the more cracks were observed.

The structural transformation of different caking coals when heated was investigated by Zubkova [2005]. Different rank Ukrainian coals with different caking capacities were the subject of the study (3-0 mm). The macromolecule fragments in the organic mass of the highly caking coals developed segmental movement with an increase in temperature. The fluidity of coal is

the result of these movements and destruction processes with increasing temperature. When highly caking coal re-solidifies, the carbon crystallites and layers may coalesce and an increase in the ordered structure can be seen because of the growth of crystallite structure. In poorly caking coals, the ordered phase also increases due to the presence of nuclei of crystallite structures and the growth of existing crystallites. Non-caking coals are found to develop a structural deformation process when heated, causing crystallites to degrade [Zubkova, 2005].

# Chapter 3

## Background on experimental analytical techniques

*In this chapter the background relating to the experimental techniques used during this study will be discussed. Experimental conditions and instrument specifications will be included in Chapter 4, which discusses experimental procedures.*

*The various chemical and physical analyses include:*

- *Proximate analysis*
- *Ultimate analysis*
- *Thermogravimetric- and mass spectrometer analysis (TG-MS)*
- *X-Ray Fluorescence (XRF)*
- *X-Ray Diffraction (XRD)*
- *Diffuse Reflectance Infrared Fourier Transform Spectroscopy (DRIFT).*
- *CO<sub>2</sub> surface area (BET)*
- *Scanning electron microscopy (SEM)*
  
- **3.1 Proximate analysis**

Proximate analysis of coal can be described as the basis of coal characterization and is in contrast to the ultimate analysis where the elemental composition of a sample is determined. The characteristics measured by proximate analysis include moisture, volatile matter, ash and fixed carbon content [Speight, 2005].

The moisture present in coal is the most evasive component and can be removed when the coal sample is gently heated. The reported moisture content in coal ranges from 2% to 15% in bituminous coals and up to 45% in lignite [Speight, 2005]. Different methods have been described to determine the total moisture content in coal: 1) thermal methods such as distillation; 2) extraction methods; 3) a desiccator method; 4) electrical methods; and 5) chemical methods [Illingworth, 1922; Speight, 2005].

Volatile matter in coal refers to various gaseous compounds which are evolved during the pyrolysis of coal. The weight loss observed during the evolution of the volatile matter is usually due to light hydrocarbons, CO, CO<sub>2</sub>, water and condensable organic compounds which are

driven off with increasing temperature. The data retrieved from volatile matter calculations are an important part in the classification system of coal. The volatile matter content in coal samples, when reported in the absence of ash and moisture, varies between 2% and 50%. The basis of coal evaluation and determining the suitability for various processing applications relies on the volatile matter present in coal.

Ash is the remaining, non-combustible residue after coal combustion and it is formed from the mineral matter or inorganic components in the coal. The properties and amount of ash formed will be influenced by the combustion conditions, as well as the composition of the mineral matter present in the coal [Speight, 2005].

*Fixed carbon* is known as the non-volatile, combustible material within the coal. The amount of fixed carbon in coals may range from 50% to 98%. The fixed carbon content is determined by subtracting the moisture, volatile matter and ash content values from 100. Fixed carbon content in coal is used to determine the effectiveness of coal-burning equipment, as well as to provide an indication of coke yield in coking processes [Speight, 2005].

- **3.2 Ultimate analysis**

Ultimate analysis provides information regarding the weight percentages of the main chemical elements present in coal i.e. carbon, oxygen, nitrogen, hydrogen and sulfur [Leonard III and Hardinge, 1991; Niksa, 1995; Speight, 2005]. This chemical analysis is important for the accurate calculation of a material balance and calorific value of coal. The ultimate analysis of carbon, hydrogen, sulfur and nitrogen are typically expressed on a moisture free basis.

To determine the percentage carbon, both the mineral carbonate as well as the organic carbon within the coal substances must be included. The nitrogen observed is assumed to be present in the coal samples' organic matrix. With regards to the determination of the hydrogen content, the hydrogen within the organic materials of coal, as well as the hydrogen in the water associated with coal, is included. Sulfur is present in various forms and the total value for sulfur is used when determining the ultimate analysis. The different forms of sulfur in coal include organic sulfur, inorganic sulfates, and inorganic sulfides in the form of pyrites and marcasite [Speight, 2005]. The percentage oxygen is calculated by difference [Schuhmann, 1952].

- **3.3 Thermogravimetric (TG) analysis**

The thermogravimetric analyser (TGA) can be used to gain quantitative information regarding the behaviour of coal samples during pyrolysis. The mass of the sample is measured

continuously as a function of time and temperature, while the temperature is maintained within a controlled atmosphere according to a specific program. The heating range can vary from 0.1°C/min to 100°C/min with high temperatures of up to 1400°C [TA instruments, 2010; Collins, 2014]. Inside the TGA, two sample pans are supported by thermobalances which are cooled or heated within a furnace during the experiment. A thermocouple is placed inside the furnace, as close as possible to the sample pans, and measures the temperature, which usually differs by approximately 2°C from the operating temperature. The purge gas manages the constant atmosphere, while the mass loss of the sample is monitored during the experiment. A schematic representation of the TGA is presented in Figure 3.1. A variety of TGA instruments are available and can be used to study different processes which include: pyrolysis, decarboxylation, decomposition, oxidation, weight % ash, weight % filler and the loss of water, solvent or plasticizer [TA instruments, 2010].

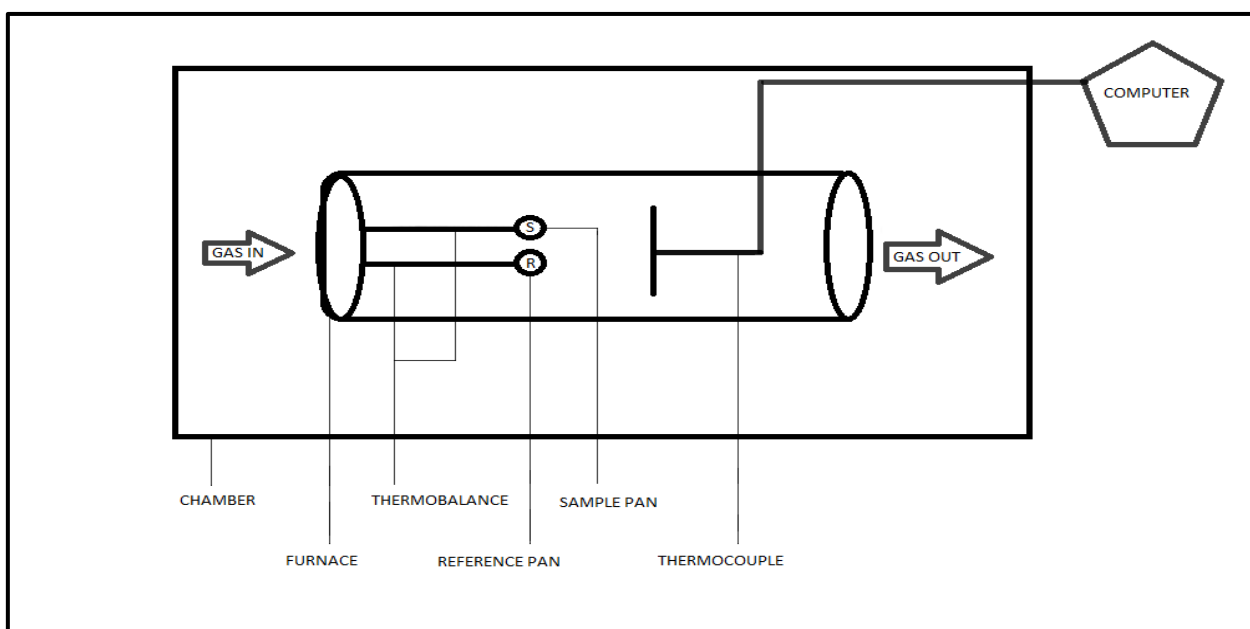


**Figure 3.1: Components of the TGA.**

A typical TG thermal decomposition curve is displayed in Figure 3.2. Temperature is on the x-axis and weight percentage on the y-axis. The mass loss of a sample with an increase in temperature can be observed from the descending curve.



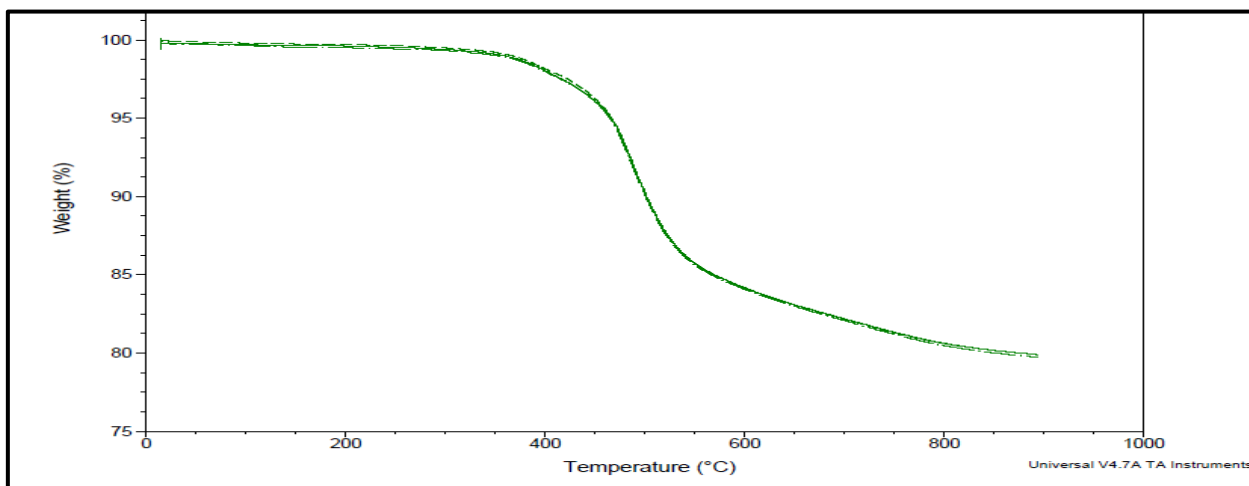


**Figure 3.2:** A typical TGA thermal curve.

The first derivative (DTG) of the weight loss curve is presented in Figure 3.3 as example. This first derivative curve can be used to do further characterizations on specific samples. The peak of this first derivative curve indicates the temperature at the maximum rate of the reaction [Perkin Elmer, Inc., 2010].

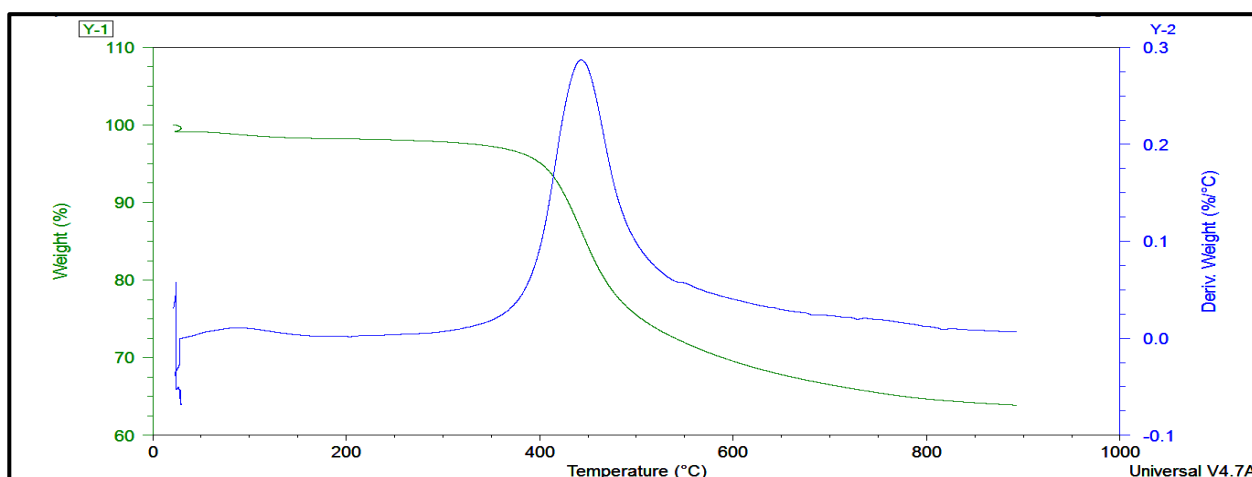


**Figure 3.3:** A first derivative curve (DTG).

The effects of pyrolysis, combustion, gasification and hydrogenation on coal samples can be observed when using the TG analysis technique [Fangxian *et al.*, 2009]. Reproducible results can be obtained when using the TGA and therefore accurate assumptions can be made about the various weight loss reactions within the coal structure during pyrolysis. Additional information about the coal sample can be gained by changing variables of the TGA such as the purge gas type and heating rate [Huang *et al.*, 1980].

Thermal analysis is essential in research regarding coal processes for both practical and fundamental investigations. The thermogravimeter is a very useful instrument because of its rapid analysis time and minimum equipment necessary. Further advantages of the TGA include accurate analysis under a controlled atmosphere with large temperature ranges and smaller sample sizes [TA instruments, 2010].

By connecting a mass spectrometer (MS) to the TGA, the analysis of the evolved gases can be recorded [Skoog et al, 2007]. When the sample is heated, volatile materials may be released, which are transferred to the MS to identify the components. When the gaseous compounds enter the MS via the capillary tube, they form positively charged radicals by colliding with a beam of electrons. These positively charged ions separate according to their different masses when moving through the mass analyser. The ion detector records these ion masses and converts the data to an electrical signal. The mass spectrum is then generated [Silverstein et al, 2005]. This pathway followed by the gaseous compounds is illustrated in Figure 3.4.

The TG-MS is a very powerful technique where quality control, product development and safety are important because it can detect very low levels of material.

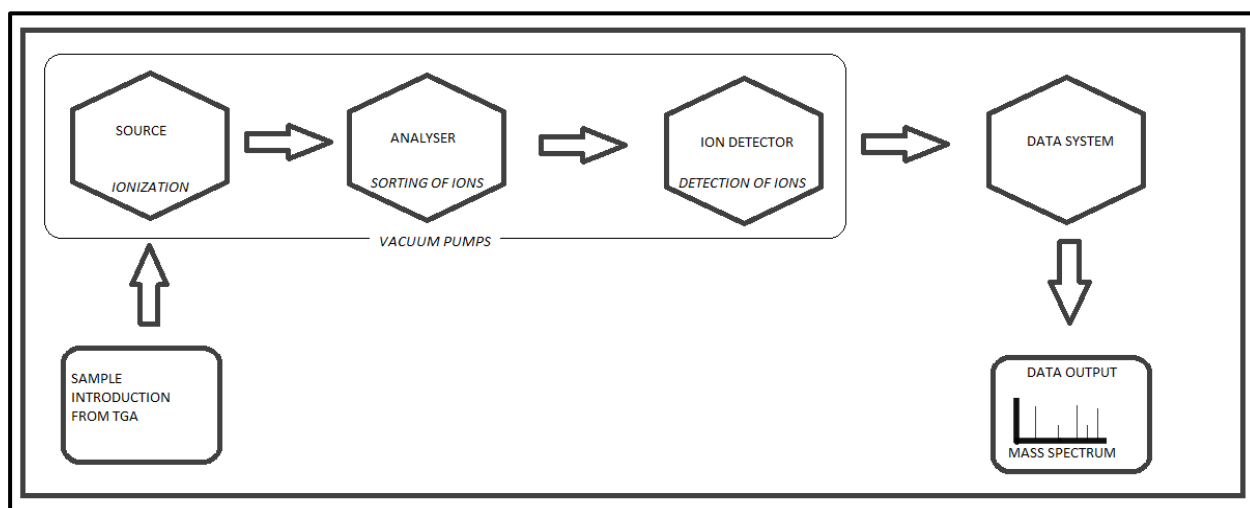


**Figure 3.4:** A schematic diagram of the components within the MS.

### 3.4 X-ray Fluorescence (XRF)

XRF analysis is used to determine the inorganic elemental content in the sample and is reported as oxides. This technique allows excitation of analytical X-rays by using an X-ray tube to generate secondary X-rays. In this tube, electrons are produced by a cathode with a current of 40 to 60 milliamps, which causes the electrons to accelerate and fire at the target anode. The cathode, as well as the target, is under vacuum to minimize air absorption of X-rays and to

avoid oxidation. After the electrons have been fired at the target, they generate high heat and broadband continuum X-rays which are directed at the sample. These X-rays cause the sample to emit X-rays which are characteristic of the elements present. An analysing crystal diffracts the X-rays in a spectrometer, which then measures the intensities with detectors on a goniometer [Skoog *et al.*, 1998].

By comparing the standard X-rays with the intensities of the emitted X-rays from the sample, the metal oxide content of the sample can be calculated [Johnson *et al.*, 1989]. A schematic diagram of an XRF spectrograph is presented in Figure 3.5, and in Figure 3.6 a typical XRF graph is displayed. Large homogeneous samples are mainly characterized by using XRF, although trace elements can also be determined to the parts-per-million (ppm) level. The accuracy of an XRF analysis of inorganic materials depends on the particle size, surface, matrix effects, concentration, and the quality of standard materials. This accuracy falls between 2% and 10% [Johnson *et al.*, 1989].

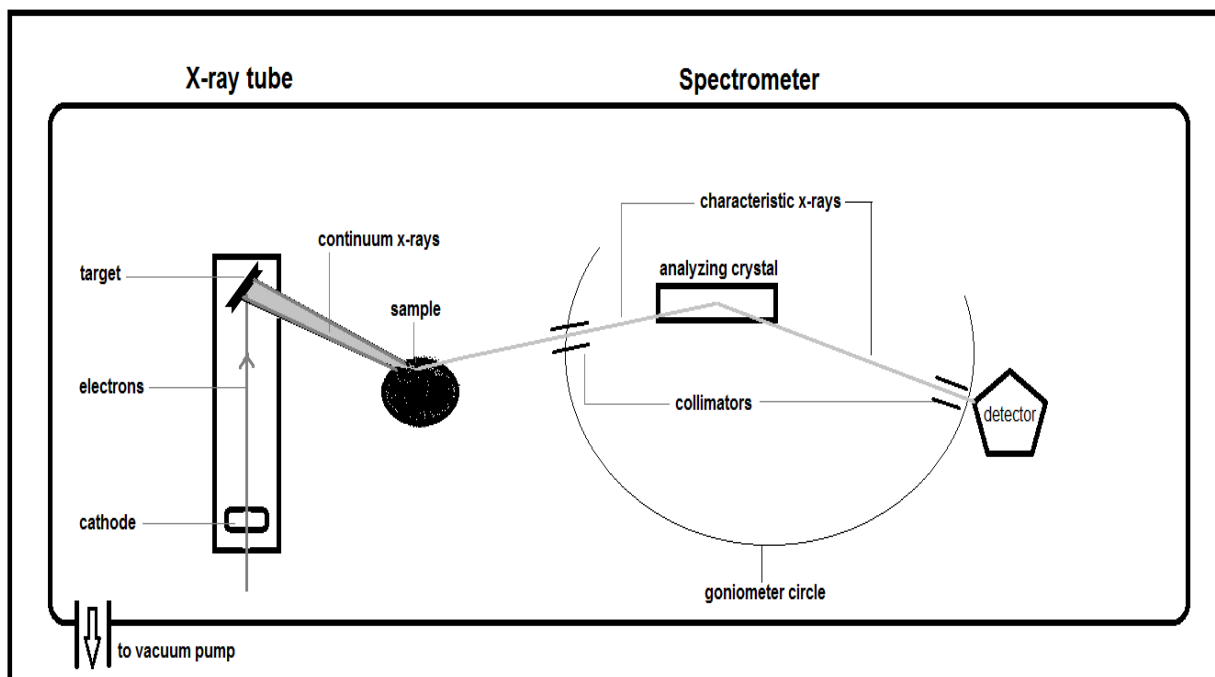


Figure 3.5: Diagram of XRF spectrograph [adapted from Skoog *et al.*, 1998].

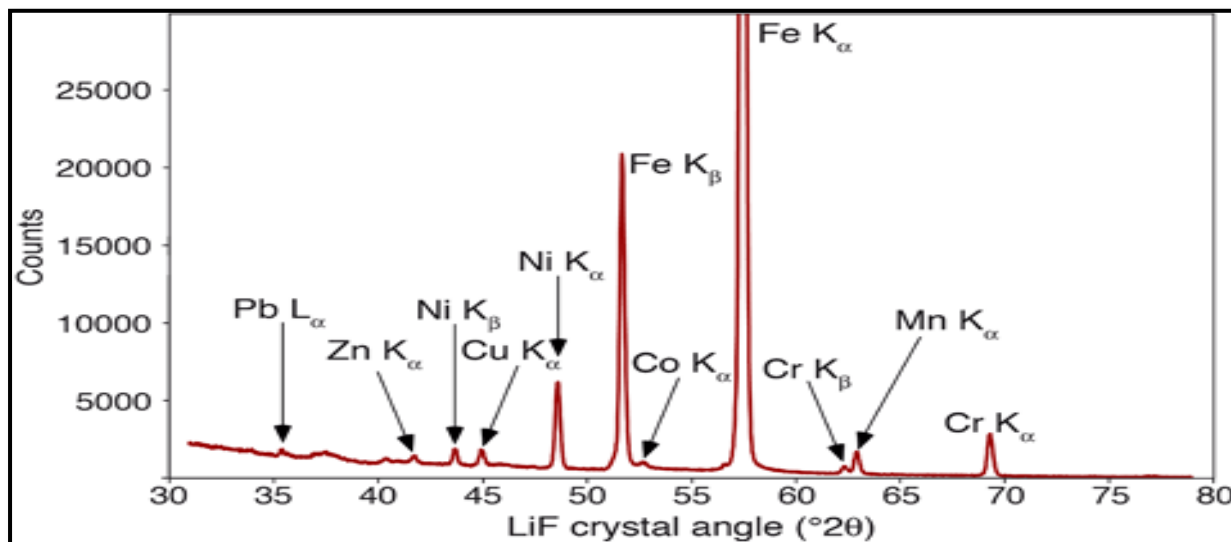


Figure 3.6: Typical XRF graph.

When using XRF analysis on coal, 11 inorganic elements present can be determined with an accuracy of 2% to 10%. The restricted availability of reference samples and the manner in which the coal samples are stored are important limiting factors of XRF spectroscopy of coal samples [Johnson *et al.*, 1989]. XRF analysis is very useful for rapid and accurate analysis of trace elements within coal samples. It is also adaptable to larger scale coal surveys because of the simplicity and speed of the analysis technique [Kuhn *et al.*, 1975].

XRF and XRD analyses can be regarded as complimentary when used for coal characterization. XRF analysis reports the concentration of elements in the samples and reported as oxides, for example 50%  $\text{Al}_2\text{O}_3$  and 30%  $\text{SiO}_2$ , while XRD can be used to distinguish between different crystalline phases in the samples, for example  $\text{Al}_2\text{O}_3$ ,  $\text{SiO}_2$ ,  $\text{Al}_2\text{Si}_2\text{O}_5(\text{OH})_4$  or  $\text{Al}_6\text{Si}_2\text{O}_{13}$ , or any of these combinations [Johnson *et al.*, 1989].

### 3.5 X-ray diffraction (XRD)

X-ray diffraction (XRD) analysis is used to identify the crystalline phases or compounds present in a solid sample [Takagi *et al.*, 2004]. XRD is a crystallography technique in which the pattern of atoms in a crystal is recorded by the diffraction of X-rays. This pattern is then analysed to detect the nature of the samples' lattices. By understanding the nature of the lattice, the material and molecular structure of the specific sample are revealed. Materials can be identified by using the patterns of powder diffraction peaks, while the crystal size, texture and purity can be determined from the changing widths and positions of the peaks [Takagi *et al.*, 2004].

During XRD analysis the sample is placed in a sample spinner, while the X-ray beam reflects the sample at angles from 20 to 80 degrees. The principle on which the XRD analysis functions is displayed in Figure 3.7.

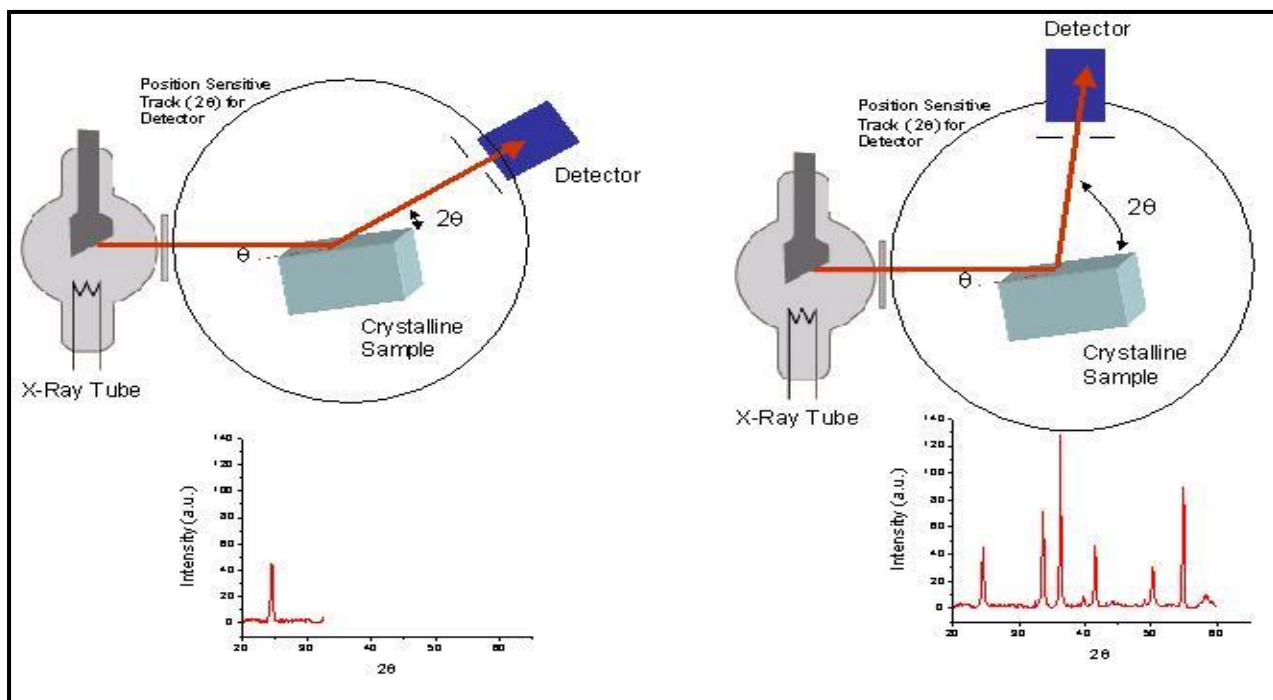


**Figure 3.7: Principle of XRD analysis [Azhagurajan and Nagaraj, 2009].**

The results from the diffraction are obtained as a graph which represents the amount of diffraction. The width of the peak at half its height, also known as the Full Wave Half Maximum (FWHM) value is tabulated along with the D-spacing values which are used for further calculations [Azhagurajan and Nagaraj, 2009].

The crystalline mineral material is assigned to the strongest peak relating to the peak position with the best fit first. Weaker peaks corresponding to that same mineral are used as conformation of the presence of the specific mineral. A set of peaks can only be used once to identify a mineral. The smaller remaining peaks are solved using the same method, until every peak has been assigned to a specific mineral [Moore and Reynolds, 1997].

XRD analysis provides information regarding the mineral composition of coal samples. It can be used in coal characterization to qualitatively and quantitatively evaluate the crystalline mineral matter present in the coal structure [Skoog *et al.*, 1998].

### 3.6 Diffuse reflectance spectroscopy (DRIFT)

Qualitative analysis of the functional groups within the coal samples can be achieved by DRIFT spectroscopy [Sobkowiak and Painter, 1995]. During DRIFT analysis, a beam of radiation is reflected from an ellipsoidal mirror in the direction of the sample. The beam is scattered, reflected and absorbed, due to different elements with a variety of orientations within the sample, before being directed to the detector. KBr is used as a diluent and is mixed with the sample before analysis, thus a reference KBr sample is run as background [Skoog *et al.*, 1998]. In Figure 3.8 a schematic diagram represents the fundamentals of DRIFT spectrometry within a FTIR cell compartment.

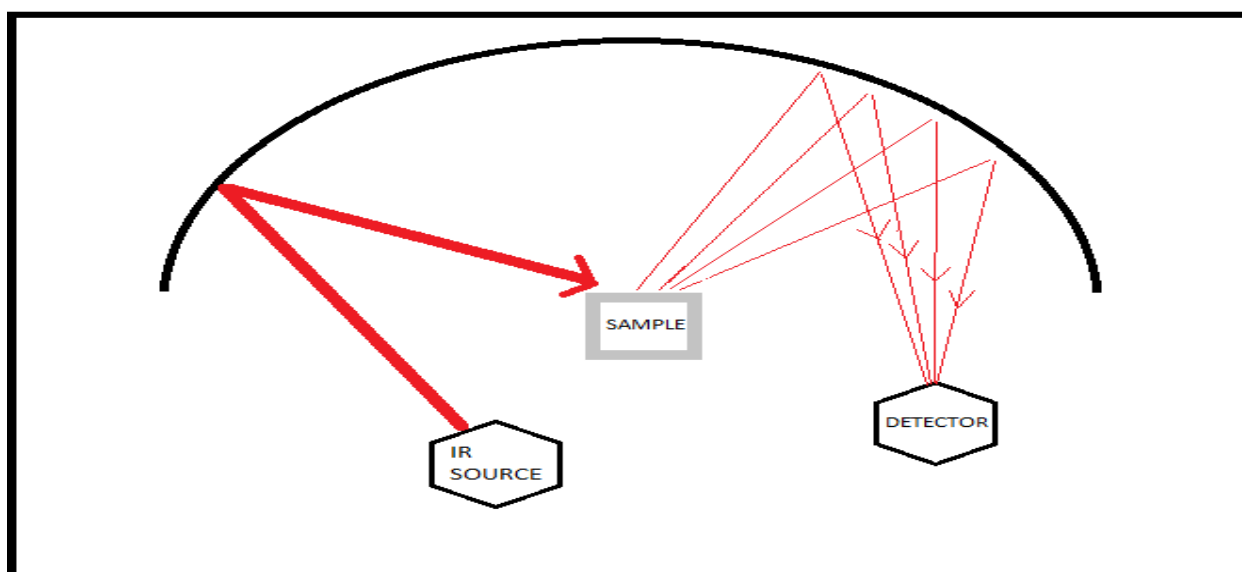


**Figure 3.8:** Principle of DRIFT spectroscopy.

The advantage of DRIFT spectra compared to FTIR using a KBr pellet is the well-resolved bands and the flat baselines [Sobkowiak and Painter, 1995].

DRIFT spectroscopy is based on the Kubelka-Munk law and interpretations of coal samples has been done extensively [Fuller and Griffiths, 1978; Ito *et al.*, 1988; Ito, 1992; Sobkowiak and Painter, 1995; Van Niekerk *et al.*, 2008; Xin *et al.*, 2014]. These studies investigated the relationship between the intensity of functional groups and the coal rank, and also the degree of coalification and carbonization of some coal samples. The results obtained from DRIFT spectra can, however, be only semi-quantitative due to various functional groups present in coal samples, which overlap on the spectra [Machnikowska *et al.*, 2002].

### 3.7 BET surface analysis

The Brunauer, Emmett and Teller (BET) theory is an extension of the Langmuir theory, which relates to the adsorption of gas molecules onto a solid surface at a specific temperature. The BET theory extends the Langmuir theory to adsorption onto multilayers. Adsorption of gas molecules occurs when the gases condense onto solid surfaces, made up from both internal and external surfaces as well as pore systems [Gregg and Sing, 1967]. The BET surface area theory is used to determine the amount of gas molecules adsorbed between relative pressures of 0.02 and 0.35 [Nandi and Walker, 1964; Hurt *et al.*, 1991; Malumbazo, 2011].

CO<sub>2</sub> has become the accepted adsorbent gas when determining coal surface area due to its relatively small molecular mass as well as high critical temperature. The adsorption and desorption of carbon dioxide have a higher activation energy when compared to nitrogen, and therefore carbon dioxide diffuses through the complex pore system of coal at lower temperatures [Van Niekerk *et al.*, 2008]. With CO<sub>2</sub> adsorption, the area of the entire pore system is reported [Larsen *et al.*, 1995].

Information regarding the reactivity of coal samples is provided when the surface areas of coal-char samples are investigated. The surface area of coal-char samples can be determined by using the Dubinin-Radushkevich model and CO<sub>2</sub> as adsorbent gas at low pressures [Collins, 2014].

### 3.8 Scanning electron microscope (SEM)

SEM is an analytical technique which can be used to investigate the microscopic structure of the sample. SEM images are obtained with a high-energy beam which produces secondary electrons when the beam reaches the sample. These secondary images are processed to display a digital image. The SEM generates signals at the surface of the samples using a focused beam of electrons with high-energies. Signals derived from these interactions between the electrons and the sample reveal information about the crystalline structure of the sample, i.e. external morphology, the chemical composition, and the orientation of the compounds present in the sample. A 2-dimensional image displays the variation of these properties, and the data can be collected over selected areas ranging from 5 microns to 1 cm in width.

Combined analysis can be achieved when fitting different detectors to the SEM instrument. The most common is combining an energy-dispersive X-ray spectroscope with the SEM to analyse sintering, agglomeration and elements responsible for transformation. The high-energy electron beam operates under vacuum and uses magnetic lenses to focus on the sample [Skoog *et al.*, 1998]. A schematic diagram of a SEM detector is displayed in Figure 3.9.

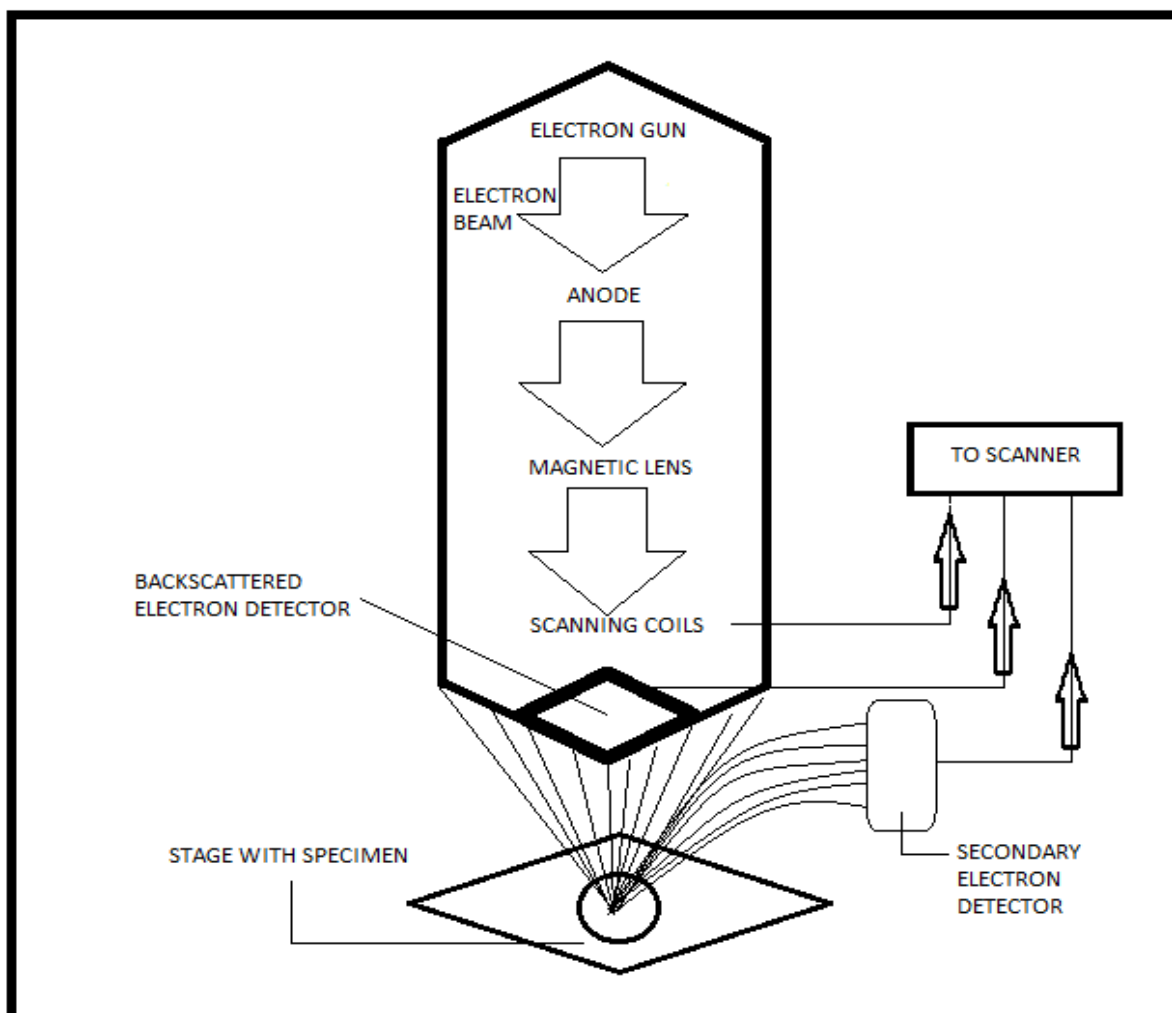


**Figure 3.9:** Schematic diagram of a typical SEM.

SEM analysis is non-destructive, thus the x-rays from the electron interactions do not cause loss of sample, making multiple analyses of the same sample possible [Swapp, 2012]. SEM analyses the morphological changes, which provides detailed information about the physical properties of crystallinity and size of the phases present in the sample [Azhagurajan *et al.*, 2009].



# CHAPTER 4

## Experimental procedure

*The specifications of the experimental procedures used during this study will be discussed in this chapter. The sample preparation conducted will be explained in detail, as well as the instrumental specifications given for the different analytical techniques. The following topics are addressed:*

*4.1 Experimental plan*

*4.2 Coal samples*

*4.3 Sample preparation*

*4.4 Thermogravimetry-Mass Spectrometry (TG-MS)*

*4.5 Char preparation in the tube furnace*

*4.6 Sample analysis techniques*

- **4.1 Experimental plan**

The experimental procedures and analytical techniques used in this study are summarized in Figure 4.1.

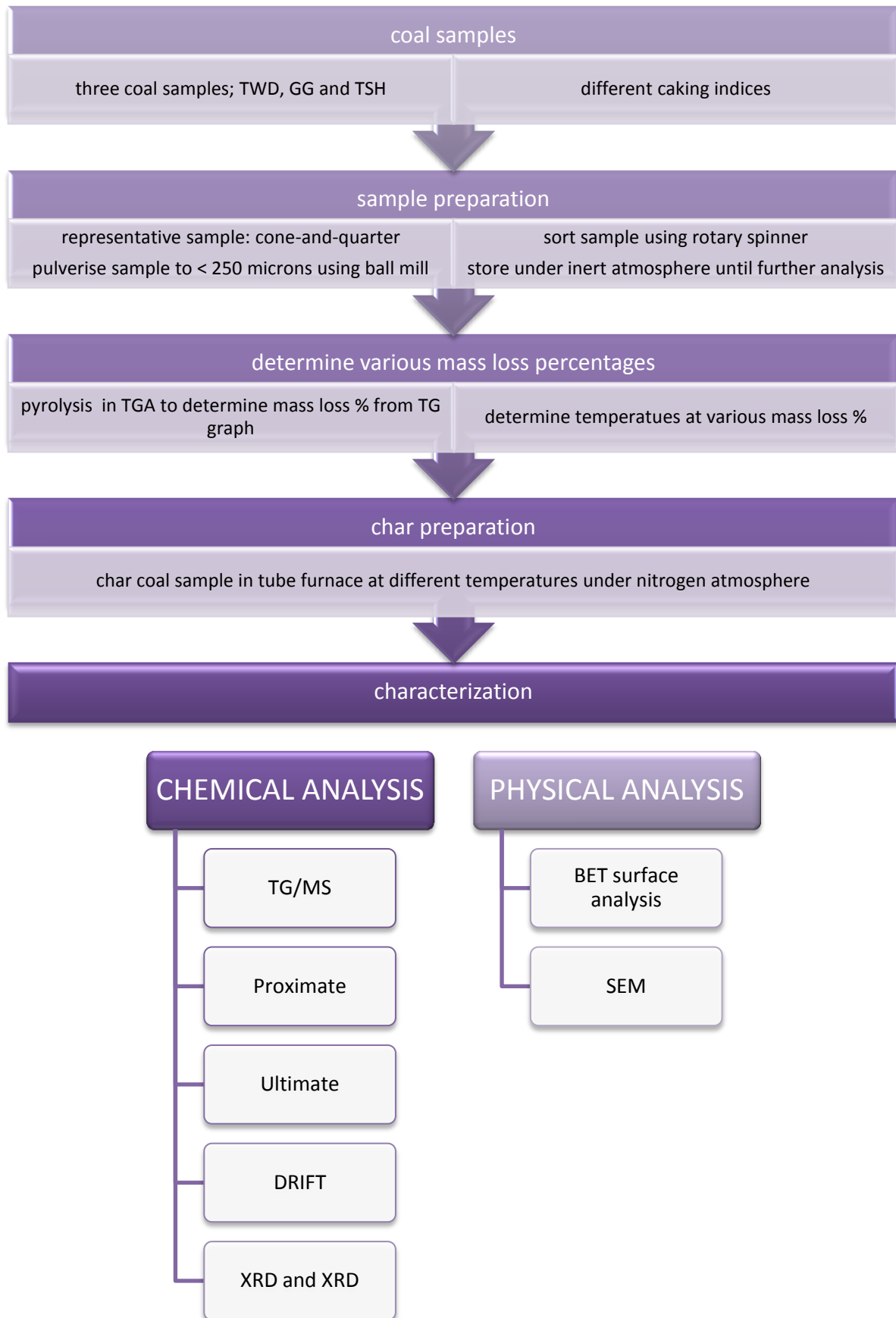


Figure 4.1: Diagram of experimental work and analysis.

## 4.2 Coal samples

Three South African coals with different caking propensities were chosen for this study. The first coal sample was from the Highveld region with a free swelling index (FSI) of 0, and classified as a bituminous medium rank-C coal. This Highveld coal comes from permian seams of the Vryheid Formation (345-230 Ma). This coal reserve area yields a low-ash export product from the beneficiation process. The raw ash content of the lower seam varies between 18 and 36%, and this seam is the major contributor to the production process.

The second sample was a Grootegeluk coal from the Waterberg region, also a bituminous medium rank-C coal, with a FSI of 6.5. The Grootegeluk Mine is in the Waterberg Coalfields and has 12 different zones. An increase in the ratio of bright to dull coal is characteristic of Zones 4 to 11, while semi-soft coking coals can be found from Zone 6 to 11. The thin coal seams are combined with carbonaceous mudstone [Jeffrey, 2005].

The Tshikondeni coal (the third coal sample) came from the Limpopo region, and is a bituminous medium rank-B coal with the highest FSI of 9. The Tshikondeni Colliery is the only operation exploiting the Soutpansberg Coalfield, and produces hard coking coal. These coking coals are useful in the steelmaking and metallurgical industries [Jeffrey, 2005].

When caking coals are heated they soften and become fluid (known as the plastic stage) and then re-solidify, leaving a coherent solid residue. In the case of non-caking coals, this plastic stage is absent when heated, and the char that remains after heating is weak or non-coherent [Zubkova, 2005]. Investigating the differences in the chemical and physical properties of these three coals, the changes occurring during pyrolysis will be better understood and explained for different types of caking coals.

## 4.3 Sample preparation

Representative samples of the coal were obtained using the cone and quarter method proposed by Allen [1981] as illustrated in Figure 4.2. The bulk coal sample was emptied and thoroughly mixed, leaving a uniform conical pile (A in Figure 4.2). This pile of coal was then divided into four equal parts. Only two quarters opposite each other (B1 and B2), are mixed into another conical pile (D) and the other two quarters are removed (C1 and C2). This process of mixing and dividing was repeated four times to obtain enough coal, approximately 3 kg, for the test work programme.

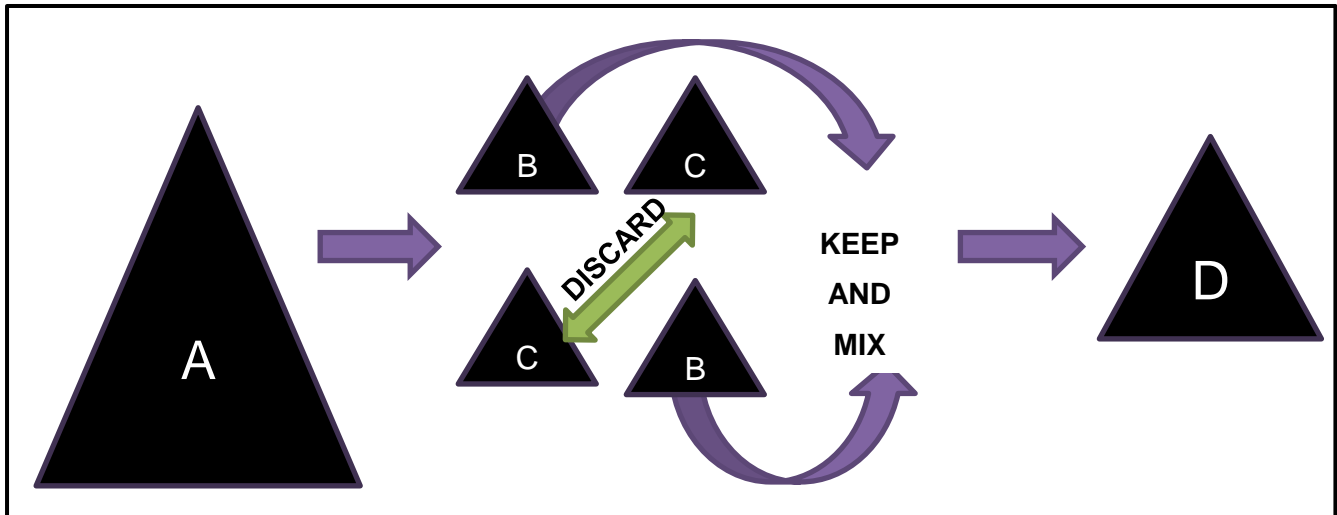


**Figure 4.2: The cone and quarter method.**

The coal was then crushed and ground using a Samuel Osborne (SA) LTD jaw crusher, model: 66YROLL, to break down the bigger particles to smaller than 1 mm. A ball mill containing stainless steel balls was used to further mill the coal. The milled coal was then sieved, and particles smaller than 250 microns were used, while the bigger particles were milled again until all the oversized particles were below 250 micron. These crushed and milled samples were sieved using a Spartan vibratory sieve-shaker, Fritsch Analysette (type 03.5025; 4822). A rotary riffle splitter, illustrated in Figure 4.3, was used to divide the milled coal into multiple samples in one single operation. The coal is inserted into the feed hopper and the vibratory feeder moves the coal with a constant flow to the rotating turntable. This turntable contains six sample holders and rotates at a constant speed. The sample holders are uniformly filled, which ensures that smaller coal samples are still representative of the bigger bulk coal sample [Allen, 1981]. The prepared coal samples are sensitive to oxidation and were immediately dried in a vacuum oven overnight at 80°C before vacuum sealing it until further analysis.

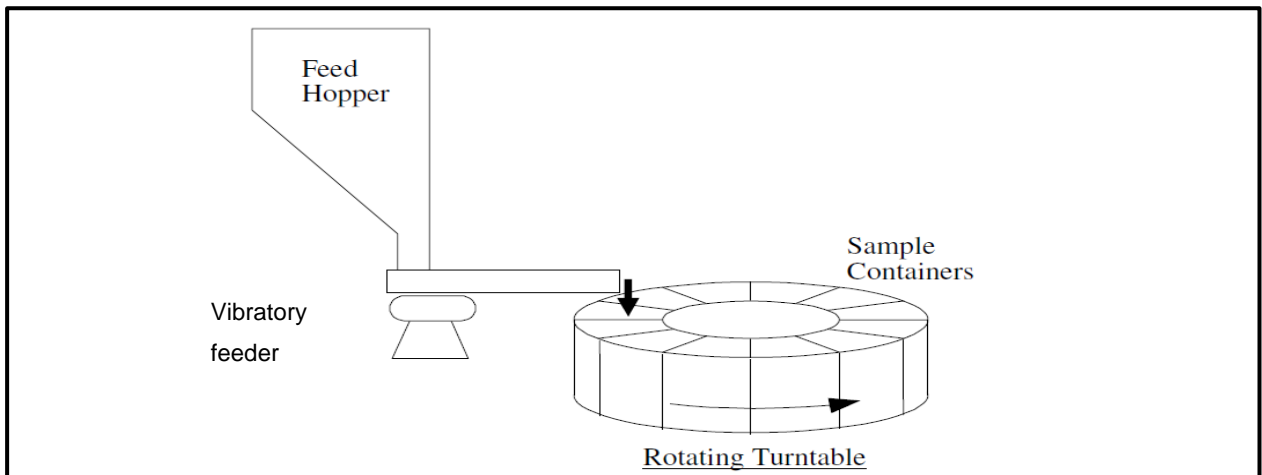


Figure 4.3: Rotary riffle splitter dividing coal into six identical fractions [Allen, 1981].

#### 4.4 Thermogravimetry-Mass Spectrometry (TG-MS)

The Thermogravimetric analyser was used to analyse the mass loss of the coal samples under a nitrogen atmosphere. Coupling the TG to a quadrupole mass spectrometer (TG-MS) made it possible to determine the composition of different gaseous compounds formed during pyrolysis in a nitrogen atmosphere. The TG-MS experimental set-up is displayed in Figure 4.4.

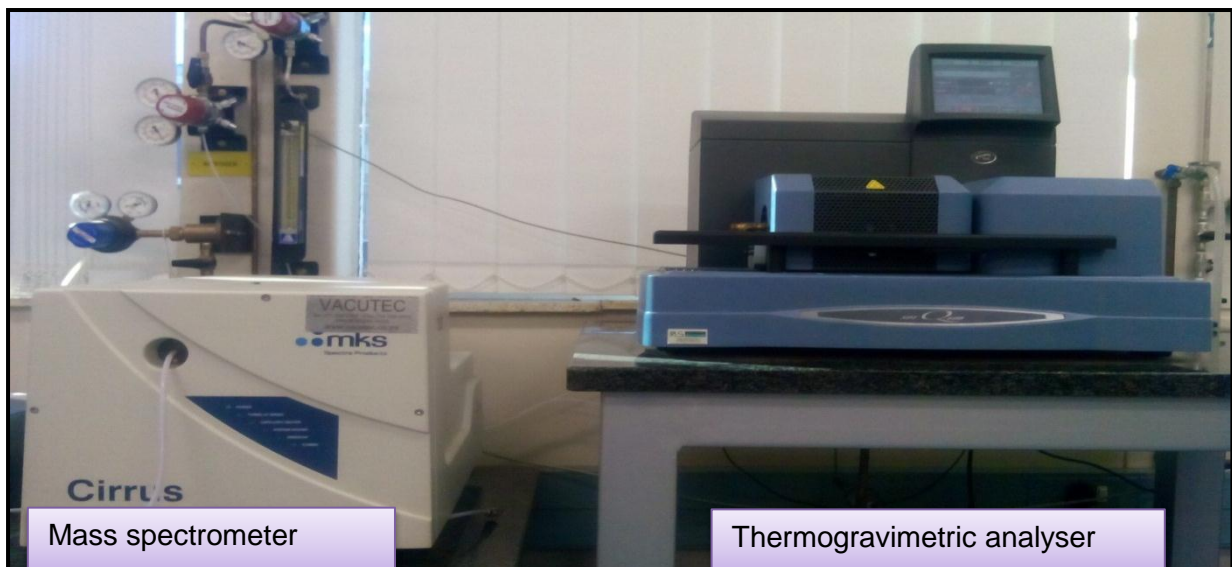


Figure 4.4: TG-MS experimental set-up.

## 4.5 Thermogravimetric (TG) analysis

The mass losses during pyrolysis were determined using a SDTQ 600 thermogravimetric analyser. 90  $\mu\text{L}$  alumina crucibles were used, with approximately 20 mg of coal sample per measurement, and placed on the thermobalance in the TG. The sample was heated in a nitrogen atmosphere up to 900°C. A continuous flow of nitrogen prevented the sample from oxidization while cooling down in situ to room temperature. The results were recorded with mass loss as a function of temperature. Three runs were performed of each sample. The first differential curves (DTG), generated electronically from the mass loss data, show the rate of change in mass of the sample.

The experimental conditions for the pyrolysis under nitrogen atmosphere are summarized in Table 4.1.

---

**Table 4.1: Experimental conditions for the pyrolysis process.**

Nitrogen atmosphere: flow rate 100 mL/min

Operating temperature up to 900°C at a rate of 10°C/min

Coal particle size: < 250 micron

20 mg of coal sample

---

## 4.6 Mass Spectrometer (MS)

The MS results were obtained from a Cirrus mass spectrometer equipped with a dual Faraday detector (model: LM92-00111019). Figure 4.4 shows the MS as connected to the outgas port of the TG. The evolved gases were detected while the TG was running and fed through a heated capillary from the outgas port to the MS. The MS was only used to detect the temperature ranges of the gaseous products which are released during pyrolysis in the TG, and no quantitative analyses of the gases were done.

#### 4.7 Char preparation in the tube furnace

Coal samples were heated in a Lenton tube furnace, model TSH12/75/610, displayed in Figure 4.5. The maximum operating temperature of this furnace is 1200°C and it has a ceramic tube of 75 mm diameter with a heating zone of 610 mm.



**Figure 4.5:** Lenton tube furnace used to prepare the char samples.

Approximately 20 g of coal sample was loaded in a ceramic sample pan and heated up to 900°C at 10°C/min. The nitrogen flow was set at 100 ml/min so that these conditions were similar to the heating conditions of the TG. After loading two sample pans in the tube furnace, it was closed and purged with nitrogen to remove the air present before the heat treatment was started.

Using the TG graphs of mass loss as a function of temperature, the different temperatures correlating respectively to 20%, 40%, 60%, 80% and 100% of mass loss up to 900°C can be determined. The experimentally derived temperatures from the TG experiments are summarised in Table 4.2.

The specified temperatures are given corresponding to the respective mass loss of the coal. Samples were heated up to the specific temperature in the tube furnace and cooled down under nitrogen atmosphere to prevent oxidation. Each sample was weighed to determine the mass loss percentage and vacuum sealed until further analysis.

**Table 4.2: Temperatures at which specific mass loss observed from TGA.**

<u>Highveld TWD</u>		<u>Grootegeluk GG</u>		<u>Tshikondeni TSH</u>	
<i>Sample</i>	<i>Temperature (°C)</i>	<i>Sample</i>	<i>Temperature (°C)</i>	<i>Sample</i>	<i>Temperature (°C)</i>
TWD 1 at 20%	433	GG 1 at 20%	424	TSH 1 at 20%	457
TWD 2 at 40%	468	GG 2 at 40%	450	TSH 2 at 40%	490
TWD 3 at 60%	535	GG 3 at 60%	482	TSH 3 at 60%	520
TWD 4 at 80%	657	GG 4 at 80%	571	TSH 4 at 80%	612
TWD 5 at 100%	900	GG 5 at 100%	900	TSH 5 at 100%	900

#### 4.8 Proximate and ultimate analyses

Raw coal, as well as the char samples, prepared at specified mass loss percentages, were sent to the Bureau Veritas Testing and Inspections South Africa laboratories for proximate and ultimate analyses.

These analyses were done to determine the changes in the chemical composition at the various temperatures. During proximate analysis the mass percentages of the samples' moisture, ash, fixed carbon (FC) and volatile matter (VM) were determined, while the ultimate analysis was used to determine the mass percentages of the chemical components in the coal and char samples (sulfur, carbon, hydrogen, nitrogen and oxygen).

Table 4.3 presents the different analytical procedures used.



**Table 4.3: Analytical procedures and test methods.**

<u>Description</u>	<u>Procedure / Test Method</u>
<b>Sample preparation</b>	ACT-TPM-001 based on ISO 13909-4: 2001
<b>Moisture content (%)</b>	ACT-TPM-010 based on ISO11722: 1999
<b>Ash content (%)</b>	ACT-TPM-011 based on ISO 1171: 2010
<b>Volatile matter content (%)</b>	ACT-TPM-012 based on ISO 562: 2010
<b>Total sulfur (%)</b>	ACT-TPM-013 based on ISO 19579: 2006
<b>Ash composition</b>	ASTM D4326 XRF – By fusion bead (Subcontracted Test)
<b>Ultimate analysis</b>	ACT-TPM-027 based on ISO 29541:2010
<b>Crucible Swelling number</b>	ACT-TPM-015 based in ISO 501:2003

#### 4.9 X-Ray Fluorescence (XRF)

XRF analysis was performed to determine the ash composition of the coal, i.e. the major and minor elements present. The raw coal and the char samples were sent to the Bureau Veritas Testing and Inspections South Africa laboratories for analysis; the ASTM D4326 XRF analysis method was used.

#### 4.10 X-Ray Diffraction (XRD)

Samples were sent to XRD Analytical and Consulting for the qualitative and quantitative determination of the crystalline compounds present in the various samples. A back loading preparation method was used to prepare the samples for the XRD analysis. Analyses were done on a PANalytical Empyrean diffractometer with PIXcel detector and fixed slits with Fe filtered Co-K<sub>α</sub> radiation. X'Pert Highscore plus software was used to determine the crystalline phases. The Rietveld method was used to estimate the relative phase concentrations (weight %).

#### 4.11 Diffuse Reflectance Infrared Fourier Transform (DRIFT) spectroscopy

Raw coal samples, as well as the char samples, were analysed with the DRIFT technique to characterize the different functional groups present and their behaviour during increasing temperature. The interpretation of the DRIFT spectra was based on publications by Van Niekerk *et al.* [2008] and Painter *et al.* [1981].

The samples were prepared by adding 200 mg potassium bromide (KBr) to 20 mg of coal or char sample. This was then mixed in a Wig-L-Bug for 1 minute and stored in a vacuum oven at 60 °C for 24 hours. The samples were placed in a desiccator for approximately 30 minutes to cool down before analysis. Pure KBr was used as background spectrum and was also stored in the vacuum oven at 60 °C for 24 hours before use.

A DRIFT sampling holder, containing the sample, was placed in the Bruker VERTEX 70 FTIR spectrometer (Figure 4.6) to obtain the IR spectra. The spectra were acquired with a mid-infrared region (MIR) KBr beam splitter, and a resolution of 4 was observed for the 400 scans per sample. Scanning of samples was performed from a wavenumber of 4000  $\text{cm}^{-1}$  to 370  $\text{cm}^{-1}$ .



Figure 4.6: Vertex FTIR spectrometer with DRIFT sample holder.

### 4.12 CO<sub>2</sub> BET surface analysis

The CO<sub>2</sub> BET surface adsorption analyses were conducted using a Micrometrics ASAP 2010 Analyser as presented in Figure 4.7. The coal-char sample was dried in a vacuum oven for at least 6 hours to remove the excess moisture present in the sample. 0.2 g of the coal sample was placed in a glass tube and degassed at 25°C for 48 hours. After the degassing process was completed, the glass tube was connected to the analysing port for the adsorption analysis. The analyses were conducted according to the short coal method using CO<sub>2</sub> as adsorbent gas. Ice was used to keep the analysis temperature constant at 273.15 K. The Dubinin-Radushkevich method was used to calculate the surface areas of the samples [Sobolik *et al.*, 1992].



Figure 4.7: The Micrometrics ASAP analyser used for CO<sub>2</sub> surface analyses.

A; Degassing port	D; Analysis port
B; Sample tube being degassed	E; Sample tube being analysed
C; Thermal jacket	F; Container filled with ice as cooling medium

### 4.13 SEM

SEM analyses were performed using a FEI QUANTA 250 FEG ESEM analyser. The images were gathered by the Laboratory for Electron Microscopy (LEM) at the NWU (North West University). Images were taken at various magnifications.

# Chapter 5

## Results and discussion: changes in the chemical properties of caking coals during pyrolysis

*In this chapter the various chemical analyses performed on the coal-derived char samples will be discussed. These results will give insight into the chemical changes occurring in the coal structure and the effect of pyrolysis on the composition of the coal. 18 samples were subjected to these analyses; the three raw coals and their various char samples prepared at different temperatures correlating to the different mass loss percentages.*

*Results from the following techniques are discussed in this chapter:*

*5.1 Conventional analyses*

*5.2 Thermogravimetric and mass spectrometer analysis (TG-MS)*

*5.3 X-Ray Fluorescence (XRF)*

*5.4 X-Ray Diffraction (XRD)*

*5.5 Diffuse Reflectance Infrared Fourier Transform Spectroscopy (DRIFT)*

*5.6 Summary*

- **5.1 Conventional analyses**

The raw coals as well as the coal-derived char samples were submitted for conventional analyses which included the proximate and ultimate analyses. The results obtained were used to characterize the coal and are summarized in Table 5.1 to Table 5.4. Background on the proximate and ultimate analyses are described in Chapter 3.1.1 and 3.1.2, respectively, while the experimental procedures as well as the ISO standards for the various analyses are given in Chapter 4.6.1. The results from the proximate and ultimate analyses for the three raw coal samples are summarized in Table 5.1. The results for the TWD, GG and TSH raw coals, as well as for the coal-derived char samples are respectively reported in Table 5.2 to Table 5.4. These results are reported on a moisture free basis (m.f.b) as well as on a dry basis (d.b). The abbreviations used for the samples are summarized in Table 4.2.

Table 5.1: Conventional analysis results for the three raw coals.

	TWD raw		GG raw		TSH raw	
	<i>m.f.b</i>	<i>d.b</i>	<i>m.f.b</i>	<i>d.b</i>	<i>m.f.b</i>	<i>d.b</i>
<b>Proximate analysis</b>						
<b>Inherent moisture</b>	0.0	4.5	0.0	2.9	0.0	0.7
<b>Ash</b>	14.2	13.6	8.0	7.8	15.0	14.9
<b>Volatile matter</b>	28.3	27.1	36.9	35.8	21.5	21.4
<b>Fixed carbon</b>	57.4	54.8	55.1	53.5	63.5	63.0
	<u>100</u>	<u>100</u>	<u>100</u>	<u>100</u>	<u>100</u>	<u>100</u>
<b>Ultimate analysis</b>	<i>m.f.b</i>	<i>d.b</i>	<i>m.f.b</i>	<i>d.b</i>	<i>m.f.b</i>	<i>d.b</i>
<b>Sulfur</b>	0.8	0.7	1.1	1.0	0.8	0.7
<b>Carbon</b>	79.4	65.1	82.0	73.3	89.7	75.8
<b>Hydrogen</b>	4.2	3.5	5.3	4.8	5.1	4.3
<b>Nitrogen</b>	2.2	1.8	1.8	1.6	2.1	1.8
<b>Oxygen</b>	13.2	10.8	9.7	8.7	2.3	1.9
	<u>100</u>	<u>81.9</u>	<u>100</u>	<u>89.4</u>	<u>100</u>	<u>84.4</u>
<b>Atomic O/C ratio</b>		0.13		0.09		0.02
<b>Atomic H/C ratio</b>		0.64		0.77		0.67
<b>FSI</b>		0		6.5		9.0

The raw coal samples can be characterized (Table 5.1) as low to medium ash yield coals because the ash yields ranged between 8.0 wt.% and 15.0 wt.% (m.f.b.). The GG raw coal sample contained the largest amount of volatile matter with a value of 36.9 wt.% (m.f.b.), followed by the TWD coal with 28.3 wt.% (m.f.b.), and then the TSH coal with 21.5 wt.% (m.f.b.). The fixed carbon content present in the raw coal samples was the largest for the TSH coal with a value of 63.5 wt.% (m.f.b.), followed by TWD coal with 57.4 wt.% (m.f.b.), and the GG coal

contained the lowest amount of fixed carbon with a value of 55.1 wt.% (m.f.b.). It is important to note that the TSH raw coal sample contained substantially less inherent moisture with a value of 0.7 wt.% (d.b.).

From the ultimate analysis (Table 5.1) it is clear that the total sulfur values for the raw coals were between 0.8 wt.% and 1.1 wt.% (m.f.b.). Elevated levels of carbon content can be observed for all three raw coals, with TWD containing the lowest amount with a value of 79.4 wt.% (m.f.b.) and TSH containing the highest amount of carbon with a value of 89.7 wt.% (m.f.b.). No significant differences between the hydrogen and nitrogen contents could be observed for the three raw coal samples. Oxygen present in the coal samples were determined by difference, and substantially less oxygen was observed for the TSH sample with a value of only 2.3 wt.% (m.f.b.). The TWD coal and GG coal contained between 9.7 wt.% and 13.2 wt.% (m.f.b.) oxygen as determined by ultimate analysis.

Table 5.1 also includes the atomic H/C and O/C ratios as calculated from the ultimate analysis. When the three raw coal samples are compared, the O/C ratio was highest for TWD (0.13), followed by GG (0.09), and lowest for TSH (0.02). The relatively low O/C ratio of the TSH sample suggests that this coal has the highest aromaticity [Hatting, 2012].

The free swelling index (FSI) values are also reported in Table 5.1. TWD is a non-caking coal with an FSI of 0. GG is a medium caking coal with an FSI of 6.5, while TSH is a high caking coal with an FSI of 9.

When comparing the proximate analysis results, on a moisture free basis (Table 5.2), of the TWD raw coal sample (TWD 1) with the coal-derived char samples prepared at the different temperatures (TWD 2 – 6), it can be observed that the the volatile matter content decreased from the raw coal sample with a value of 28.3 wt.% (m.f.b.) to the TWD 6 sample, (prepared at 900°C), containing 2.4 wt.% (m.f.b) of volatile matter. As a result of the evolution of volatile matter the ash content increased with an increase in temperature as expected. The fixed carbon content was determined and also increased from 57.4 wt.% (m.f.b.) to a value of 77.3 wt.% (m.f.b.) with the increase in temperature during pyrolysis.

Table 5.2: Conventional analysis results of Highveld coal samples.

	TWD 1 (raw coal)		TWD 2 20% mass loss		TWD 3 40% mass loss		TWD 4 60% mass loss		TWD 5 80% mass loss		TWD 6 100% mass loss	
	<i>m.f.b</i>	<i>d.b</i>	<i>m.f.b</i>	<i>d.b</i>	<i>m.f.b</i>	<i>d.b</i>	<i>m.f.b</i>	<i>d.b</i>	<i>m.f.b</i>	<i>d.b</i>	<i>m.f.b</i>	<i>d.b</i>
<b>Proximate analysis</b>												
<b>Inherent moisture</b>	0.0	4.5	0.0	1.9	0.0	2.0	0.0	2.5	0.0	2.7	0.0	3.5
<b>Ash</b>	14.2	13.6	15.1	14.8	16.3	16.0	16.6	16.2	18.3	17.8	20.3	19.6
<b>Volatile matter</b>	28.3	27.1	24.1	23.7	17.3	16.9	12.2	11.9	8.9	8.7	2.4	2.3
<b>Fixed carbon</b>	57.4	54.8	60.8	59.6	66.4	65.1	71.2	69.4	72.8	70.8	77.3	74.6
	<u>100</u>	<u>100</u>	<u>100</u>	<u>100</u>	<u>100</u>	<u>100</u>	<u>100</u>	<u>100</u>	<u>100</u>	<u>100</u>	<u>100</u>	<u>100</u>
<b>Ultimate analysis</b>	<i>m.f.b</i>	<i>d.b</i>	<i>m.f.b</i>	<i>d.b</i>	<i>m.f.b</i>	<i>d.b</i>	<i>m.f.b</i>	<i>d.b</i>	<i>m.f.b</i>	<i>d.b</i>	<i>m.f.b</i>	<i>d.b</i>
<b>Sulfur</b>	0.8	0.7	0.8	0.7	0.8	0.6	0.7	0.6	0.7	0.6	0.8	0.6
<b>Carbon</b>	79.4	65.1	81.8	68.1	84.3	69.1	87.2	71.0	90.7	72.2	96.7	74.4
<b>Hydrogen</b>	4.2	3.5	3.9	3.3	3.3	2.7	2.6	2.1	1.9	1.5	0.2	0.1
<b>Nitrogen</b>	2.2	1.8	2.4	2.0	2.5	2.0	2.5	2.0	2.6	2.1	2.1	1.6
<b>Oxygen</b>	13.2	10.8	11.1	9.2	9.1	7.4	6.9	5.7	4.1	3.3	0.2	0.1
	<u>100</u>	<u>81.9</u>	<u>100</u>	<u>83.2</u>	<u>100</u>	<u>81.9</u>	<u>100</u>	<u>81.4</u>	<u>100</u>	<u>79.6</u>	<u>100</u>	<u>76.9</u>
<b>Atomic O/C ratio</b>	0.13		0.10		0.08		0.06		0.03		0.00	
<b>Atomic H/C ratio</b>	0.64		0.57		0.47		0.36		0.24		0.02	

A significant decrease in the volatile matter content can be observed between the samples TWD 2 (20% mass loss) and TWD 3 (40% mass loss), and between TWD 5 (80% mass loss) and TWD 6 (100% mass loss). The temperatures correlating to these significant changes are from 433°C to 468°C and 657°C to 900°C, respectively.



A significant increase of the fixed carbon content could be observed at similar stages during pyrolysis as a result of this evolution of the volatile matter. During pyrolysis under the specified conditions, a substantial decrease could be observed in the oxygen content from the raw coal up to the char at 900°C, as expected. Between TWD 2 (20% mass loss) and TWD 3 (40% mass loss), and again from TWD 5 (80% mass loss) to TWD 6 (100% mass loss), the hydrogen content, decreased significantly due to the loss of moisture and the aliphatic hydrogen as expected. This corroborates with the decrease in the volatile matter content as determined by the proximate analysis. An increase in the carbon content can be observed at similar stages as the decrease in hydrogen content. This increase in carbon is expected due to the release of volatile matter.

For the TWD coal sample the atomic O/C ratio decreased to  $\pm 0.01$  at a relatively constant rate with an increase in pyrolysis temperature. However, the atomic H/C ratio decreased to  $\pm 0.02$  at a significantly faster rate, especially from TWD 5 (80% mass loss) to TWD 6 (100% mass loss). This is due to reactions of the carbonaceous material which is present at temperatures higher than  $\pm 600^\circ\text{C}$ . Hambly [1998] obtained results where the H/C ratios of the coal samples also decreased with an increase in temperature. This decrease was related to the increase in aromaticity. The H/C ratios against the O/C ratios are presented in Appendix A.

The results from the conventional analyses of the GG coal and coal-derived char samples are reported in Table 5.3 on a moisture-free as well as on an air-dried basis. As expected, a decrease in the volatile matter content can be observed. As a result of the decrease in volatile matter content, the fixed carbon, determined by difference, increased with an increase in temperature. The volatile matter evolved at a constant rate, with an increase in the evolution rate between the GG 2 (20% mass loss) and GG 3 (40% mass loss) samples, thus from 424°C to 450°C. This increase in the rate of evolution can be attributed to the metaplast occurring at  $\pm 430^\circ\text{C}$  [Serio *et al.*, 1987].

From the ultimate analysis results it can be observed that the hydrogen and oxygen contents decreased significantly, as expected. Yu *et al.* [2007] reported that, during stage I of pyrolysis, i.e. the primary pyrolysis stage, a decrease in hydrogen bonding occurs with an increase in temperature. This was also reported in literature where the pyrolysis process was divided into nine reaction steps [Serio *et al.*, 1987; Solomon *et al.*, 1988; Yu *et al.*, 2007]. The major decrease was between the GG 5 (80% mass loss) and GG 6 (100% mass loss) samples, thus at temperatures above  $\pm 570^\circ\text{C}$ . The carbon content increased with the increase in temperature, and a significant increase can be observed from GG 5 to GG 6.

Table 5.3: Conventional analysis results of Grootegeluk samples

	GG 1		GG 2		GG 3		GG 4		GG 5		GG 6	
	raw coal		20% mass loss		40% mass loss		60% mass loss		80% mass loss		100% mass loss	
<i>Proximate analysis</i>	<i>m.f.b</i>	<i>d.b</i>	<i>m.f.b</i>	<i>d.b</i>	<i>m.f.b</i>	<i>d.b</i>	<i>m.f.b</i>	<i>d.b</i>	<i>m.f.b</i>	<i>d.b</i>	<i>m.f.b</i>	<i>d.b</i>
<b>Inherent moisture</b>	0.0	2.9	0.0	0.8	0.0	1.2	0.0	2.1	0.0	2.5	0.0	2.9
<b>Ash</b>	8.0	7.8	8.0	7.9	9.4	9.3	9.9	9.7	10.2	9.9	11.7	11.3
<b>Volatile matter</b>	36.9	35.8	32.9	32.6	21.9	21.6	16.0	15.6	9.6	9.3	1.6	1.5
<b>Fixed carbon</b>	55.1	53.5	59.2	58.7	68.7	68.0	74.2	72.6	80.3	78.3	86.8	84.3
	<u>100</u>	<u>100</u>	<u>100</u>	<u>100</u>	<u>100</u>	<u>100</u>	<u>100</u>	<u>100</u>	<u>100</u>	<u>100</u>	<u>100</u>	<u>100</u>
<i>Ultimate analysis</i>	<i>m.f.b</i>	<i>d.b</i>	<i>m.f.b</i>	<i>d.b</i>	<i>m.f.b</i>	<i>d.b</i>	<i>m.f.b</i>	<i>d.b</i>	<i>m.f.b</i>	<i>d.b</i>	<i>m.f.b</i>	<i>d.b</i>
<b>Sulfur</b>	1.1	1.0	1.1	1.0	1.0	0.9	1.0	0.9	0.9	0.8	0.9	0.8
<b>Carbon</b>	82.0	73.3	81.5	74.4	84.5	75.7	86.6	76.5	89.1	78.1	95.7	82.1
<b>Hydrogen</b>	5.3	4.8	5.1	4.6	4.3	3.9	3.6	3.2	2.6	2.3	0.2	0.2
<b>Nitrogen</b>	1.8	1.6	1.8	1.7	2.1	1.9	2.1	1.9	2.2	1.9	1.8	1.6
<b>Oxygen</b>	9.7	8.7	10.4	9.5	8.0	7.2	6.6	5.8	5.2	4.5	1.3	1.1
	<u>100</u>	<u>89.4</u>	<u>100</u>	<u>91.3</u>	<u>100</u>	<u>89.5</u>	<u>100</u>	<u>88.3</u>	<u>100</u>	<u>87.6</u>	<u>100</u>	<u>85.7</u>
<b>Atomic O/C ratio</b>	0.09		0.1		0.07		0.06		0.04		0.01	
<b>Atomic H/C ratio</b>	0.77		0.74		0.61		0.5		0.35		0.03	

During pyrolysis under the set conditions, the O/C and H/C atomic ratios decreased as expected. The H/C atomic ratio decreased significantly between GG 5 (80% mass loss) and GG 6 (100% mass loss). Hambly [1998] observed a decrease in the H/C ratios, accompanied by the increase in aromaticity with an increase in temperature.

The characterization results from the conventional analyses of the TSH coal sample are reported in Table 5.4.

When observing the proximate analysis results for the TSH coal and coal-derived char samples, the fixed carbon content increased during pyrolysis as expected. The volatile matter content decreased with a significant rate up to the TSH 3 (40% mass loss) sample, and then evolved at a slower rate from TSH 3 to TSH 5 (80% mass loss). The decrease in volatile matter content occurred at a substantially faster rate from the TSH 5 to TSH 6 samples at 900°C. Similar results were reported in literature where the changes in the coal with heat treatment can be observed after the formation of the metaplast. The temperature of maximum fluidity for the TSH coal is at 467°C (between 20 and 40% mass loss), thus explaining the release of volatile matter up to 40% mass loss and the decrease in the evolution rate from 40 to 80% mass loss. The increase in the rate of evolution from the 80 to 100% mass loss can be ascribed to the evolution of secondary gases during secondary pyrolysis [Serio *et al.*, 1987; Yu *et al.*, 2004].

From the ultimate analysis results, a significant decrease in the hydrogen content occurred from TSH 5 (80% mass loss) to TSH 6 (100% mass loss), i.e., from 610°C up to 900°C. This decrease could be related to the secondary reactions occurring during secondary pyrolysis occurring from  $\pm 550^\circ\text{C}$  [Serio *et al.* 1987, Yu *et al.*, 2004]. The carbon content remained constant up to TSH 3 (40% mass loss), after which it increased to 96.5 wt.% (m.f.b.). Zubkova [2005] reported that the carbon layers coalesce with the carbon crystallites during the re-solidification of the metaplast. For the TSH coal the re-solidification occurred at 508°C, thus from 60% mass loss, explaining the increase in the carbon content. A small increase in the oxygen content could be observed initially, however at TSH 3 the oxygen content decreased substantially to 0.3 wt.% (m.f.b.).

Table 5.4: Conventional analysis of Tshikondeni samples.

	TSH 1		TSH 2		TSH 3		TSH 4		TSH 5		TSH 6	
	raw coal		20% mass loss		40% mass loss		60% mass loss		80% mass loss		100% mass loss	
<i>Proximate analysis</i>	<i>m.f.b</i>	<i>d.b</i>	<i>m.f.b</i>	<i>d.b</i>	<i>m.f.b</i>	<i>d.b</i>	<i>m.f.b</i>	<i>d.b</i>	<i>m.f.b</i>	<i>d.b</i>	<i>m.f.b</i>	<i>d.b</i>
<b>Inherent moisture</b>	0.0	0.7	0.0	0.6	0.0	0.5	0.0	0.8	0.0	1.7	0.0	2.4
<b>Ash</b>	15.0	14.9	16.7	16.6	16.8	16.7	17.1	17.0	18.3	18.0	19.1	18.7
<b>Volatile matter</b>	21.5	21.4	17.9	17.8	13.6	13.5	10.7	10.6	7.3	7.2	1.4	1.4
<b>Fixed carbon</b>	63.5	63.0	65.4	65.0	69.6	69.3	72.2	71.6	74.4	73.1	79.4	77.5
	<u>100</u>	<u>100</u>	<u>100</u>	<u>100</u>	<u>100</u>	<u>100</u>	<u>100</u>	<u>100</u>	<u>100</u>	<u>100</u>	<u>100</u>	<u>100</u>
<i>Ultimate analysis</i>	<i>m.f.b</i>	<i>d.b</i>	<i>m.f.b</i>	<i>d.b</i>	<i>m.f.b</i>	<i>d.b</i>	<i>m.f.b</i>	<i>d.b</i>	<i>m.f.b</i>	<i>d.b</i>	<i>m.f.b</i>	<i>d.b</i>
<b>Sulfur</b>	0.8	0.7	0.8	0.7	0.8	0.6	0.8	0.7	0.8	0.6	0.8	0.6
<b>Carbon</b>	89.7	75.8	89.9	74.4	89.6	74.2	90.9	74.8	92.3	74.1	96.5	76.1
<b>Hydrogen</b>	5.1	4.3	4.6	3.8	4.3	3.6	4.3	3.5	3.3	2.6	0.4	0.3
<b>Nitrogen</b>	2.1	1.8	2.2	1.8	2.2	1.8	2.2	1.8	2.3	1.9	2.1	1.6
<b>Oxygen</b>	2.3	1.9	2.5	2.1	3.0	2.5	1.8	1.4	1.4	1.1	0.3	0.2
	<u>100.0</u>	<u>84.4</u>	<u>100.0</u>	<u>82.8</u>	<u>100.0</u>	<u>82.7</u>	<u>100.0</u>	<u>82.2</u>	<u>100.0</u>	<u>80.3</u>	<u>100.0</u>	<u>78.9</u>
<b>Atomic O/C ratio</b>	0.02		0.02		0.03		0.01		0.01		0.00	
<b>Atomic H/C ratio</b>	0.67		0.61		0.58		0.56		0.42		0.04	

The O/C and H/C atomic ratios, as expected, decreased as the temperature increased. For the H/C ratio it could be observed that a significant decrease occurred from TSH 5 to TSH 6, which correlates to a decrease in the volatile matter content as determined by the proximate analysis. This decrease may be related to the depletion of the aliphatic hydrogen at the end of primary pyrolysis [Serio *et al.*, 1987].

The fixed carbon content (m.f.b.) determined by the proximate analysis and the percentage carbon determined from the ultimate analysis (m.f.b.) were compared, and can be observed in Figures 5.1 to 5.3 for the respective coal samples investigated. The curves showing the carbon content present in the TWD coal samples converge just before the TWD 6 sample, thus at  $\pm 900^{\circ}\text{C}$ . For the GG coal samples, the curves converge at the GG 5 sample, i.e. at  $\pm 570^{\circ}\text{C}$ , while the curves in Figure 5.3 for the TSH coal, (the high caking coal), converge between TSH 5 and TSH 6, thus at temperatures between  $610^{\circ}\text{C}$  and  $900^{\circ}\text{C}$ . These graphs converge at different temperatures, which correlate to the depletion of carbon associated with the volatile matter.

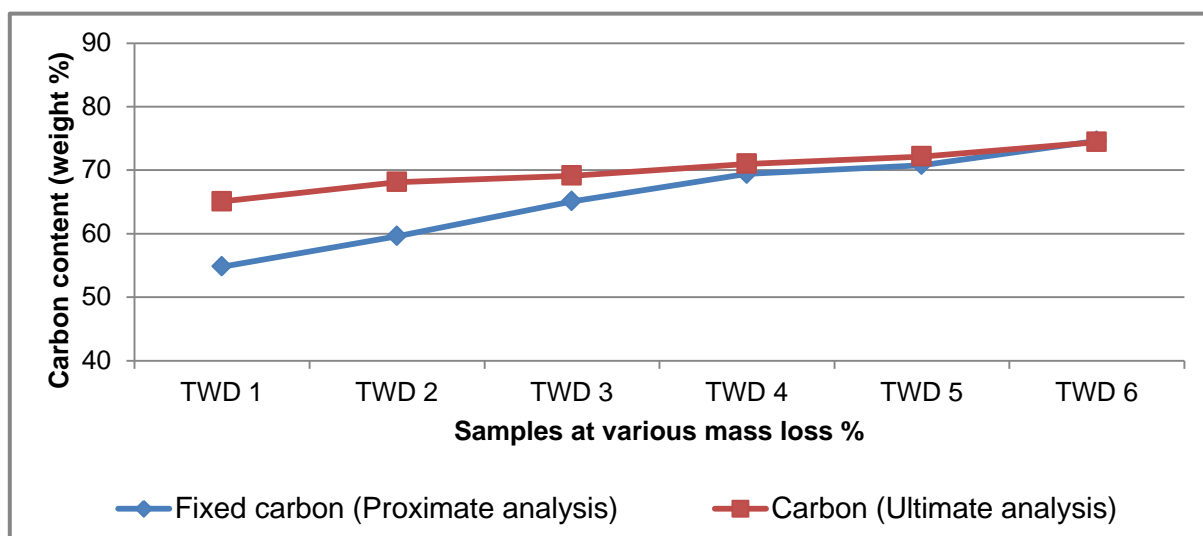


Figure 5.1: Carbon contents for Highveld (m.f.b.).

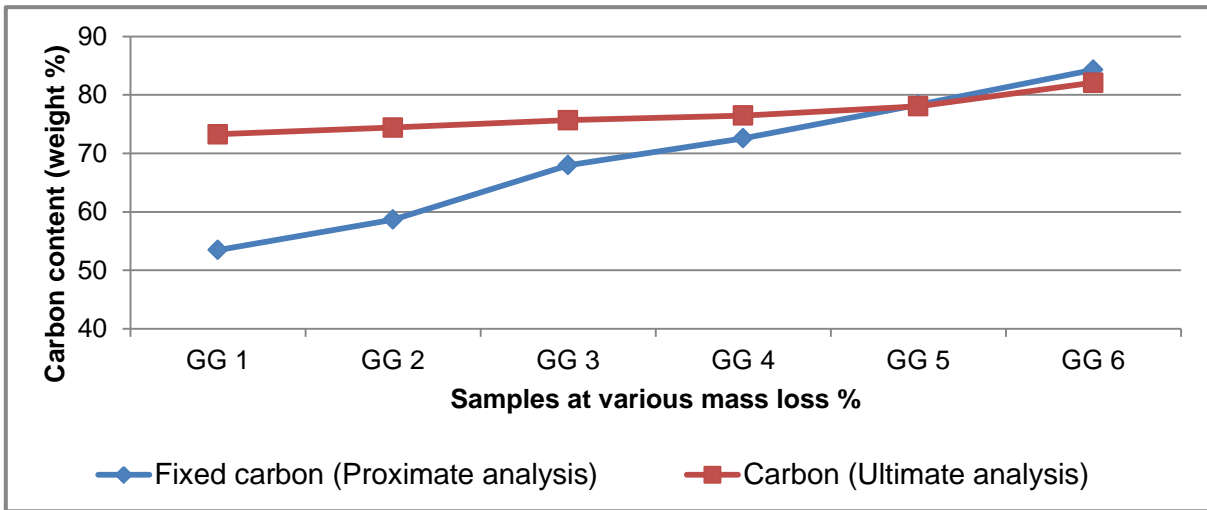


Figure 5.2: Carbon contents for Grootegeluk (m.f.b.).

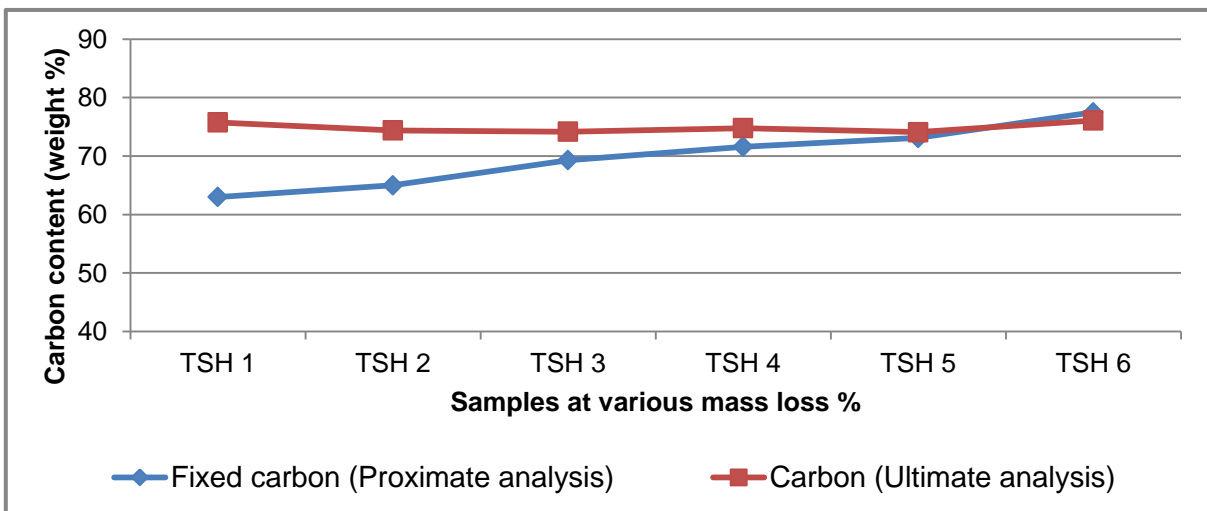


Figure 5.3: Carbon contents for Tshikondeni (m.f.b.).

Wang *et al.* (2010) and Oboirien *et al.* (2011) reported the aromaticity factor for coal samples by using the results obtained from the proximate and ultimate analyses (Eq. (1)).

$$f_a = \frac{1200 \times (100 - V_{db})}{1240 \times C_{db}} \quad (1)$$

The aromaticity factor is represented by  $f_a$ ,  $V_{db}$  is the volatile matter on a dry basis and the  $C_{db}$  is the carbon content on a dry basis as determined by the ultimate analysis.

**Table 5.5: Aromaticity factors of the coal and coal-derived char samples.**

Samples	Raw coal	20 %	40%	60%	80%	100%
		mass loss	mass loss	mass loss	mass loss	mass loss
<b>TWD</b>	1.08	1.08	1.16	1.20	1.22	1.27
<b>GG</b>	0.85	0.88	1.00	1.07	1.12	1.16
<b>TSH</b>	1.00	1.07	1.13	1.16	1.21	1.25

The aromaticity factors are reported in Table 5.5 and are shown in Figure 5.4. These results include the aromaticity of the raw coal samples, as well as at the various decomposition stages of the samples. The highest aromaticity was observed for the TWD coal sample, while the GG coal had the lowest aromaticity. As expected, an increase in the aromaticity could be observed for all three coal samples with an increase in temperature up to 900°C. The TWD coal sample revealed a substantial increase in aromaticity from the TWD 2 sample (20% mass loss) to the TWD 3 sample (40% mass loss), whereafter the aromaticity increased with a constant rate up to the TWD 6 sample at 100% mass loss. The lowest aromaticity was observed for the GG coal sample, and a substantial increase in the aromaticity was observed from the GG 2 sample (20% mass loss) to the GG 3 sample (40% mass loss). A continuous increase in the aromaticity was observed from the GG 3 sample to the GG 6 sample (100% mass loss). A significant increase was observed for the aromaticity of the TSH coal sample up to the TSH 3 sample (40% mass loss) and thereafter the aromaticity increased with a constant rate. An increase in aromaticity during heat treatment is also reported in literature [Oboirien *et al.* 2011, Wang *et al.*, 2010].

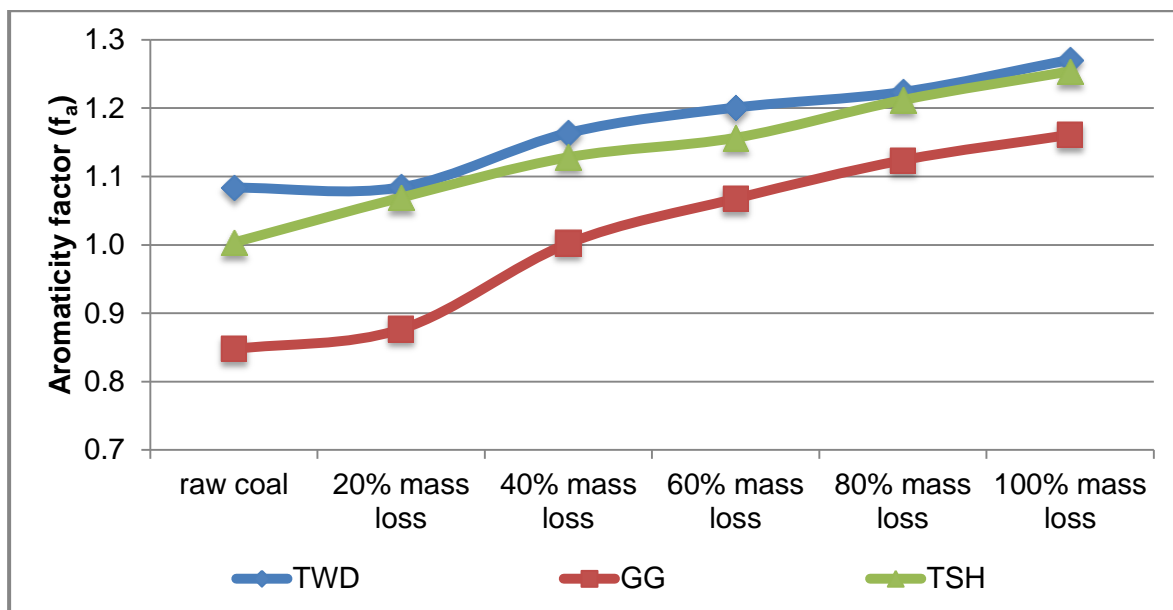


Figure 5.4: Aromaticity factors for the three coal samples.

Petrographic analyses were conducted by Coetzee *et al.* [2014] on these three South African coal samples. The vitrinite content (vol.%, m.m.f.b.) of the TWD coal was 59% and the inertinite content (vol.%, m.m.f.b.) was 37%. GG coal contained 86% vitrinite and 8% inertinite, while TSH consisted of 82% vitrinite and 18% inertinite. Thus the conclusion can be drawn that these samples are all three vitrinite-rich coals. According to Oboirien *et al.* [2010], the proportions of the vitrinite and inertinite macerals within the coal sample contribute to the changes occurring in the carbon structure. Higher vitrinite content may lead to chars with higher graphitised order carbon structures, while inertinite-rich coals will transform to structurally disordered chars.

The coal samples are classified by Coetzee *et al.* [2014] as follows; the TWD as well as the GG coal samples are classified as bituminous, medium rank C coals, while the TSH coal sample is classified as a bituminous, medium rank B coal.

- **5.2 Thermogravimetric and mass spectrometric analyses (TG-MS) results.**

Thermogravimetric experiments were used to determine the different temperatures relating to specific percentages of mass loss using set conditions as discussed in Chapter 4.4. The mass loss profiles for the three raw coal samples are presented in Figure 5.5. Repeatability was ensured by repeating the TG runs at least three times to calculate the average curves for use in further analysis. These profiles can be observed in Appendix B.



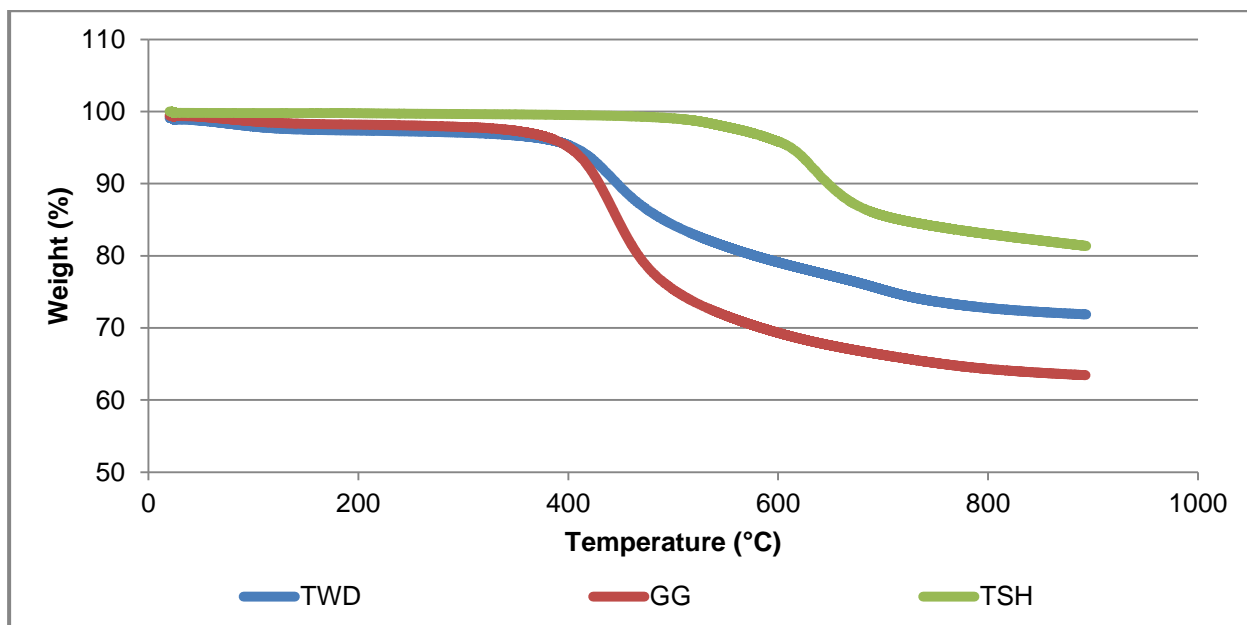


**Figure 5.5:** Thermogravimetric weight loss curves for the raw coal samples during pyrolysis.

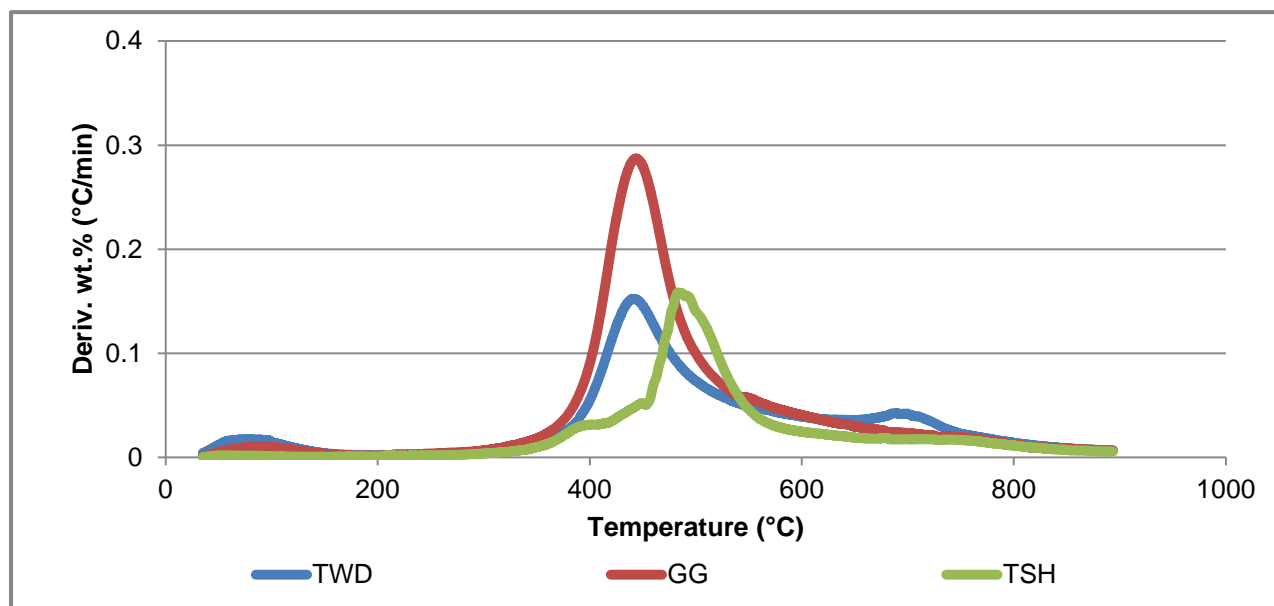
Noticeable mass loss ( $\pm 3\%$ ) occurred for the TWD and GG samples below  $350^\circ\text{C}$ . The mass loss was due to the loss of moisture as also indicated by the proximate analysis (Table 5.1). TSH contained only 0.7 wt.% moisture and no significant mass loss was observed for this sample below  $350^\circ\text{C}$ .

The decomposition process for the TWD and GG coals started at a similar temperature of  $\pm 380^\circ\text{C}$ . A significant increase in the rate of mass loss for the GG coal could be observed between  $400^\circ\text{C}$  and  $500^\circ\text{C}$ , this sample also had the highest weight loss percentage of 36% after heat treatment up to  $900^\circ\text{C}$ . The TWD coal reacted at a more constant rate and revealed a weight loss of 28% after the pyrolysis process. The TSH coal started to react at a much higher temperature of approximately  $500^\circ\text{C}$ , with an increase in the rate of mass loss between  $580^\circ\text{C}$  and  $670^\circ\text{C}$ . After pyrolysis (at  $900^\circ\text{C}$ ), only a 20% weight loss was observed for TSH. The GG coal sample contained the most volatile matter and therefore showed the highest weight loss percentage, whereas the TSH coal sample had the lowest weight loss percentage and also consisted of the lowest amount of volatile matter. These weight loss percentages relate to the amount of volatile matter determined by proximate analysis (see tables 5.1 to 5.4).

Characteristic properties could be derived from the DTG curves presented in Figure 5.6.  $T_{\max}$  represents the temperature where the maximum rate of mass loss occurred, and  $T_i$  is the initial temperature of thermal decomposition. These parameters are presented in Table 5.5.

**Table 5.6: Parameters from DTG curves.**

	TWD	GG	TSH
$T_{max}$	440°C	440°C	480°C
$T_i$	280°C	260°C	310°C

**Figure 5.6: DTG curves of the three raw coal samples.**

When investigating the DTG curves, small peaks can be observed for the TWD and GG coals at approximately 100°C, and these are due to the loss of moisture. Initial mass loss for the TWD coal occurred at  $\pm 280^\circ\text{C}$  and another peak can be observed at  $\pm 680^\circ\text{C}$ . The temperature where maximum rate of mass loss occurred is at 440°C for both the TWD and the GG samples. The GG coal reacted at the lowest temperature of 260°C, as can be observed from the TG curves as well. When observing the DTG curve for the TSH coal, the maximum rate of initial mass loss occurred at 310°C, and the maximum rate of the second step of mass loss occurred at 480°C. It is also important to notice the small shoulder peaks at  $\pm 390^\circ\text{C}$  and  $\pm 450^\circ\text{C}$  for the TSH coal. These shoulder peaks correlate to the softening and maximum fluidity temperatures of the TSH coal and are an indication of the metaplast phase occurring with an increase in temperature.

The distinctive DTG peaks between 400°C and 600°C for all three coal samples can be explained by primary pyrolysis, as discussed in Chapter 2.4.2. De-polymerization reactions dominate the main pyrolysis zone, i.e. the primary pyrolysis, and lead to the breaking of aliphatic bridges between the macromolecular networks. As a result, the functional groups are decomposed causing the formation of gases and tars. Condensable tars and light hydrocarbons are evolved from coal samples at approximately 500°C [Serio *et al.*, 1987; Cai *et al.*, 2008].

- **5.3 Mass Spectrometry (MS) results**

TG-MS analyses were done on the three raw coal samples in order to investigate the temperature ranges of the evolved gaseous species. The MS records the mass-to-charge ratio ( $m/z$ ) corresponding to the volatile matter evolved at specific temperatures. Only qualitative analyses were done on the three raw coal samples. Chapter 4.4 provides a detailed description of the TG-MS connection.

The evolution profiles of the major gaseous compounds are presented in Figures 5.7 to 5.9. The remaining profiles are given in Appendix C.

### **H<sub>2</sub> evolution**

The temperature ranges of evolution of H<sub>2</sub> were determined by observing the H<sub>2</sub><sup>+</sup> mass spectroscopic peaks ( $m/z = 2$ ). The MS profiles for the three raw coal samples are presented in Figure 5.7. The top graph represents the TWD coal, in the middle is the graph for the GG coal sample and the TSH coal is represented by the bottom graph. These profiles are used to determine the temperature where maximum rate of H<sub>2</sub> evolution occurred in the samples. As expected, the profiles presented similar peak maximum values, as well as shapes, with the maximum rate of H<sub>2</sub> evolution occurring at approximately 720°C. The degradation reactions responsible for the evolution of H<sub>2</sub> were similar for the TWD, GG and TSH coal samples. Sources of H<sub>2</sub> evolution are related to the decomposition of functional groups present in the coal samples. According to Yu *et al.* [2007], H<sub>2</sub> present during pyrolysis causes an increase in the tar yield as well as in the fluidity of coal. Therefore, changes in the char's morphology may occur because of the strong relation between the evolution of volatile matter, thermoplastic properties and the char structure.

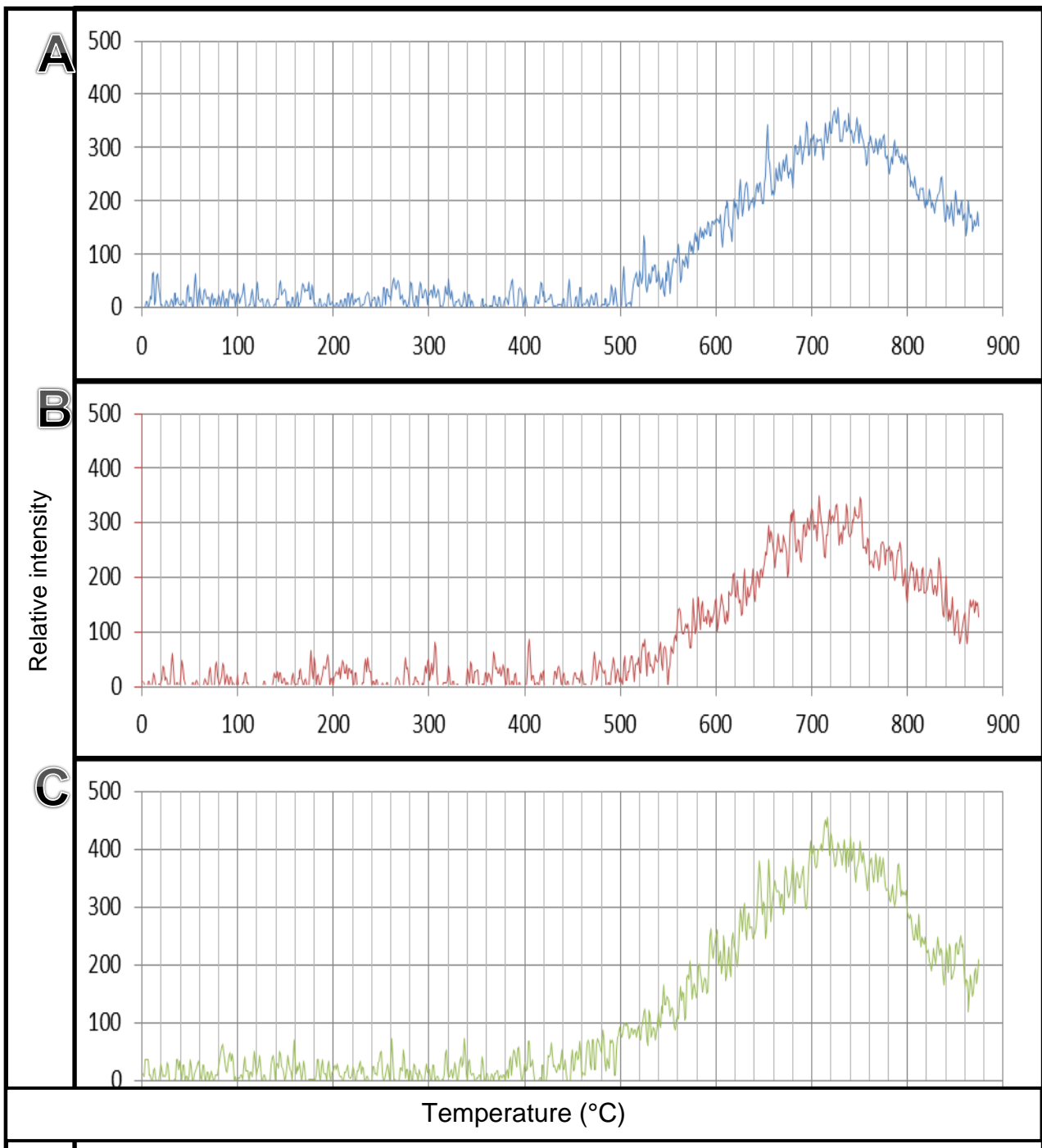
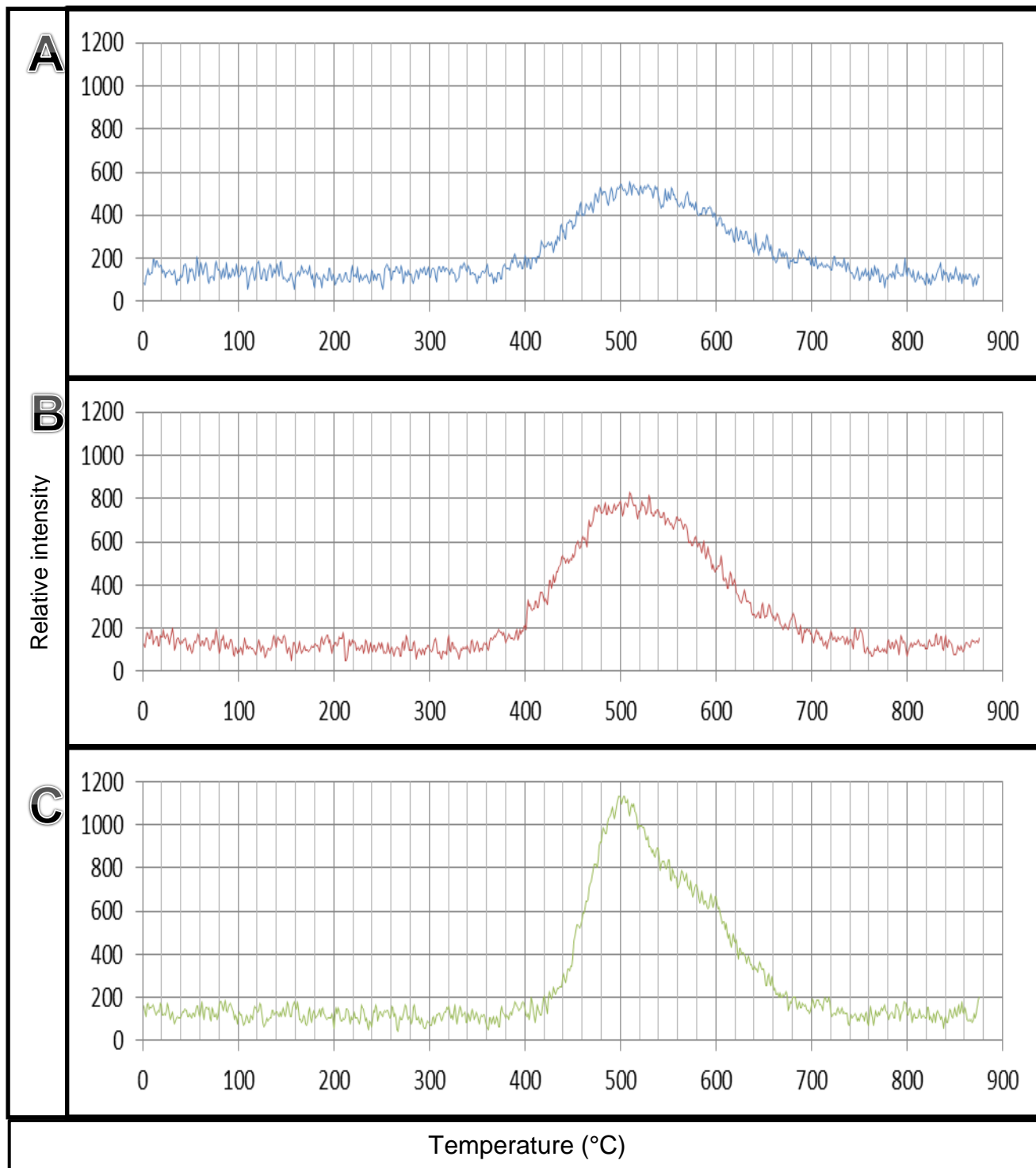


Figure 5.7: Mass spectra of H<sub>2</sub> (m/z = 2) evolution for (A) TWD, (B) GG and (C) TSH coal.

### CH<sub>4</sub> evolution

Figure 5.8 presents the profiles for the evolution of CH<sub>3</sub><sup>+</sup>, measured at an m/z of 15. When determining the evolution of methane (CH<sub>4</sub>) at an m/z of 16, interference from oxygen (m/z = 16) may occur, thus the CH<sub>4</sub> evolution was represented by the CH<sub>3</sub><sup>+</sup> fragment.

For the TWD sample (Figure 5.8 (A)), the evolution of methane started just below 400°C and reached a maximum at ± 520°C. The onset of evolution for the GG coal (Figure 5.8 (B)) occurred at a similar temperature than for the TWD coal with a maximum evolution occurring at ± 520°C. The intensity of the CH<sub>4</sub> peak was, however, much higher for the GG coal than for the TWD coal. CH<sub>4</sub> evolution in the TSH coal (presented in Figure 5.8 (C)) started at a higher temperature of ± 420°C and reached a maximum at approximately 500°C. The TSH coal had the highest intensity of methane evolution under the similar experimental conditions. The presence of CH<sub>4</sub> is due to the decomposition of functional groups which may cause re-polymerization. It is evident from these results that caking coals experience more reactions during the secondary pyrolysis stage than the non-caking coal. According to Serio *et al.* [1987], the evolution of functional groups will cause re-polymerisation and lead to the formation of CH<sub>4</sub>, where a methyl group is released through substitution reactions.



**Figure 5.8:** Mass spectra of  $\text{CH}_3^+$  ( $m/z = 15$ ) evolution for (A) TWD, (B) GG and (C) TSH coal.

## H<sub>2</sub>O evolution

The H<sub>2</sub>O evolution from the raw coal samples during pyrolysis are presented in Figure 5.9. Initial release of H<sub>2</sub>O could be observed for all three coals below 100°C, with the highest intensity occurring for the GG coal sample, and substantially less evolution of H<sub>2</sub>O observed in the TSH sample. This could also be observed in the DTG curves (Figure 5.6). Another peak maximum could be observed for the TWD coal (A) at ± 480°C, with the onset of the evolution occurring at ± 340°C. The evolution of H<sub>2</sub>O for the GG coal started at approximately 360°C, with a maximum rate occurring between 440°C and 500°C. H<sub>2</sub>O evolution in the TSH sample was detected at a higher onset temperature of ± 440°C and a maximum rate was observed at ± 510°C. The degradation of H<sub>2</sub>O occurred due to condensation reactions; and although only semi-quantitative, the highest intensity of evolution was observed for the TWD coal, followed by the GG coal, and was substantially less for the TSH coal. This evolution correlates with the amount of oxygen content present in the coal samples (as determined by ultimate analysis, Table 5.1). The TWD coal sample contained 13.2 wt.% (m.f.b.) oxygen, while the GG coal sample contained 9.7 wt.% (m.f.b.) oxygen, and the TSH coal sample had the lowest amount of oxygen, at a value of only 2.3 wt.% (m.f.b.). The main cause for this H<sub>2</sub>O release is due to the liberation of lattice water.

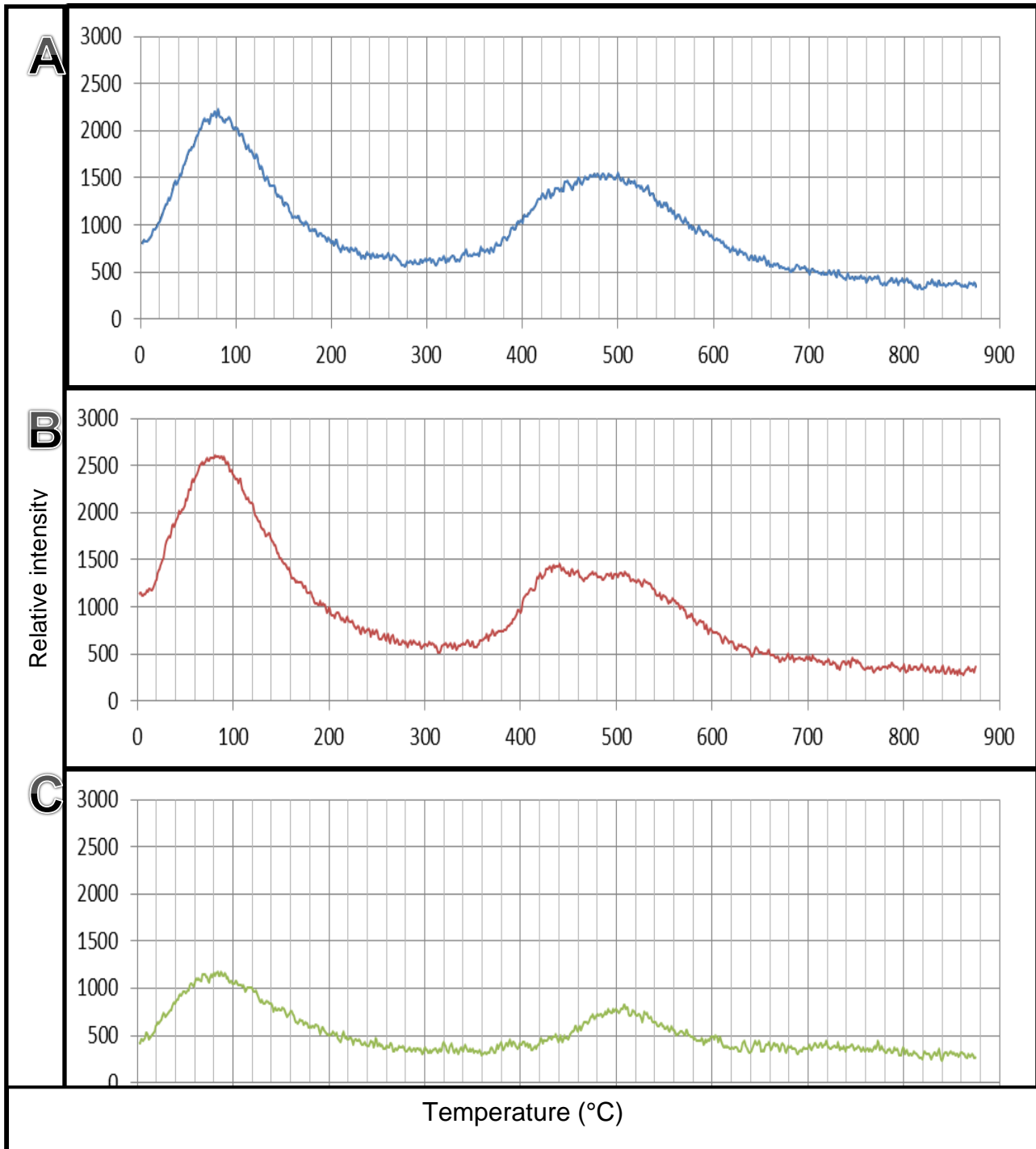


Figure 5.9: Mass spectra of  $\text{H}_2\text{O}$  ( $m/z = 18$ ) evolution for the three coal samples.



- **5.4 X-Ray Fluorescence (XRF) results**

The 18 coal-derived char samples were submitted for XRF analysis and the results obtained are presented in Table 5.7. The experimental conditions for the XRF analysis are discussed in Chapter 4.6.2.

The results from the XRF analysis revealed that the three raw coal ash samples mainly consisted of Al which is reported as aluminium oxide ( $\text{Al}_2\text{O}_3$ ) and Si which is reported as silica oxide ( $\text{SiO}_2$ ). The TSH and GG coal samples showed elevated levels of Si, while TWD coal contained substantially less Si. The Al levels were between 20% and 30% for the three raw coal samples.

When the results were compared for each individual sample heated up to  $900^\circ\text{C}$ , no significant changes in the elemental composition of the major and minor elements were observed due to the thermal stability of the mineral matter elements. Although the results are reported as oxides, they are representative of the elemental composition of the ash, which consists of aluminosilicates [Xianglin *et al.* 1999].

Table 5.7: XRF analysis results for the coal samples.

	TWD 1	TWD 2	TWD 3	TWD 4	TWD 5	TWD 6	GG 1	GG 2	GG 3	GG 4	GG 5	GG 6	TSH 1	TSH 2	TSH 3	TSH 4	TSH 5	TSH 6
<b>Al<sub>2</sub>O<sub>3</sub></b>	28.03	28.09	29.17	28.91	29.19	28.27	20.27	20.01	20.59	20.33	29.19	20.31	26.02	26.19	26.30	26.39	29.19	26.23
<b>CaO</b>	10.84	10.48	10.83	10.74	10.69	10.32	1.78	1.72	1.68	1.48	1.45	1.52	2.79	2.71	2.73	2.73	2.66	2.64
<b>Cr<sub>2</sub>O<sub>3</sub></b>	0.07	0.07	0.03	0.03	0.06	0.14	0.13	0.07	0.13	0.12	0.12	0.40	0.01	0.01	0.00	0.01	0.02	0.20
<b>Fe<sub>2</sub>O<sub>3</sub></b>	3.71	3.51	3.52	3.43	3.54	3.73	7.39	7.18	6.99	6.81	6.55	7.80	4.10	3.90	3.93	3.93	3.77	4.60
<b>K<sub>2</sub>O</b>	0.59	0.59	0.60	0.60	0.60	0.59	0.97	1.01	0.97	1.01	1.00	0.96	1.56	1.58	1.56	1.56	1.57	1.58
<b>MgO</b>	3.46	3.35	3.49	3.45	3.41	3.31	0.78	0.66	0.72	0.69	0.69	0.70	1.24	1.22	1.25	1.24	1.25	1.22
<b>MnO</b>	0.13	0.13	0.13	0.13	0.12	0.13	0.11	0.17	0.10	0.09	0.09	0.10	0.04	0.04	0.04	0.04	0.04	0.04
<b>Na<sub>2</sub>O</b>	0.55	0.54	0.56	0.59	0.55	0.56	0.12	0.30	0.20	0.16	0.11	0.13	0.33	0.34	0.33	0.33	0.34	0.34
<b>P<sub>2</sub>O<sub>5</sub></b>	1.81	1.79	1.86	1.84	1.85	1.81	0.16	0.15	0.20	0.15	0.15	0.18	0.60	0.63	0.59	0.60	0.59	0.59
<b>SiO<sub>2</sub></b>	42.18	41.48	42.92	42.60	43.11	41.88	63.52	63.16	63.60	64.82	64.53	63.13	58.38	58.47	59.02	58.78	59.75	58.64
<b>TiO<sub>2</sub></b>	1.48	1.45	1.50	1.51	1.50	1.46	3.19	3.18	3.16	3.21	3.20	3.23	1.26	1.22	1.22	1.24	1.21	1.22

Chapter 5: Results and discussion

	TWD 1	TWD 2	TWD 3	TWD 4	TWD 5	TWD 6	GG 1	GG 2	GG 3	GG 4	GG 5	GG 6	TSH 1	TSH 2	TSH 3	TSH 4	TSH 5	TSH 6	
<b>V<sub>2</sub>O<sub>5</sub></b>	0.04	0.04	0.04	0.03	0.04	0.04	0.30	0.31	0.30	0.31	0.32	0.31	0.03	0.03	0.03	0.03	0.03	0.03	0.03
<b>ZrO<sub>2</sub></b>	0.08	0.08	0.09	0.08	0.09	0.08	0.37	0.34	0.37	0.37	0.37	0.37	0.08	0.07	0.07	0.07	0.08	0.08	0.08
<b>Ba</b>	0.36	0.34	0.37	0.36	0.37	0.36	0.10	0.10	0.10	0.10	0.10	0.09	0.25	0.24	0.24	0.24	0.24	0.24	0.24
<b>Sr</b>	0.72	0.68	0.73	0.72	0.73	0.70	0.06	0.06	0.06	0.06	0.06	0.06	0.15	0.14	0.14	0.15	0.14	0.14	0.14
<b>SO<sub>3</sub></b>	5.93	7.38	4.18	4.98	4.14	6.62	0.75	1.58	0.84	0.29	0.86	0.72	3.16	3.21	2.53	2.66	1.88	1.88	2.00

---

- **5.5 X-Ray Diffraction (XRD) results**

The XRD results obtained for the raw coal and the coal-derived char samples are presented in Table 5.8. The crystalline phases present in the sample were determined by the XRD analyses, i.e. for the raw coal samples and the char samples prepared at different temperatures (up to 900°C) relating to the different mass loss percentages. The experimental conditions are explained in Section 4.5.2.

Kaolinite is present as the main clay mineral in most coal resources [Yu *et al.*, 2007; Nel, 2010]. Nel [2010] concluded that the transformation of kaolinite during heat treatment occurs in three main steps: (1) from 100 to 120°C absorbed water is released, (2) endothermic dehydroxylation occurs from 400 to 600°C, which results in the release of lattice water, (3) the metaplast can undergo exothermic transformation from 950°C and above. The decrease in kaolinite, observed for all three coal samples, could have been expected, since kaolinite is more reactive than quartz at temperatures below 800°C.

Mineral matter of coal mainly consists of quartz [Yu *et al.*, [2007]. Quartz undergoes transformation from low quartz to high quartz during pyrolysis, i.e. at temperatures of  $\pm 570^\circ\text{C}$ . The melting point of quartz is 1600°C, making it a thermally stable component. The quartz reacts with other minerals and forms the aluminosilicates present in the coal ash [Salmang, 1961; Reifenstein *et al.*, 1999].

Pyrite can transform to different states of iron during heat treatment, resulting in different melting behaviours for the ash [Wu *et al.*, 2009]. Pyrite decomposes at relatively low temperatures, i.e. from 330 to 630°C, to form pyrrhotite.

Calcite is the main calcium-containing mineral in coal. The decomposition temperature of calcite is in the range of 600 to 950°C [Nel, 2010].

It could be observed that different crystalline phases were present in the three coal samples.  $\text{TiO}_2$  in the anatase phase was only present in the TWD raw coal sample, and as expected the rutile phase formed only at the TWD 3 coal-derived char sample (at 40% mass loss). For the TSH raw coal sample, the  $\text{TiO}_2$  crystalline phase was present as rutile and transformed to anatase at the TSH 2 coal-derived char sample (at 20% mass loss) [Heald and Weiss, 1972]. The presence of anatase in coking coals was reported by Sakurovs *et al.* [2007]. Calcite ( $\text{CaCO}_3$ ) was only present in the TSH sample, but in small amounts only. Siderite ( $\text{FeCO}_3$ ) was present in the GG and TSH raw coal samples, but not in the TWD raw coal sample. Siderite

decomposes from 400°C and CO<sub>2</sub> is formed as a result, thus explaining the decrease of siderite with an increase in temperature [Nel, 2010].

Closer investigation of the crystalline phases within the TWD raw coal and coal-derived char samples revealed that the crystalline phases partially decomposed with increasing temperature, with the exception of three crystalline compounds. A significant decrease in the content of kaolinite, as well as the contents of chlorite and pyrite could be observed in the TWD 3 coal-derived char sample (at 40% mass loss) while quartz transformed from low quartz to high quartz. The carbon content measured as graphite increased relatively to the other crystalline phases as the temperature increased up to 900°C. This increase in the graphite content occurred at a significant rate from the TWD 3 coal-derived char sample to the TWD 4 coal-derived char sample (representing 20 and 40% mass loss, respectively).

For the GG coal sample, similar trends were observed as for the TWD coal sample. Kaolinite content decreased substantially from the GG 4 coal-derived char sample (at 60% mass loss), with chlorite and pyrite contents also decreasing with an increase in temperature. The graphite content started to increase from the GG 3 coal-derived char sample (40% mass loss) to the GG 4 coal- char sample, while a significant increase was observed from the GG 4 to the GG 5 coal-derived char samples (representing 60 and 80% mass loss, respectively). This increase in the graphite content continued up to the GG 6 char sample, prepared at 900°C and representing 100% mass loss.

In the TSH 3 coal-derived char sample (at 40% mass loss), a significant decrease was observed for kaolinite content while the pyrite content increased. The remaining crystalline phases decreased from the raw coal sample to the TSH 6 char sample (at 900°C). The carbon content, measured as graphite, decreased initially from the TSH 1 sample (raw coal sample) to the TSH 2 coal-derived char sample (at 20% mass loss). However, an increase was observed in the graphite content from the TSH 2 coal-derived char sample to the TSH char sample (at 100% mass loss).

Table 5.8: XRD results for raw coal and coal-derived char samples.

		TWD 1	TWD 2	TWD 3	TWD 4	TWD 5	TWD 6
<b>Anatase</b>	TiO <sub>2</sub>	0.25	0.23	0.22	0.02	0.13	0.13
<b>Chlorite</b>	((Mg,Fe) <sub>5</sub> Al(AlSi <sub>3</sub> O <sub>10</sub> )(OH) <sub>8</sub> )	3.23	3.17	2.89	1.63	1.6	1.47
<b>Dolomite</b>	(CaMg)(CO <sub>3</sub> ) <sub>2</sub>	3.15	2.52	2.33	2.29	1.77	0.01
<b>Carbon content</b>	C	72.44	74.11	76.41	84.46	88.4	92.42
<b>Halite</b>	NaCl	-	-	-	-	0.05	0.6
<b>Kaolinite</b>	Al <sub>2</sub> Si <sub>2</sub> O <sub>5</sub> (OH) <sub>4</sub>	13.92	13.29	12.46	6.48	3.23	2.66
<b>Microcline</b>	KAlSi <sub>3</sub> O <sub>8</sub>	0.79	0.77	0.54	0.81	0.56	0.24
<b>Muscovite</b>	(KAl <sub>3</sub> Si <sub>3</sub> O <sub>10</sub> (OH) <sub>2</sub> )	0.58	0.79	0.34	0.12	0.44	0.15
<b>Plagioclase</b>	NaAlSi <sub>3</sub> O <sub>8</sub> – CaAl <sub>2</sub> Si <sub>2</sub> O <sub>8</sub>	0.59	0.41	0.3	0.46	0.48	0.58
<b>Pyrite</b>	FeS <sub>2</sub>	0.87	0.78	0.69	0.42	0.09	0.01
<b>Quartz</b>	SiO <sub>2</sub>	4.19	3.92	3.8	3.21	3.26	1.67
<b>Rutile</b>	TiO <sub>2</sub>	-	-	0.04	0.02	-	-
<b>Siderite</b>	FeCO <sub>3</sub>	-	-	-	0.07	-	0.06
		GG 1	GG 2	GG 3	GG 4	GG 5	GG 6
<b>Anatase</b>	TiO <sub>2</sub>	-	-	-	-	-	-
<b>Chlorite</b>	((Mg,Fe) <sub>5</sub> Al(AlSi <sub>3</sub> O <sub>10</sub> )(OH) <sub>8</sub> )	3.17	0.36	2.55	1.4	1.44	1.07
<b>Dolomite</b>	(CaMg)(CO <sub>3</sub> ) <sub>2</sub>	0.08	0.16	0.22	0.11	-	-
<b>Carbon content</b>	C	79.08	79.72	80.62	82.69	87.52	91.57
<b>Halite</b>	NaCl	-	-	-	-	-	0.01
<b>Kaolinite</b>	Al <sub>2</sub> Si <sub>2</sub> O <sub>5</sub> (OH) <sub>4</sub>	8.83	10.23	7.89	7.66	3.38	2.31

<b>Microcline</b>	$\text{KAlSi}_3\text{O}_8$	0.36	0.23	0.19	0.35	0.33	0.3
<b>Muscovite</b>	$(\text{KAl}_3\text{Si}_3\text{O}_{10}(\text{OH})_2)$	0.39	0.59	0.33	0.32	0.18	0.07
<b>Plagioclase</b>	$\text{NaAlSi}_3\text{O}_8 - \text{CaAl}_2\text{Si}_2\text{O}_8$	0.34	0.34	0.51	0.73	0.73	0.52
<b>Pyrite</b>	$\text{FeS}_2$	0.55	0.56	0.5	0.46	0.14	0.08
<b>Quartz</b>	$\text{SiO}_2$	6.82	7.79	7.05	6.26	6.27	4.06
<b>Rutile</b>	$\text{TiO}_2$	-	-	-	-	-	-
<b>Siderite</b>	$\text{FeCO}_3$	0.39	0.38	0.12	-	-	-
		<b>TSH 1</b>	<b>TSH 2</b>	<b>TSH 3</b>	<b>TSH 4</b>	<b>TSH 5</b>	<b>TSH 6</b>
<b>Anatase</b>	$\text{TiO}_2$	-	0.05	0.17	0.23	0.12	-
<b>Calcite</b>	$\text{CaCO}_3$	0.09	-	-	-	0.07	0.05
<b>Chlorite</b>	$((\text{Mg,Fe})_5\text{Al}(\text{AlSi}_3\text{O}_{10})(\text{OH})_8)$	2.43	0.19	-	-	-	-
<b>Dolomite</b>	$(\text{CaMg})(\text{CO}_3)_2$	1.65	1.72	1.41	0.72	0.54	-
<b>Carbon content</b>	C	75.79	73.74	76.62	80.23	85.3	90.69
<b>Kaolinite</b>	$\text{Al}_2\text{Si}_2\text{O}_5(\text{OH})_4$	10.98	13.57	12.07	10.96	5.33	2.25
<b>Microcline</b>	$\text{KAlSi}_3\text{O}_8$	0.5	0.68	0.31	0.44	0.84	0.63
<b>Muscovite</b>	$(\text{KAl}_3\text{Si}_3\text{O}_{10}(\text{OH})_2)$	1.31	2.06	1.93	0.6	1.62	0.56
<b>Plagioclase</b>	$\text{NaAlSi}_3\text{O}_8 - \text{CaAl}_2\text{Si}_2\text{O}_8$	0.92	0.61	0.47	0.22	0.93	1.66
<b>Pyrite</b>	$\text{FeS}_2$	0.24	0.25	0.26	6.44	0.1	0.12
<b>Quartz</b>	$\text{SiO}_2$	5.54	6.71	6.49	0.06	4.92	3.83
<b>Rutile</b>	$\text{TiO}_2$	0.11	-	0.05	0.09	0.24	0.21
<b>Siderite</b>	$\text{FeCO}_3$	0.44	0.44	0.23	-	-	-

### • 5.6 Diffuse Reflectance Infrared Fourier Transform Spectroscopy results

The changes in the intensities of functional groups with heat treatment were observed from the DRIFT spectra which were obtained for the three raw coal samples, as well as for the coal-derived char samples. The background and experimental procedure regarding the DRIFT analytical technique are described in Chapter 3.1.6 and Chapter 4.6.4, respectively. The DRIFT spectra for the raw coals are presented in Figure 5.10, and the interpretation of these spectra is based on research reported in literature [Painter *et al.*, 1981; Sobkowiak and Painter, 1995; Machnikowska *et al.*, 2002; Van Niekerk *et al.*, 2008; Morga, 2010; Xin *et al.*, 2014].

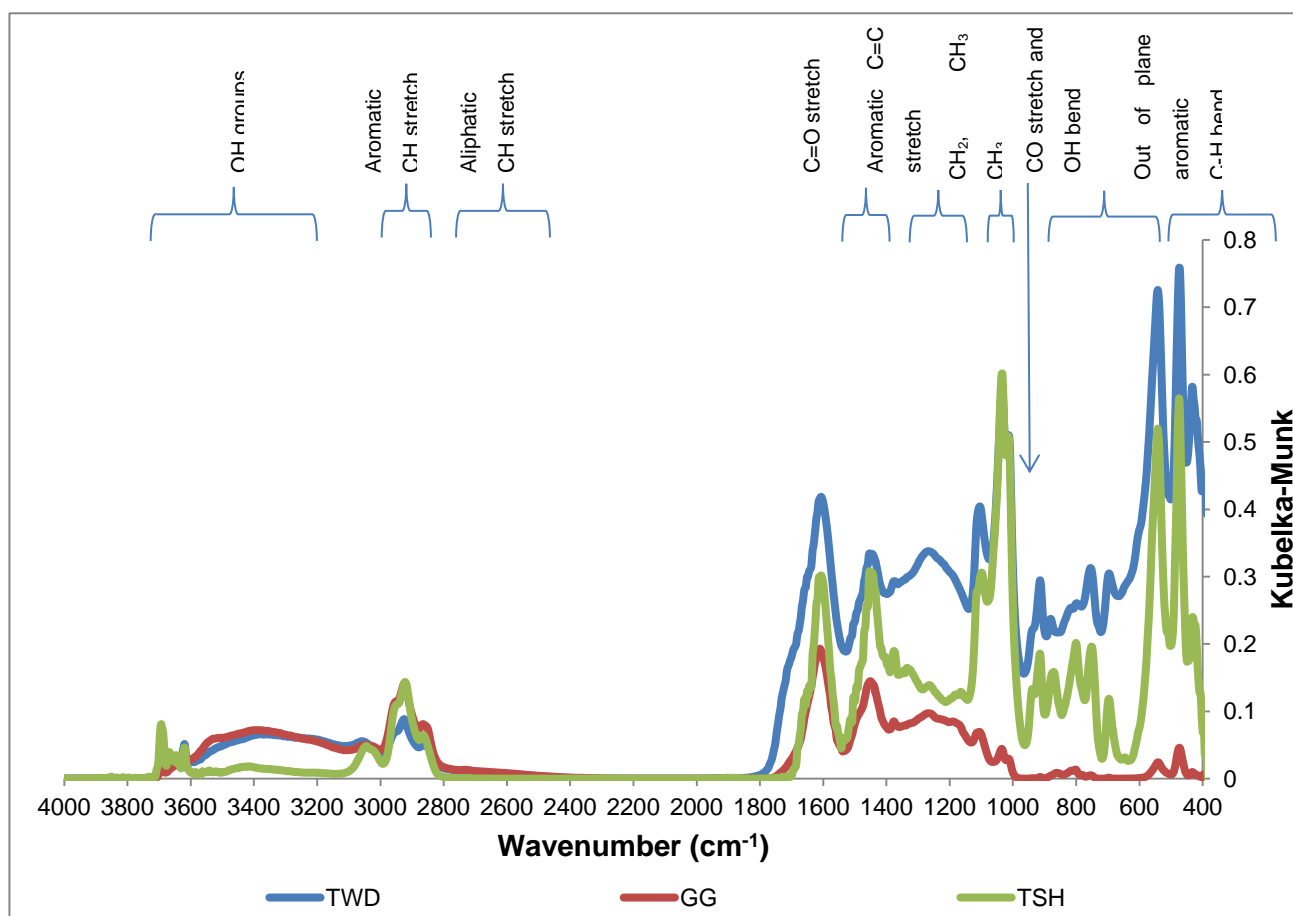


**Figure 5.10: DRIFT spectra for three raw coal samples.**

DRIFT spectroscopy is based on the Kubelka-Munk law and is considered for qualitative interpretation only. The peaks observed at 3800 – 3600  $\text{cm}^{-1}$  could be assigned to mineral matter present in all three coal samples. O-H stretch vibrations in the region of 3700 to 3100  $\text{cm}^{-1}$  could be observed for all three coals, with TSH coal consisting of substantially lower intensities of the OH groups. Various types of free OH groups and combinations of hydrogen bonds within the coal samples contribute to the peaks observed in this region. The aromatic C-



H stretch mode (3100 to 3000  $\text{cm}^{-1}$ ), as well as the aliphatic C-H stretch mode (3000 to 2800  $\text{cm}^{-1}$ ) was present in all three coal samples. The aliphatic C-H stretch region was divided into three distinct peaks and assigned to the following vibrations; i.e. the shoulder peak at 2950  $\text{cm}^{-1}$  to the asymmetric  $\text{CH}_3$  vibration, the 2920  $\text{cm}^{-1}$  peak represented the asymmetric  $\text{CH}_2$  vibration, and the peak observed at 2850  $\text{cm}^{-1}$  was assigned to the symmetric vibrations of  $\text{CH}_2$  and  $\text{CH}_3$ . The next distinctive peak for all three coal samples was observed at 1600  $\text{cm}^{-1}$ , and this was due to the C=C stretching vibrations within the aromatic ring structure. C=O stretch vibrations were assigned to the shoulder peaks which could be observed on the side of the 1600  $\text{cm}^{-1}$  peak. TWD coal contained two C=O stretching vibrations, while one C=O vibration could be observed for TSH coal. This variation of the C=O vibrations in the coal samples may be due to the different types of C=O groups, which included aldehydes, carboxyl and ketone functional groups.

The peak observed at 1450  $\text{cm}^{-1}$  could be assigned to the aliphatic C-H bending vibrations while the shoulder peak at 1490  $\text{cm}^{-1}$  corresponded to the C=C aromatic stretch modes. The small peak observed for all three spectra at 1375  $\text{cm}^{-1}$  was assigned to  $\text{CH}_3$  groups. Distinctive intensity bands at 1035  $\text{cm}^{-1}$  was observed for the TWD and the TSH samples, but not for the GG coal. This peak was assigned to the aliphatic C-O-C stretch vibrations. Out of plane aromatic C-H vibrations (in the region from 900 to 700  $\text{cm}^{-1}$ ) were observed for the TWD and the TSH coal samples, while the intensities of these peaks were substantially less for the GG coal sample. According to Van Niekerk *et al.* [2008], the differences in the intensity of these C-H modes can be used as an indication of the different substitution patterns occurring at the aromatic ring structures within the coal samples. The DRIFT results indicated that the hydrogen bonding was substantially more evident for the TWD and the GG coal than for the TSH coal sample. This is in good relation to the ultimate analysis, where substantially less hydrogen content was reported for the TSH coal sample.

The high intensity of the aliphatic C-H stretch modes in the region of 3000 – 2800  $\text{cm}^{-1}$  suggested that these coal structures were strongly aliphatic. From the petrographic analysis results reported by Coetzee *et al.* [2014], it is evident that these coal samples are vitrinite-rich coals. Van Niekerk *et al.* [2008] investigated vitrinite-rich South African coals and concluded that the structure is mainly aliphatic.

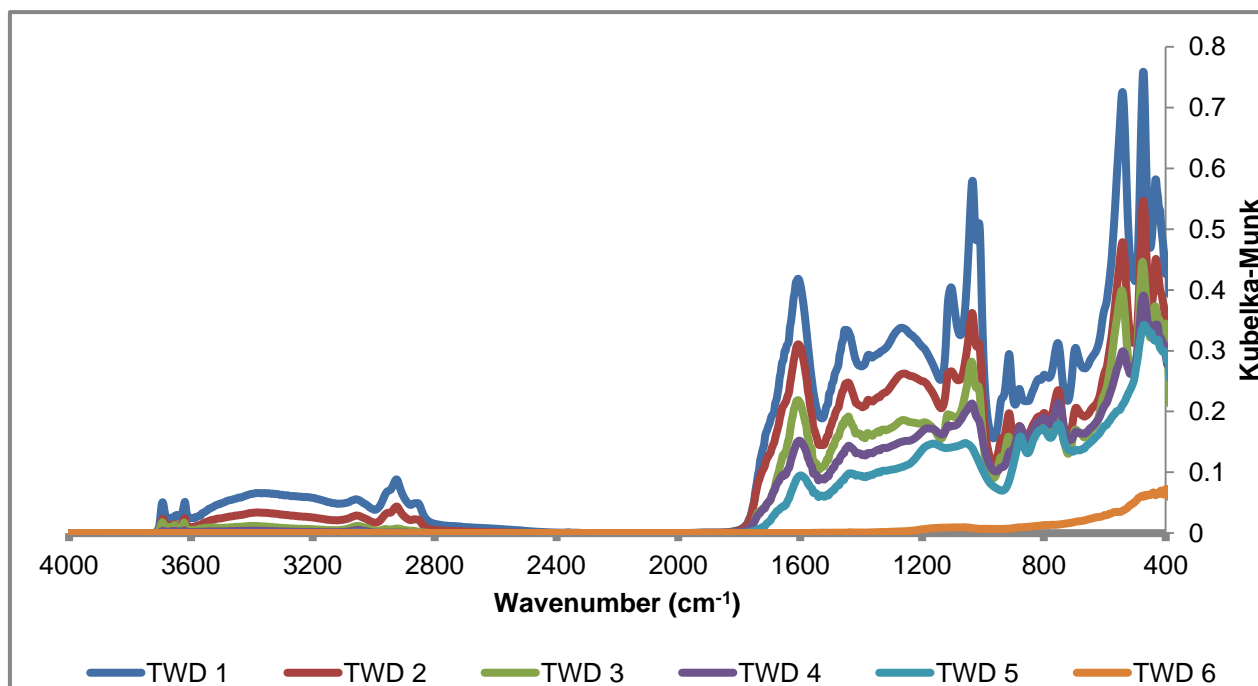


**Figure 5.11: DRIFT spectra of TWD raw coal and coal-derived char samples.**

The DRIFT spectra for the raw coal samples and their coal-derived char samples, prepared at different temperatures correlating to various mass loss percentages, are presented in Figures 5.11 to 5.13. An interactive integration method was used to integrate the distinctive peak areas observed for the coal samples and the values of these integrated peak areas are reported in Appendix D. The intensities of the absorption peak areas were compared in relation to other absorption peaks observed in the same DRIFT spectrum.

Although semi-quantitative measurements were performed, the peak intensity values were compared with each other and the results are given in the next section. The DRIFT spectra for the TWD raw coal and coal-derived char samples can be observed in Figure 5.11. The intensity of the O-H groups ( $3700$  to  $3100$   $\text{cm}^{-1}$ ) decreased significantly with an increase in temperature, i.e. from the TWD 1 sample (raw coal) to the TWD 6 coal-derived char sample (100% mass loss). The aliphatic CH peak area decreased significantly from the TWD 2 coal-derived char sample (20% mass loss) to the TWD 3 coal-derived char sample (40% mass loss), while the intensity of the aromatic CH peak area decreased at a more constant rate. The peak area for the C=C stretch vibration decreased at a constant rate from the raw coal sample to the TWD 6 coal-derived char sample (at  $900^\circ\text{C}$ ). The absorption peak areas in the TWD 6 char sample decreased almost completely. It is evident that the functional groups containing hydrogen and oxygen decomposed with an increase in temperature when inspecting the DRIFT spectra of the TWD 6 sample at 100% mass loss.

The DRIFT spectra for the GG coal and coal-derived char samples can be observed in Figure 5.12. As expected, the OH groups decreased with an increase in temperature. The intensity of the CH<sub>2</sub>, CH<sub>3</sub> stretch (1530 – 1400 cm<sup>-1</sup>) as well as the intensity of the C=C aromatic vibrations (1600 cm<sup>-1</sup>) increased from the GG 2 sample (20% mass loss) to the GG 3 sample (40% mass loss) before it decreased with an increase in temperature up to 900°C (GG 6 char sample). This increase in the intensity of the absorption peak areas from the GG 2 sample to the GG 3 coal-derived char sample was also observed for the C-O stretch at 1035 cm<sup>-1</sup>, as well as for the aromatic CH modes in the region of 900 – 700 cm<sup>-1</sup>. The absorption peak areas decreased dramatically with an increase in temperature up to the GG 6 char sample (100% mass loss) at 900°C. This is the result of the decomposition of the functional groups containing hydrogen and oxygen with an increase in temperature [Serio *et al.*, 1987].

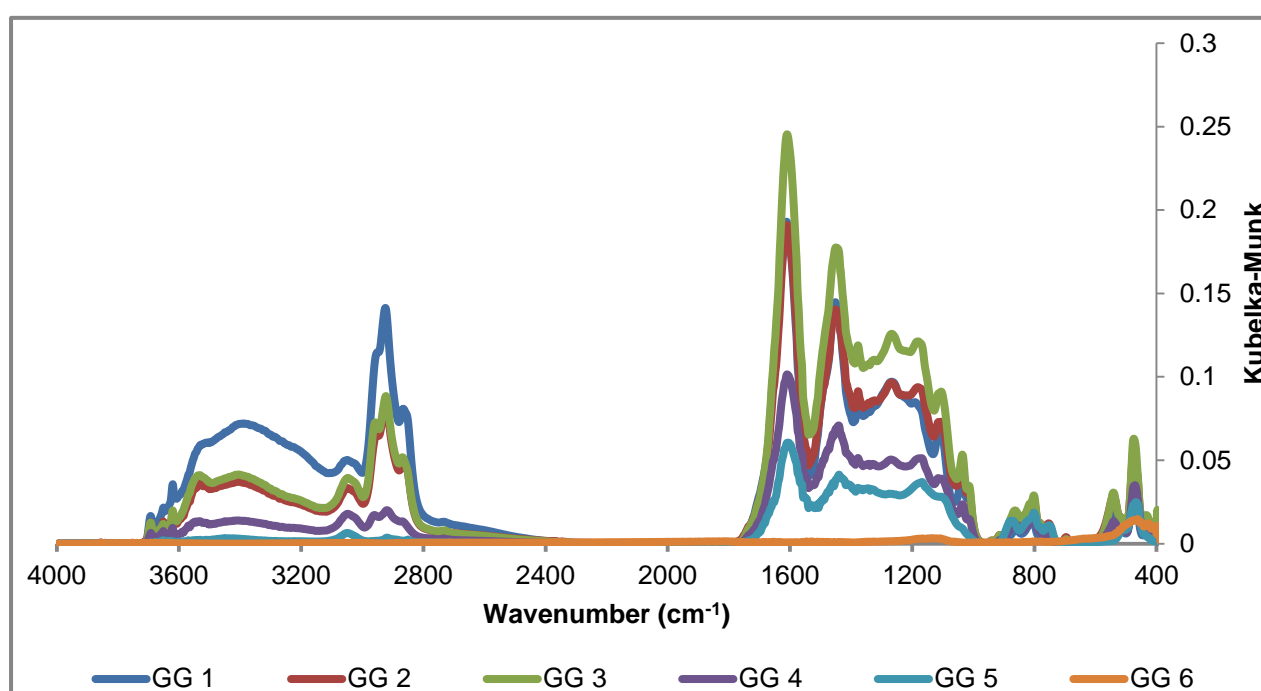


**Figure 5.12: DRIFT spectra of GG coal and coal-derived char samples.**

The DRIFT spectra for the TSH coal and coal-derived char samples are presented in Figure 5.13, and revealed significant differences in comparison to the DRIFT spectra for the TWD and the GG coal samples. Similar trends were observed, with an increase in temperature, for the absorption peak areas within the TSH coal sample. The intensity of the peak areas decreased substantially, to close to the baseline, from the TSH 1 (raw coal) sample to the TSH 2 coal-derived char sample (20% mass loss). A significant increase in the intensities of the peak areas was observed from the TSH 2 coal-derived char sample to the TSH 3 coal-derived char sample

(40% mass loss), after which it gradually decreased to close to the baseline at the TSH 6 char sample (prepared at 900°C). The observed increase may be due to the measurements being semi-quantitative only. The TSH 6 char sample showed no significant absorption peak areas except for the S-S peak at 620-400  $\text{cm}^{-1}$ , i.e. this is due to the decomposition of the functional groups with an increase in temperature.

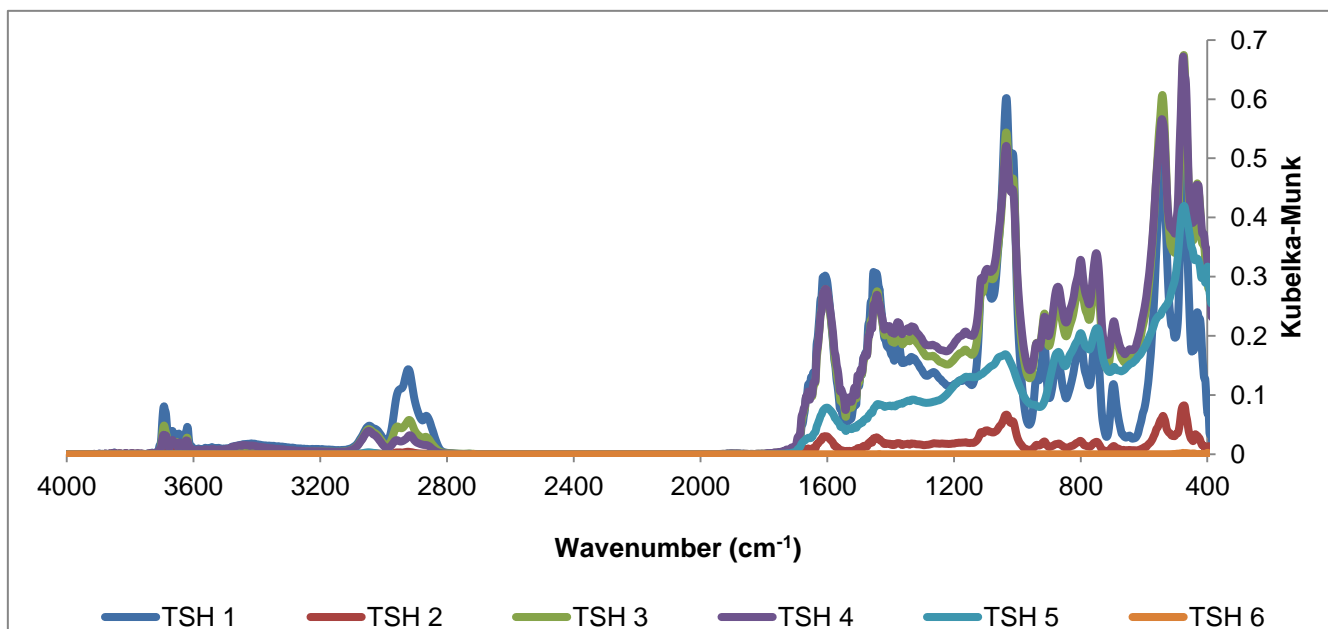


**Figure 5.13: DRIFT spectra for TSH coal and coal-derived char samples.**

The changes in the chemical structure of the coal samples can be described using the following ratios of the integrated areas of the spectral bands:

- A)  $\text{CH}_{\text{ar}}$  (900-700  $\text{cm}^{-1}$ ) /  $\text{CH}_{\text{al}}$  (3000-2800  $\text{cm}^{-1}$ ). The aromaticity of the coal structure can be demonstrated by the ratio of the aromatic and aliphatic hydrogen functional groups [Fujioka *et al.*, 2006].
- B)  $\text{CH}_{\text{ar}}$  (900-700  $\text{cm}^{-1}$ ) /  $\text{C}=\text{C}_{\text{ar}}$  (1650-1500  $\text{cm}^{-1}$ ). This ratio can be used to determine the aromatic ring condensation [Morga, 2010].

According to Machnikowska *et al.* [2002], these structural parameters,  $\text{CH}_{\text{ar}}/\text{CH}_{\text{al}}$  and  $\text{CH}_{\text{ar}}/\text{C}=\text{C}$  ratios, can be calculated using the DRIFT spectra in order to follow the structural rearrangement occurring within the coal sample.

The aromatic/aliphatic ( $\text{CH}_{\text{ar}}/\text{CH}_{\text{al}}$ ) CH peak area ratios are presented in Figure 5.14. An increase in this  $\text{CH}_{\text{ar}}/\text{CH}_{\text{al}}$  ratio could be observed with an increase in temperature for all three coal samples.

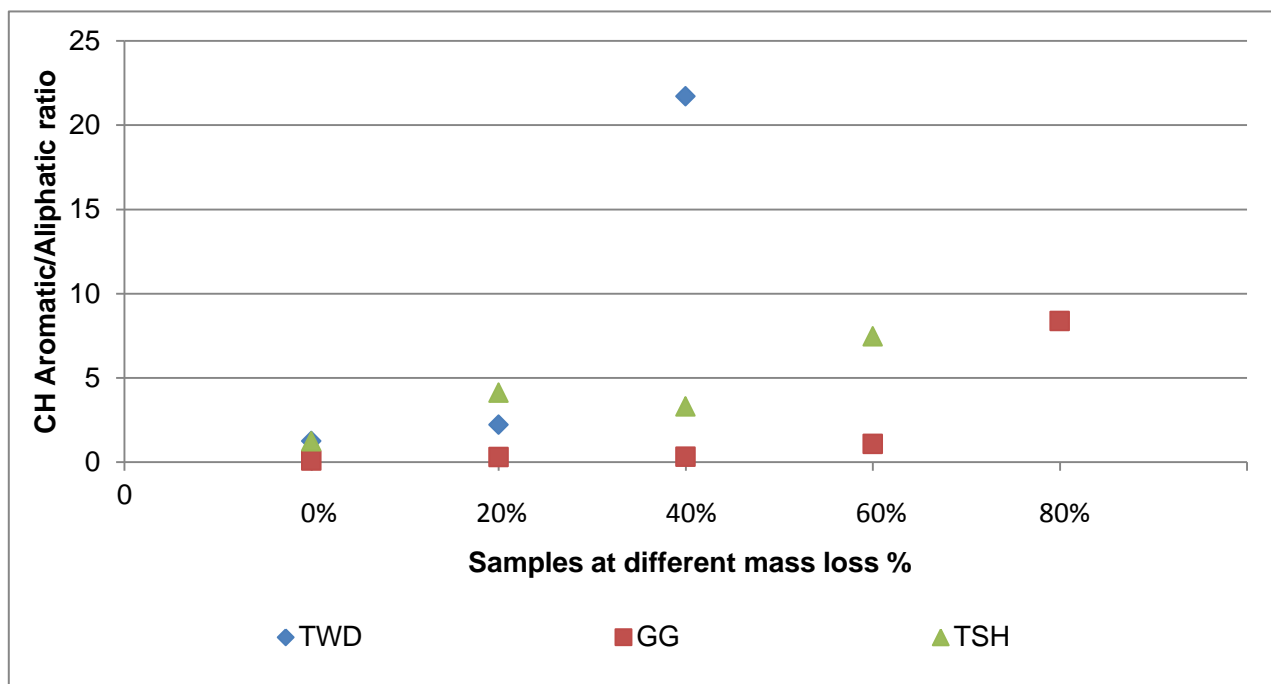


**Figure 5.14: Aromatic/Aliphatic CH peak area ratio of the three coal samples.**

The TWD coal sample showed a significant increase in aromaticity from the TWD 2 sample at 20% mass loss. No increase in the aromaticity for the GG coal sample was observed until the GG 4 sample at 60% mass loss. The aromaticity increased substantially from the 60% mass loss sample. The aromaticity for the TSH coal sample increased from the raw coal sample to the sample at 20% mass loss, after which a slight decrease was observed from the TSH 2 (20% mass loss) to the TSH 3 (40% mass loss) coal samples. An increase in the aromaticity was observed again from the TSH 4 coal sample at 60% mass loss.

The ratio of the CH aromatic peak area ( $900-700\text{ cm}^{-1}$ ) to the C=C peak area ( $1650-1500\text{ cm}^{-1}$ ) can be observed in Figure 5.15. The aromatic ring condensation can be determined from these results. The aromatic ring condensation for the TWD coal sample increased with an increase in temperature during pyrolysis. A substantial increase was observed between the TWD 3 coal-derived char sample (40% mass loss) and the TWD 4 coal-derived char sample (60% mass loss). The GG coal sample displayed the lowest amount of aromatic ring condensation, and a decrease was observed from the GG 4 coal-derived char sample (60% mass loss) to the GG 5 coal-derived char sample (80% mass loss). The TSH coal sample experienced the highest intensity aromatic ring condensation. A slight decrease was observed from the TSH raw coal to the TSH 2 sample at 20% mass loss. The ring condensation for the TSH coal sample increased significantly from the TSH 4 (60% mass loss) coal-derived char sample.

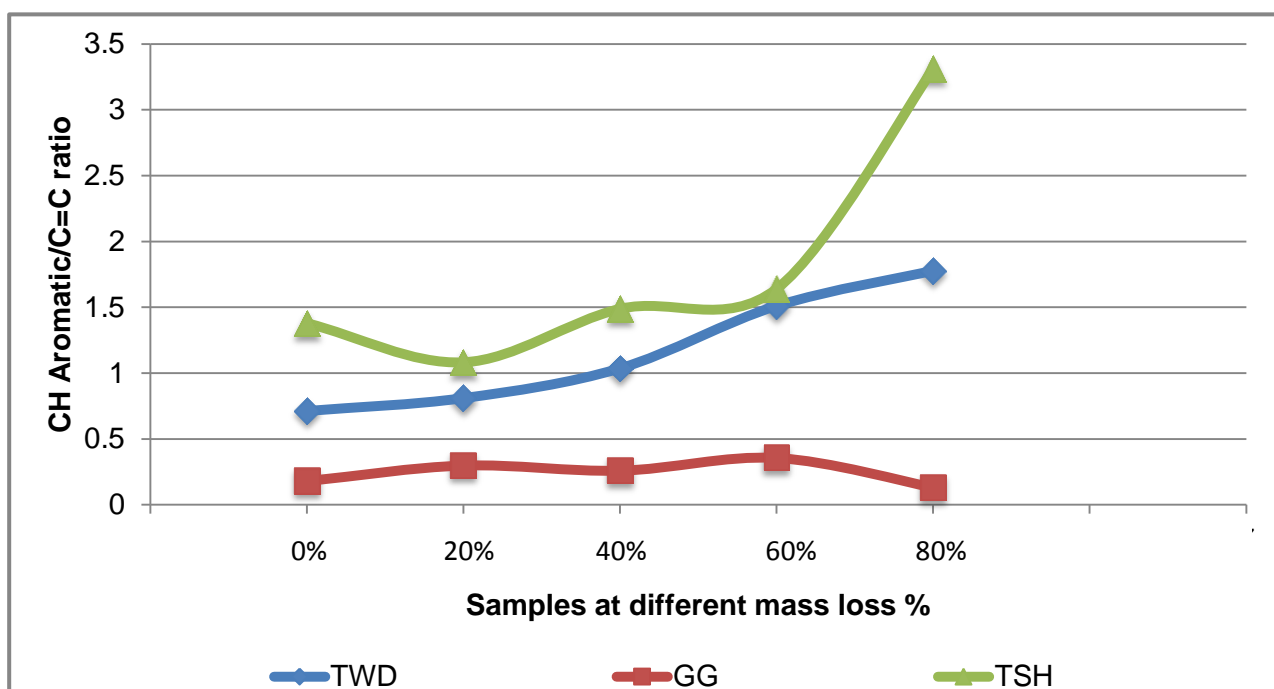


Figure 5.15: CH aromatic / C=C peak area ratio for the three coal samples.

During pyrolysis the aromaticity increased for all three coal samples with the highest aromaticity observed for the TSH coal sample, i.e. the high caking coal.

### • 5.7 Summary

The three raw coal samples as well as their various coal-derived char samples were subjected to characterization analyses in order to determine the changes in the chemical properties of the coal samples during pyrolysis, with specific relevance to caking coals.

The ultimate analyses revealed that the hydrogen and oxygen content, present in the three coal samples, decreased with an increase in temperature. This is expected since the heteroatoms and aliphatic carbons are present in the less stable bonds while these functional groups consist mainly of oxygen and hydrogen [Hambly, 1998]. The carbon content increased with an increase in temperature due to the evolution of light gaseous compounds containing  $\text{CO}_2$ ,  $\text{H}_2$  and  $\text{H}_2\text{O}$ . The evolution of these gases, prior to the formation of tar, results in the decrease of oxygen and hydrogen fractions, as well as in the increase of the carbon fraction [Hambly, 1998].

With regards to the TWD coal sample, the most significant chemical changes occurred between the TWD 2 and the TWD 3 coal-derived char samples (representing 20 and 40% mass loss, respectively) and again from the TWD 5 and the TWD 6 coal-derived char samples

(representing 80 and 100% mass loss, respectively). The TGA results revealed that the temperature of maximum mass loss occurred between the TWD 2 and TWD 3 coal-derived char samples, (433°C to 468°C). From the proximate and ultimate analyses results, it was evident that the evolution of volatile matter and hydrogen increased significantly, which led to the increase in the carbon content of the coal sample between the TWD 2 and the TWD 3 coal-derived char samples. The results derived from the DRIFT spectra revealed a significant increase in the aromaticity of the coal-derived char sample from the TWD 2 to the TWD 3 samples. This corroborates with the aromaticity factor ( $f_a$ ), which also increased significantly from the TWD 2 to the TWD 3 coal-derived char samples. Chemical changes occurring between the TWD 3 and the TWD 4 coal-derived char samples (40 and 60% mass loss, respectively) included the significant increase in the CH aromatic/C=C peak area ratio as well as an increase in the graphite content, determined by XRD analysis. The MS results indicated that the maximum temperature for H<sub>2</sub> evolution occurred between the TWD 5 and the TWD 6 coal-derived char samples (representing 80 and 100% mass loss, respectively). This evolution of the H<sub>2</sub> was confirmed by the substantial decrease observed in the atomic H/C ratios from the TWD 5 to the TWD 6 coal-derived char samples.

The proximate and ultimate analyses results indicated that significant evolution of volatile matter, hydrogen and oxygen occurred between the GG 2 (20% mass loss) and the GG 3 (40% mass loss) coal-derived char samples and again from the GG 5 (80% mass loss) to the GG 6 (100% mass loss) coal-derived char samples. The aromaticity factor ( $f_a$ ) increased significantly from the GG 2 to the GG 3 coal-derived char samples while the intensity of the peak areas, observed from the DRIFT spectra, showed a slight increase. The TGA results indicated that the maximum rate of mass loss occurred between the GG 3 and the GG 4 (60% mass loss) coal-derived char samples. An increase in the graphite content was observed in the coal-derived char sample between the GG 3 and the GG 4 samples. The DRIFT spectra revealed a decrease in the intensities of the peak areas while the maximum evolution of H<sub>2</sub>O, determined from the MS analysis, was recorded from the GG 3 to the GG 4 coal-derived char samples. The graphite content increased significantly from the GG 4 to the GG 5 coal-derived char sample while the maximum evolution of H<sub>2</sub> was recorded, by the MS analysis, for the same phase. The CH aromatic/CH aliphatic peak area ratio increased significantly while the other peak area intensities, observed from the DRIFT spectra, decreased from the GG 4 to the GG 5 coal-derived char samples. From the ultimate analysis results, it was evident that the evolution of hydrogen and oxygen reached a maximum between the GG 5 and the GG 6 coal-derived char samples. In accordance with this evolution, the atomic H/C ratios decreased substantially from the GG 5 sample to the GG 6 sample while the DRIFT spectra decreased significantly.

The TSH coal sample, with an FSI of 9, behaved completely differently under pyrolysis conditions in comparison with the TWD and the GG coal samples. The major evolution of volatile matter occurred between the TSH 1 and the TSH 2 coal-derived char samples (representing the raw coal sample and 20% mass loss, respectively). The aromaticity factor ( $f_a$ ) as well as the CH aromatic/CH aliphatic ratio, derived from the DRIFT spectra, increased significantly from the raw coal sample to the TSH 2 sample (at 20% mass loss). The intensities of the peak areas as well as the CH aromatic/C=C peak area ratio, from the DRIFT spectra, decreased as the sample was heated from the raw coal to the TSH 2 coal-derived char sample, due to the plastic range also occurring at these temperatures. The TGA results indicated that the maximum temperature of mass loss occurred at 480°C, which was between the TSH 2 and the TSH 3 (40% mass loss) coal-derived char samples. The chemical changes occurring between the TSH 2 and the TSH 3 coal samples included; the increase of the aromaticity factor, the increase in the graphite content and a slight increase in the intensities of the peak areas observed in the DRIFT spectra.

It is evident from these results that the high caking coal, the TSH sample, behaved differently and that significant chemical changes occurred at different phases during pyrolysis, compared to the TWD and the GG samples (coals with an FSI of 0 and 6.5, respectively). The reactions within the highly caking coal occurred at higher temperatures compared to the TWD and the GG coal samples.



## Chapter 6

### Results and discussion of the changes in the physical properties of caking coals during pyrolysis.

*In this chapter the results of the investigation into the structural changes during pyrolysis will be discussed. The raw coal samples as well as their coal-derived char samples, prepared at different temperatures correlating to the different mass loss percentages, were subjected to the following analytical techniques:*

- **6.1 CO<sub>2</sub> adsorption analysis results**

The micropore surface areas of the three raw coal samples as well as their coal-derived char samples, were determined by the adsorption of CO<sub>2</sub>. The experimental procedure regarding the BET surface analysis is described in Chapter 4.6.5 and the results obtained are reported in Table 6.1. The values for the micropore surface area and the monolayer capacity were determined by using the Dubinin-Radushkevich (DR) equation.

The GG coal sample exhibited the largest surface area (this includes the values for the micropore surface area, monolayer capacity, BET surface area and the Langmuir surface area), while the TSH coal had the lowest values. During pyrolysis, the reactivity of the coal sample is related to the surface area [Malumbazo, 2011], thus, considering the surface area values obtained in this investigation, the GG coal sample will have the highest reactivity, with TWD exhibiting the second highest reactivity and the TSH coal sample will show the lowest reactivity when comparing the three coal samples. When observing the TG analyses in Chapter 5.2, the GG coal exhibited the largest pyrolysis reactivity, followed by the TWD coal sample with a small difference in reactivity, while the TSH coal had the lowest reactivity. This decrease in reactivity from GG to TSH proves the correlation between surface area and reactivity to be true in the case of these coals, and thus also for caking coals.

Table 6.1: CO<sub>2</sub> physical parameters for coal and coal-derived char samples.

	<b>TWD</b>	<b>1</b>	<b>TWD</b>	<b>2</b>	<b>TWD</b>	<b>3</b>	<b>TWD</b>	<b>4</b>	<b>TWD</b>	<b>5</b>	<b>TWD</b>	<b>6</b>
	<i>(raw</i>		<i>(20%</i>		<i>(40%</i>		<i>(60%</i>		<i>(80%</i>		<i>(100%</i>	
	<i>coal)</i>		<i>mass</i>		<i>mass</i>		<i>mass</i>		<i>mass</i>		<i>mass</i>	
			<i>loss)</i>		<i>loss)</i>		<i>loss)</i>		<i>loss)</i>		<i>loss)</i>	
<b>Micropore Surface Area (m<sup>2</sup>.g<sup>-1</sup>)</b>	106.9		125.0		189.0		198.2		262.1		300.7	
<b>Monolayer capacity (cm<sup>3</sup>.g<sup>-1</sup>)</b>	23.4		27.4		41.4		43.4		57.4		65.8	
<b>BET surface area (m<sup>2</sup>.g<sup>-1</sup>)</b>	71.7		80.9		120.2		123.2		165.0		187.3	
<b>Langmuir Surface Area (m<sup>2</sup>.g<sup>-1</sup>)</b>	76.3		85.2		126.9		130.2		173.6		196.5	
	<b>GG</b>	<b>1</b>	<b>GG</b>	<b>2</b>	<b>GG</b>	<b>3</b>	<b>GG</b>	<b>4</b>	<b>GG</b>	<b>5</b>	<b>GG</b>	<b>6</b>
	<i>(raw</i>		<i>(20%</i>		<i>(40%</i>		<i>(60%</i>		<i>(80%</i>		<i>(100%</i>	
	<i>coal)</i>		<i>mass</i>		<i>mass</i>		<i>mass</i>		<i>mass</i>		<i>mass</i>	
			<i>loss)</i>		<i>loss)</i>		<i>loss)</i>		<i>loss)</i>		<i>loss)</i>	
<b>Micropore Surface Area (m<sup>2</sup>.g<sup>-1</sup>)</b>	118.2		128.1		135.9		198.0		287.0		286.2	
<b>Monolayer capacity (cm<sup>3</sup>.g<sup>-1</sup>)</b>	25.9		28.0		29.7		43.3		62.8		62.7	
<b>BET surface area (m<sup>2</sup>.g<sup>-1</sup>)</b>	77.0		85.3		87.7		126.0		178.7		176.1	
<b>Langmuir Surface Area (m<sup>2</sup>.g<sup>-1</sup>)</b>	82.6		91.2		93.4		133.3		188.7		185.7	
	<b>TSH</b>	<b>1</b>	<b>TSH</b>	<b>2</b>	<b>TSH</b>	<b>3</b>	<b>TSH</b>	<b>4</b>	<b>TSH</b>	<b>5</b>	<b>TSH</b>	<b>6</b>
	<i>(raw</i>		<i>(20%</i>		<i>(40%</i>		<i>(60%</i>		<i>(80%</i>		<i>(100%</i>	
	<i>coal)</i>		<i>mass</i>		<i>mass</i>		<i>mass</i>		<i>mass</i>		<i>mass</i>	
			<i>loss)</i>		<i>loss)</i>		<i>loss)</i>		<i>loss)</i>		<i>loss)</i>	
<b>Micropore Surface Area (m<sup>2</sup>.g<sup>-1</sup>)</b>	90.2		84.8		170.2		101.8		194.7		289.5	
<b>Monolayer capacity (cm<sup>3</sup>.g<sup>-1</sup>)</b>	19.7		18.6		37.2		22.3		42.6		63.4	
<b>BET surface area (m<sup>2</sup>.g<sup>-1</sup>)</b>	62.4		60.0		108.0		69.5		120.0		180.9	
<b>Langmuir Surface Area (m<sup>2</sup>.g<sup>-1</sup>)</b>	67.5		65.5		115.5		75.6		128.0		190.6	
<b>Standard deviation</b>	±4		±4		±4		±4		±4		±4	

Dilatation analyses were conducted in previous investigations by Coetzee *et al.* [2014] on the three coal samples in order to determine the temperature where maximum swelling and contraction occurred.

The TWD coal sample did not exhibit any contraction or softening, while the GG and the TSH coal samples reached maximum contraction between the raw coal sample and the char sample at 20% mass loss (i.e. at 418°C and 425°C, respectively). From the results reported in Table 6.1 and Figure 6.1, it can be observed that the surface areas reached a minimum during the plastic temperature range, where the maximum contraction occurred, before increasing with an increase in temperature.

The CO<sub>2</sub> BET surface area results for the three coal samples are depicted in Figure 6.1. The surface areas for the raw coal samples are within 10 m<sup>2</sup>.g<sup>-1</sup> of each other; with the TSH raw coal sample yielding the lowest surface area. At the end of pyrolysis (for the 100% mass loss samples) the surface area measurements for the three coal samples are in close agreement with each other. The highest caking coal, TSH, exhibited the lowest surface area, except during the plastic stage, where the surface area increased significantly.

An increase was observed in the surface areas from the TWD raw coal sample to the TWD 3 coal-derived char sample (at 40% mass loss). This increase can possibly be ascribed to the evolution of volatile matter and the re-ordering of the aromatic ring structures within the coal sample. The surface areas remained more or less constant from the TWD 3 sample to the TWD 4 coal-derived char sample (60% mass loss), before the significant increase in surface area from the TWD 4 coal-derived char sample to the TWD 6 coal-derived char sample occurred (100 % mass loss at 900°C). This increase in the surface area corroborates with the evolution of volatile matter and hydrogen content (determined by proximate and ultimate analyses). The volatile matter and hydrogen content decreased significantly from the TWD 2 to TWD 3 samples, and again from the TWD 5 to the TWD 6 coal-derived char samples (i.e. from 20 to 40% mass loss and again from 80 to 100% mass loss). The increase in surface area was observed between the same phases.

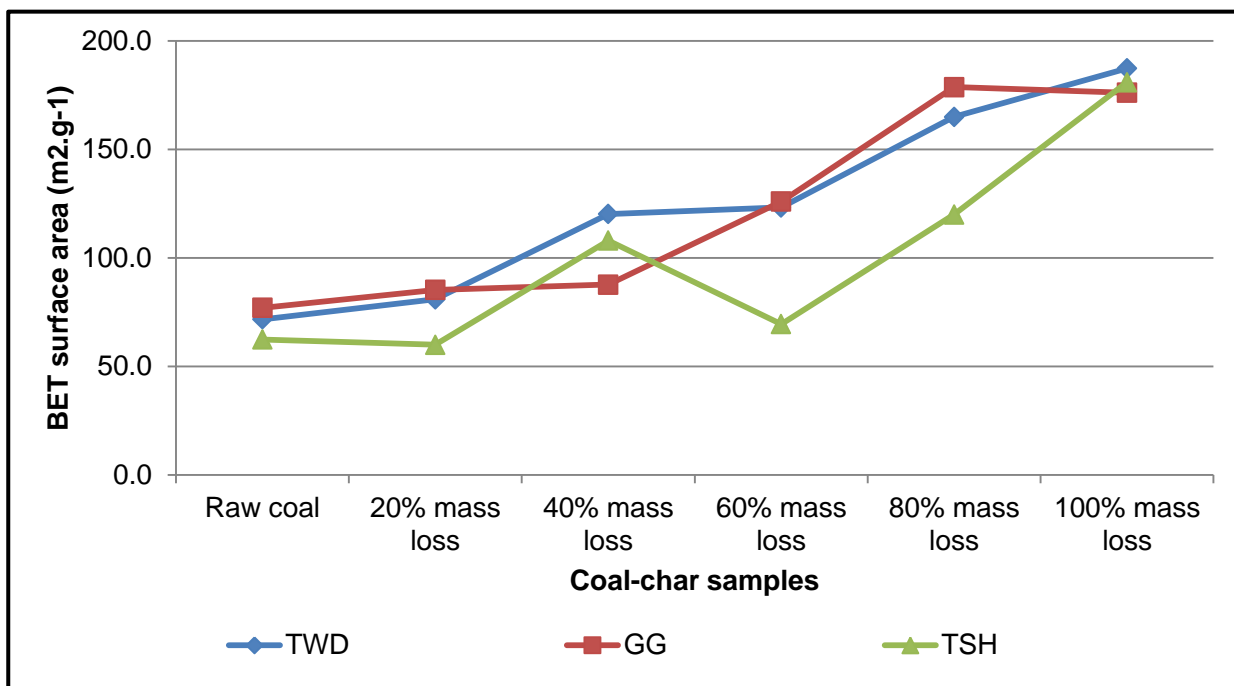


Figure 6.1: CO<sub>2</sub> BET surface areas for the three coals during pyrolysis.

The GG coal sample exhibited the highest surface area value compared to the other raw coal samples, although the values are all close. No significant increase was observed from the raw GG coal sample to the GG 3 coal-derived char sample (at 40% mass loss). From the GG 3 coal-derived char sample to the GG 5 coal-derived char sample (80% mass loss), however, a significant increase in the surface area was observed. This increase in surface area occurred at the re-solidification temperature of 457°C (determined by Coetzee *et al.*, 2014), i.e. between the GG 3 and the GG 4 samples. The surface area decreased slightly from the GG 5 coal-derived char sample (80% mass loss) to the GG 6 coal-derived char sample, prepared at 900°C. This decrease in the surface area can be explained by the swelling behaviour of the coal [Serio *et al.*, 1987].

The surface area observed for the TSH coal sample was the smallest of the three raw coal samples in this study. A slight decrease was observed initially in the surface area from the raw TSH coal sample to the TSH 2 coal-derived char sample (20% mass loss). This decrease in surface area is due to the plastic region where maximum contraction occurred (as determined by Coetzee *et al.*, 2014). The surface area increased substantially from the TSH 2 coal-derived char sample to the TSH 3 coal-derived char sample; however a decrease in the surface area was observed from the TSH 3 coal-derived char sample to the TSH 4 coal-derived char sample (representing 40 and 60% mass loss, respectively). A significant increase in the surface area

occurred from the TSH 4 coal-derived char sample (60% mass loss) up to the TSH 6 coal-derived char sample, at 100% mass loss (900°C).

The rapid increase of the CO<sub>2</sub> surface area can be explained by the creation and re-opening of micropores during pyrolysis [Malumbazo, 2011]. Similar trends in the rapid increase of the CO<sub>2</sub> surface area at the re-solidification temperature of bituminous coals (the Hazard No. 5 Seam, Kentucky) were reported by Tsai and Scaroni [1987]. For both the caking coals, GG and TSH, the re-solidification temperatures occurred between the 40 and the 60% mass loss samples. It is evident from Figure 6.1 that the increase in the surface area also occurred from the 40 to the 60% mass loss samples. This increase corroborates with the temperature region where the plastic stage occurred. The surface area increased at a similar temperature where the caking of the coal sample was observed.

The isotherm adsorption data derived from the CO<sub>2</sub> adsorption analysis are shown in Figures 6.4 to 6.6, for the three coal samples, respectively. The results, obtained from the isotherms, indicate that all three coal samples exhibited Type I behaviour during heat treatment. According to literature, a Type I isotherm can be associated with microporous material [Lowell *et al.*, 2004; Hattingh, 2012]. In Figures 6.4 to 6.6, relatively low pressures was observed, which were associated with the filling of the micropores and an increase in the rate of adsorption due to the relatively high adsorption potential and the small pore width of the microporous material [Hattingh, 2012].

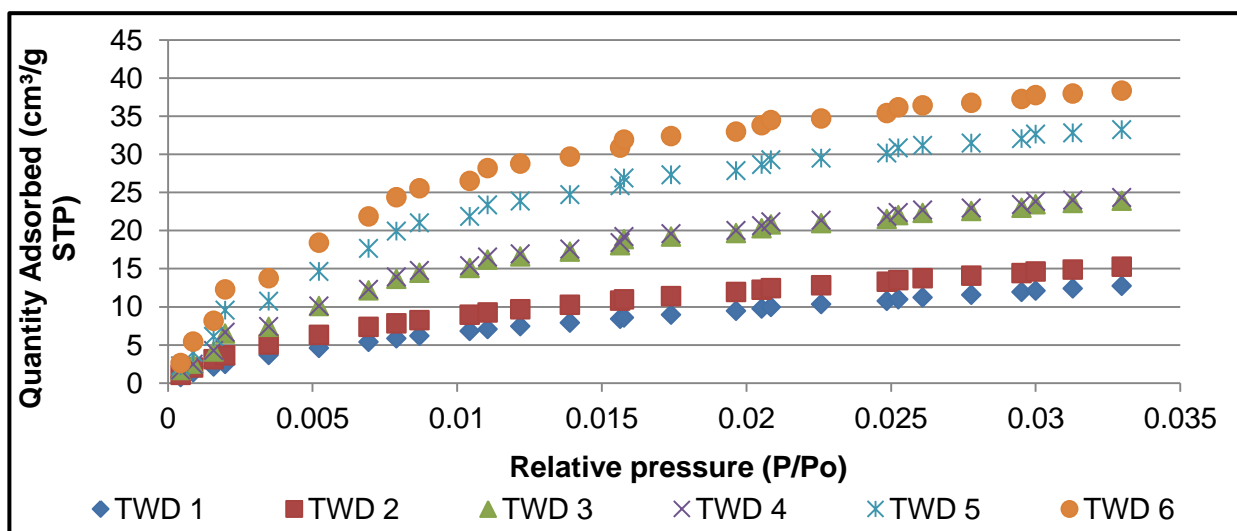


Figure 6.2: BET CO<sub>2</sub> adsorption isotherms for TWD raw coal and coal-derived char samples.

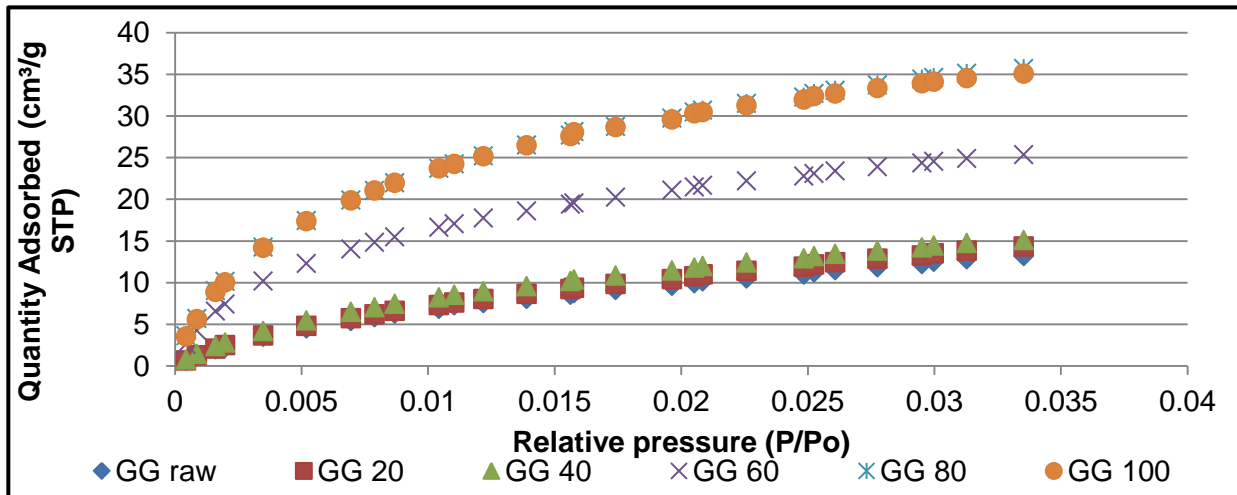


Figure 6.3: BET CO<sub>2</sub> adsorption isotherms for GG raw coal and coal-derived char samples.

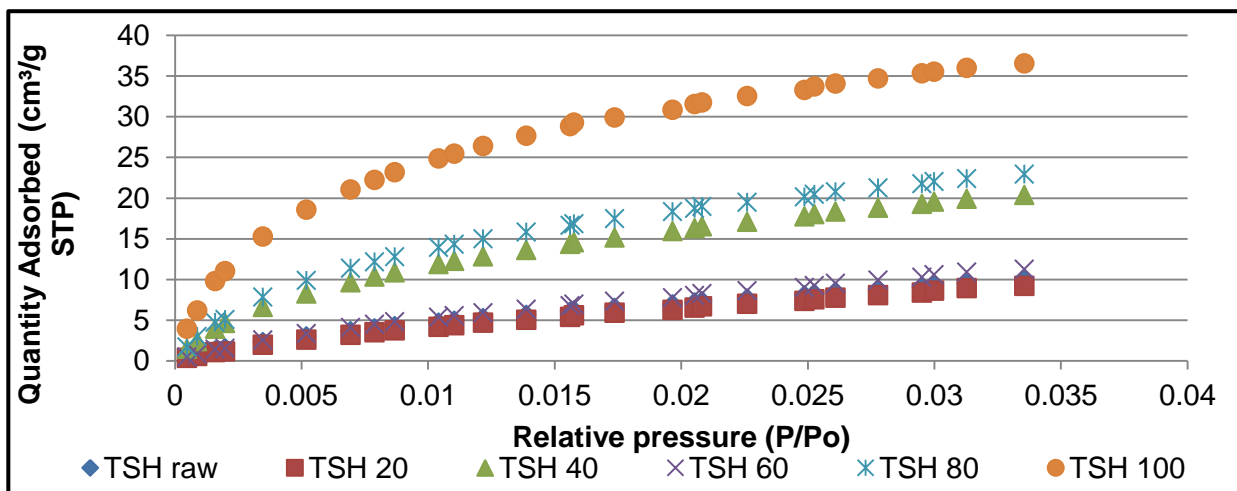


Figure 6.4: BET CO<sub>2</sub> adsorption isotherms for TSH raw coal and coal-derived char samples.

- **6.2 Scanning Electron Microscopy (SEM) results**

SEM images were recorded for the raw coal samples as well as their coal-derived char samples, representing the various mass loss percentages. The changes occurring during pyrolysis on a microscopic level can be observed in the SEM images displayed in Tables 6.2 to 6.4 for the three coal samples, respectively. The experimental procedure is described in Chapter 4.6.6.

When observing the SEM images for the three raw coal samples, it is evident that the TWD coal was a harder coal while the TSH coal sample was easily powdered into finer particles. The TWD 6 char sample (at 100% mass loss) was a more dense char, while the GG and the TSH char samples, (at 100% mass loss), showed signs of the plastic stage and bubble formation as a result of the evolution of volatile matter. The TWD char samples showed no significant signs of the molten phase. According to Yu *et al.* [2004], the swelling behaviour of a coal will influence the porosity of the char, thus higher swelling coals will form chars with greater porosity than lower swelling coals. This relationship between the swelling and the porosity is evident from the SEM images. The TSH coal sample, with a FSI of 9, formed the char with the highest porosity, while low porosity was observed for the TWD coal (non-swelling coal).

The SEM images for the TWD coal and coal-derived char samples are shown in Table 6.2. The char structure prepared at 900°C was remarkably different from the raw coal sample. The volatile matter evolved through cracks in the structure, with bubbles forming to a small extent. With the evolution of the volatile matter, the char structure became more porous and thick walls were observed. The bubble formation, due to the evolution of volatile matter, was observed from the TWD sample at 60% mass loss. The TWD 6 char sample (at 100% mass loss) exhibited the most significant visual change in the structure.

The microscopic changes in the structure of the GG coal and coal-derived char samples can be observed in Table 6.3. Bubble formation as a result of the volatile matter evolution was observed in the GG 3 sample, at 40% mass loss. The walls were thinner when compared to the TWD char samples, and the volatile matter evolved mainly through the formation of bubbles. After the volatile matter was released, the bubbles closed up again and further melting was observed.

The TSH was a softer type of coal and crushed to finer particles in comparison to the TWD and the GG coal samples. Bubble formation and signs of melting behaviour was observed in the TSH 2 coal-derived char sample (at 20% mass loss). In the TSH 3 sample, at 40% mass loss, it

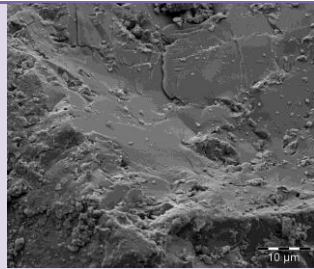
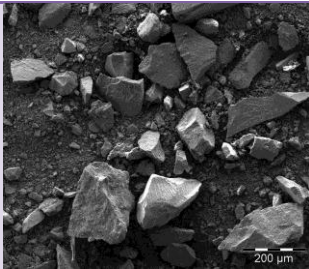
was evident that the particles melted into each other as a result of the plastic stage. The particles swelled to a great extent and formed cenospheric char particles with flow patterns on the surface. These cenospheric bubbles ruptured with a further increase in temperature due to the evolution of volatile matter. The volatile matter was released intensively; therefore the holes in the bubbles did not close again. Thin walls were observed at the 80% mass loss sample, and it was clear that the evolution of volatile matter was completed.

Classification of the char types from the SEM images was based on the threefold classification system summarized by Yu *et al.* [2004]. The TWD char sample can be classified as a type III char with a low porosity, irregular particle shape and a dense char. The GG char is a type II char with medium porosity and thick walls. The TSH char was classified as a type I char with very high porosity, spheroidal pore shapes and thin walls. Similar results were derived from SEM images on the same coal samples by Coetzee *et al.*, [2014]. The structure of the char is strongly dependent on the thermoplastic properties of the coal sample [Yu *et al.*, 2004]. Differences were therefore observed in the char structures of the three coal samples.

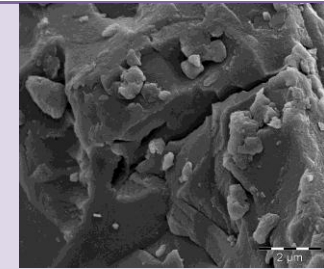
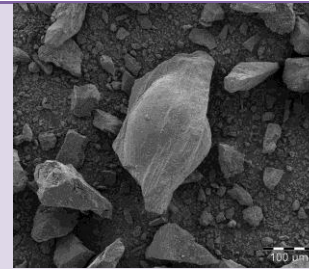


Table 6.2: SEM images for the TWD coal and coal-derived char samples.

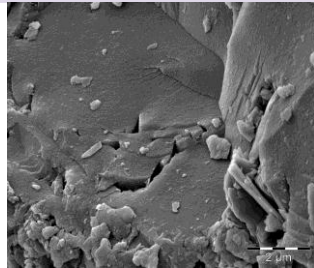
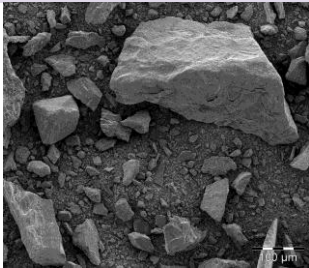
TWD raw coal



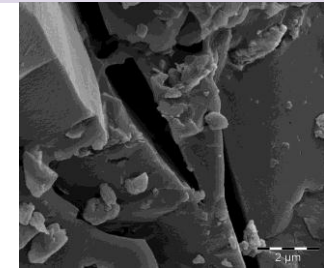
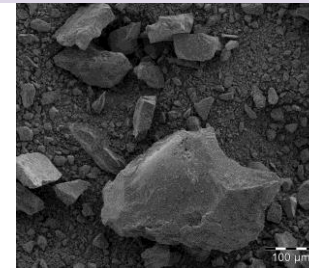
TWD 60%  
mass loss



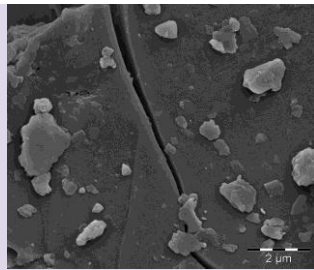
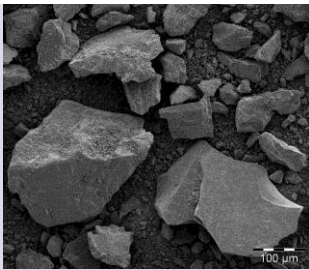
TWD 20%  
mass loss



TWD 80%  
mass loss



TWD 40%  
mass loss



TWD  
100%  
mass loss

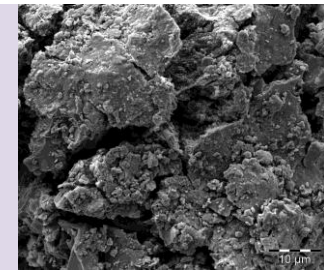
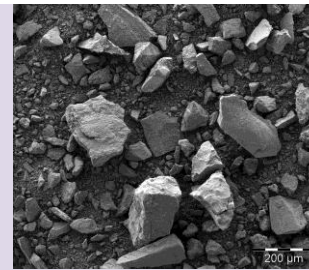


Table 6.3: SEM images for the GG coal and coal-derived char samples.

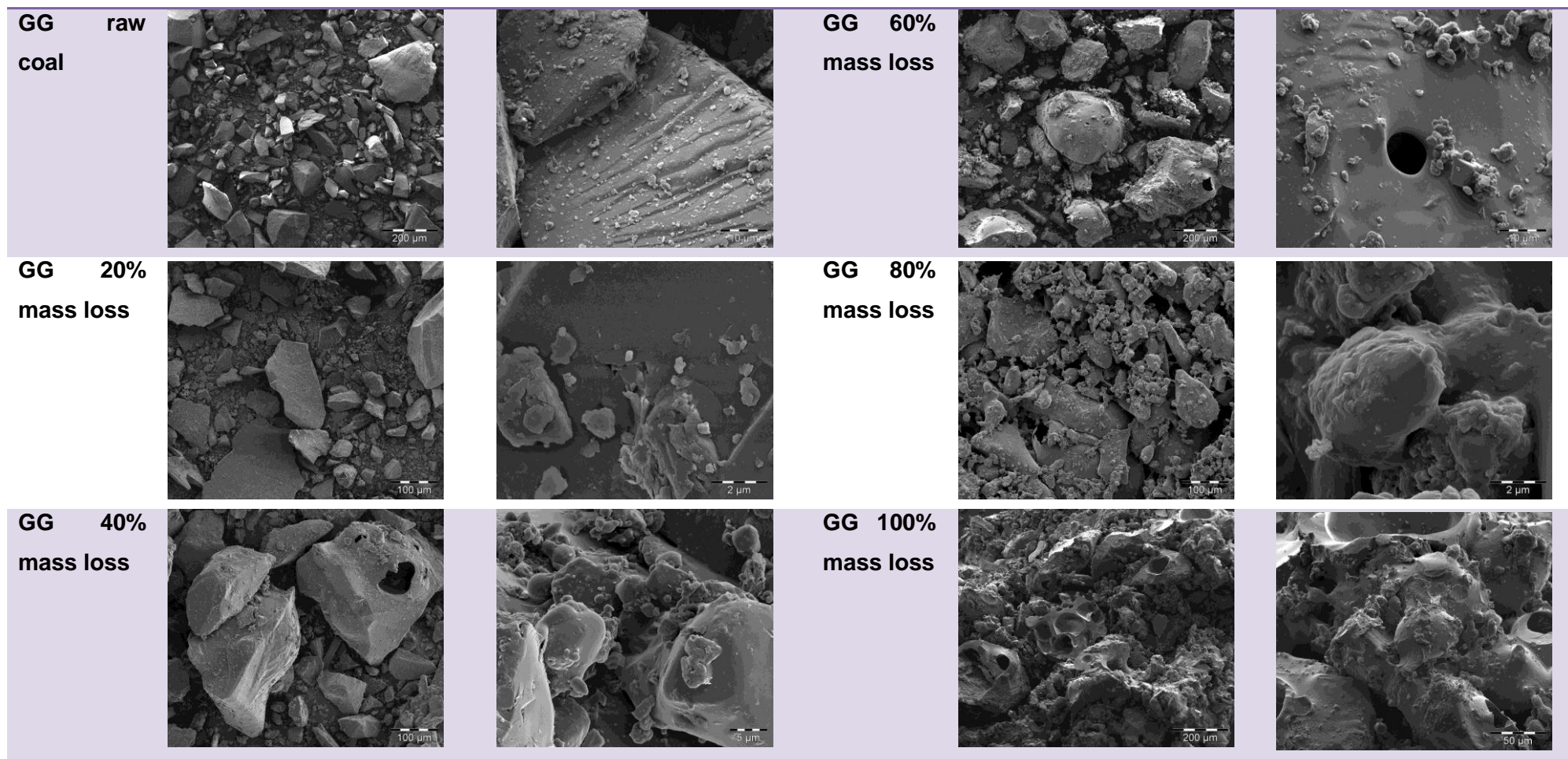
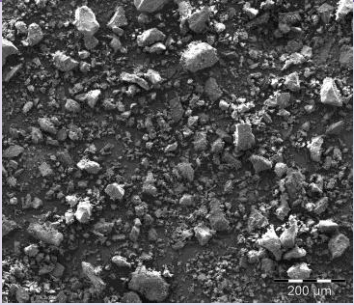
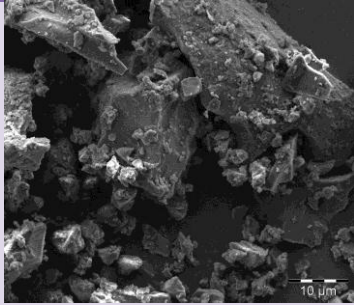
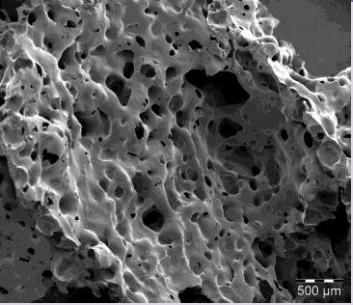
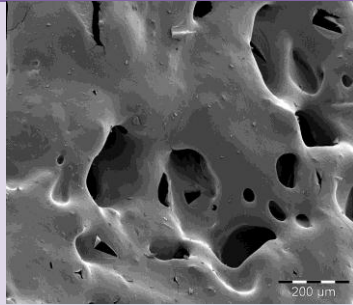
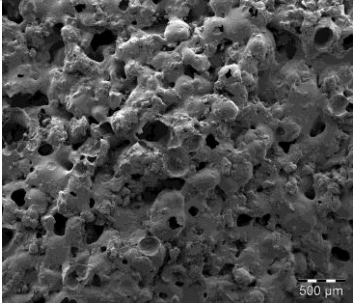
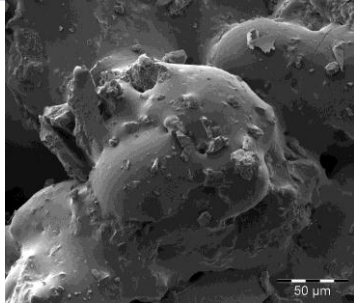
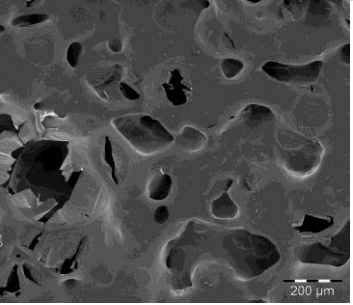
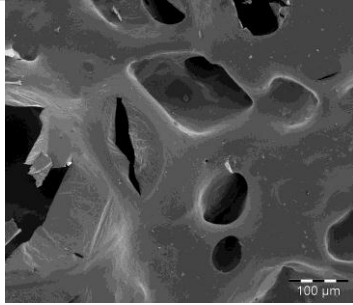
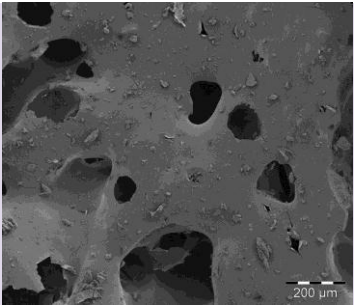
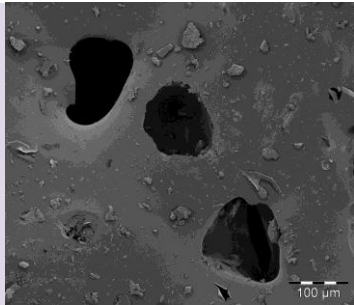
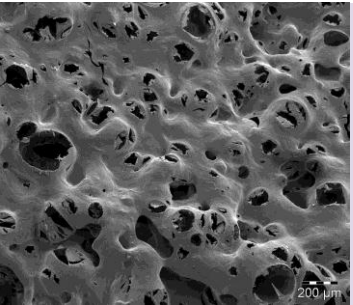
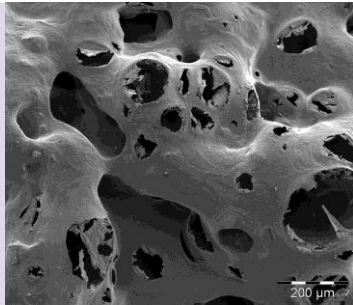


Table 6.4: SEM images for the TSH coal and coal-derived char samples.

<b>TSH raw coal</b>			<b>TSH 60% mass loss</b>		
<b>TSH 20% mass loss</b>			<b>TSH 80% mass loss</b>		
<b>TSH 40% mass loss</b>			<b>TSH 100% mass loss</b>		

- **6.3 Summary**

The physical analyses done on the three coal samples under investigation revealed that these samples were all microporous material. The TWD coal sample exhibited no plastic behaviour and can be classified as a non-softening coal. Plastic behaviour was observed for the GG coal sample which is a medium caking coal. The TSH coal sample has the highest FSI and exhibited plastic behaviour to the greatest extent. The TSH coal was also the softest coal and contained the most brittle char.

This increase in the surface area, observed for all three coal samples, corroborates with the evolution of volatile matter and hydrogen content (determined by proximate and ultimate analyses). An increase in surface area was observed during similar phases where an increase in the evolution of volatile matter and hydrogen occurred. A further increase in the surface area of the GG and the TSH samples was observed at the re-solidification temperatures.

The volatile matter was released through cracks forming on the surface of the particles, and no plastic behaviour was observed during pyrolysis of the TWD coal sample. The evolution of volatile matter leads to the formation of bubbles in the plastic range of the GG and the TSH coal samples.

# Chapter 7

## Conclusions and recommendations

*This chapter provides the main conclusions derived from this study as well as differences in behaviour observed between caking and non-caking vitrinite-rich coals during pyrolysis. Recommendations are also given for future work regarding South African caking coals and their behaviour during pyrolysis.*

- **7.1 Characteristic properties**

Conventional analyses were performed on the three raw coal samples, as well as the coal-derived char samples in order to characterize the coals and compare their behaviour during pyrolysis. The main differences between the caking and non-caking coals can be observed in Table 7.1.

**Table 7.1: Comparison of the three South African coals.**

	<b>TWD</b>	<b>GG</b>	<b>TSH</b>
<b>Coal rank</b>	Medium rank C	Medium rank C	Medium rank B
<b>FSI</b>	0	6.5	9
<b>*Softening temperature</b>	-	400°C	420°C
<b>*Maximum fluidity</b>	-	430°C	467°C
<b>*Solidification temperature</b>	-	457°C	508°C
<b>Aromaticity factors for the raw coal</b>	1.08	0.85	1
<b>Maximum temperature of mass loss</b>	440°C	440°C	480°C
<b>CH aromatic / C=C ratio for raw coal</b>	0.7	0.2	1.4
<b>CH aromatic / C=C ratio for 100% mass loss char</b>	1.8	0.1	3.3
<i>* reported by Coetzee et al. [2014]</i>			

The TWD coal was classified as a bituminous medium rank C coal with no caking propensity, thus no plastic range or caking behaviour was observed for this coal sample. The TWD coal sample consisted of 59% vitrinite and 37% inertinite (vol.%, m.m.f.b.), and could therefore be

classified as a vitrinite-rich coal. The GG coal sample was also classified as a bituminous medium rank C coal with a FSI of 6.5, thus a plastic range and caking behaviour were observed. The GG coal sample, a vitrinite-rich coal, contained the highest amount of vitrinite (with a value of 86 vol.%, m.m.f.b.), and the lowest amount of inertinite (with a value of only 8 vol.%, m.m.f.b.) in comparison with the TWD and the TSH coal samples. The GG coal contained the highest amount of volatile matter and the lowest amount of fixed carbon, as determined by proximate analysis. Maximum fluidity was observed at  $\pm 430^{\circ}\text{C}$ , with the initial softening and solidification temperatures at 400 and  $457^{\circ}\text{C}$ , respectively. The TSH coal sample is a highly caking coal, with a FSI of 9, and was classified as a bituminous medium rank B coal. This coal sample consisted of 82% vitrinite and 18% inertinite, and was also classified as a vitrinite-rich coal. The TSH coal consisted of the lowest amount of volatile matter, had the highest fixed carbon content and substantially less inherent moisture in comparison to the TWD and the GG coal samples. The initial softening temperature for the TSH coal sample was reported at  $\pm 420^{\circ}\text{C}$ , with the maximum fluidity at  $467^{\circ}\text{C}$  and the solidification temperature at  $508^{\circ}\text{C}$ . The three coal samples can be classified as mainly aliphatic coals, which are in accordance with vitrinite-rich coals.

- **7.2 Thermogravimetric analysis**

A thermogravimetric analysis was conducted on the coal samples in order to determine the temperatures where caking coals have reacted at different percentages on a mass loss basis. The specific temperatures correlating to the different mass loss percentages using a heating rate of  $20^{\circ}\text{C}/\text{min}$  in a nitrogen atmosphere are reported in Table 7.2.

Mass Loss (%)	Highveld (TWD)		Grootegeeluk (GG)		Tshikondeni (TSH)	
	Sample	Temperature ( $^{\circ}\text{C}$ )	Sample	Temperature ( $^{\circ}\text{C}$ )	Sample	Temperature ( $^{\circ}\text{C}$ )
0% mass loss	TWD 1	25	GG 1	25	TSH 1	25
20% mass loss	TWD 2	433	GG 2	424	TSH 2	457
40% mass loss	TWD 3	468	GG 3	450	TSH 3	490
60% mass loss	TWD 4	535	GG 4	482	TSH 4	520
80% mass loss	TWD 5	657	GG 5	571	TSH 5	612
100% mass loss	TWD 6	900	GG 6	900	TSH 6	900

The GG coal exhibited the highest reactivity, observed from the TG curves, followed by the TWD coal sample, while the TSH coal had the lowest reactivity. The percentage mass loss at 900°C was in good correlation to the volatile matter content, determined by proximate analysis.

From the DTG and TG curves it is evident that the TSH coal (the highly caking coal) reacted at higher temperatures than the other two coal samples, and only exhibited 20% weight loss at a pyrolysis temperature of 900°C. The shift in the maximum temperature of devolatilization, observed from the DTG curves, can be attributed to the thermoplastic behaviour, as well as the higher aromaticity observed for this TSH coal sample [Hattingh, 2012]. As described in Chapter 5.2, the maximum temperature of devolatilization is related to the primary pyrolysis stage, where de-polymerization reactions occur. The shift in the main pyrolysis region can be attributed to the delay in de-polymerization due to cross-linking reactions. These cross-link reactions can control the rate of pyrolysis after the metaplast phase, according to Cai *et al.* [2008], thus the shift in the maximum temperature is an indication of thermoplastic behaviour of the coal sample.

### • 7.3 Mass Spectrometry

TG-MS analyses were done on the three raw coal samples in order to investigate the temperature ranges of the evolved gaseous species. The main gaseous species identified were H<sub>2</sub>, CH<sub>4</sub> and H<sub>2</sub>O. The TSH coal exhibited the highest intensity of H<sub>2</sub> and CH<sub>4</sub> evolution, followed by the GG coal sample, while the TWD coal, the non-caking coal, exhibited the lowest intensity of H<sub>2</sub> and CH<sub>4</sub> evolution. The presence of H<sub>2</sub> during pyrolysis is an indication of fluidity in the coal sample [Yu *et al.*, 2007], thus confirming the metaplast phase within the TSH and GG coal samples. The higher intensities of CH<sub>4</sub> and H<sub>2</sub> obtained from the TSH coal indicated that more extensive secondary cracking occurred within this coal.

### • 7.4 Diffuse Reflectance Infrared Fourier Transform Spectroscopy (DRIFT)

DRIFT analyses were conducted in order to determine the decomposition of functional groups with an increase in pyrolysis temperature. Hydrogen bonding was more evident in the TWD and the GG coal samples than in the TSH coal sample, while the TSH coal exhibited a higher CH<sub>ar</sub>/C=C ratio.

The TSH coal showed the highest intensity ring condensation, as evident from the CH aromatic/C=C ratio. This phenomenon was confirmed by the high intensity H<sub>2</sub> evolution. According to Serio *et al.* [1987], additional H<sub>2</sub> evolution may occur during secondary pyrolysis due to ring condensation.

- **7.5 CO<sub>2</sub> Surface area**

CO<sub>2</sub> Surface area adsorption analyses were conducted to determine the behaviour of the pores within the coal samples during pyrolysis. All three coal sample can be classified as microporous materials. The non-caking TWD coal sample exhibited an increase in surface area with increasing temperature during pyrolysis, which is expected behaviour. An increase in surface area was observed for the caking coals, GG and TSH, between 40 and 60% mass loss, which relates to the end of the plastic stage and re-solidification temperatures for the coal samples. The surface area of the GG coal sample decreased slightly from 80 to 100% mass loss, i.e. according to Serio *et al.* [1987] an indication of swelling behaviour. The TSH coal showed a decrease in surface area between 40 and 60% mass loss, which is where maximum contraction occurs [Maloney *et al.*, 1982; Coetzee *et al.*, 2014].

From these results it is evident that all coal samples exhibit an increase in surface area during pyrolysis. The surface area decreased at some stage in both the caking coals. This can be used as an indication of thermoplastic behaviour and subsequent swelling of the coal samples.

- **7.6 Scanning electron microscopy (SEM)**

SEM images were recorded to visually inspect the physical changes occurring during pyrolysis. The non-caking coal (TWD) exhibited no melting or agglomeration of particles with an increase in temperature. Volatile matter evolved through cracks and led to the formation of a porous char structure with thick walls. The GG medium caking coal formed a char with thinner walls and evolution of volatile matter occurred through the formation of bubbles. Melting was observed from 40% mass loss for the GG coal sample. The highly caking TSH coal was the softest coal sample and melting of particles occurred from 20% mass loss. Cenospheric chars, with very thin walls, were formed, while the volatile matter evolved through the formation of bubbles.

- **7.7 Summary of differences between caking and non-caking coals**

The Functional Group (FG) model of coal pyrolysis, investigated by Serio *et al.* [1987], divides the pyrolysis into three stages (also described in Chapter 2). The first stage is where the metaplast is formed. This stage is not present in the TWD coal sample, but can be observed for the GG and the TSH coal samples. From the SEM images it is evident that the GG coal sample exhibited some melting of particles at the 40% mass loss char, while the TSH coal sample showed signs of melting at 20% mass loss, i.e. 457°C.



Stage 2 represents primary pyrolysis where the evolution of tar, primary gases and the formation of char occurs. In the TWD coal sample, primary pyrolysis occurred from 20 to 80% mass loss (i.e. from  $\pm 433 - 657^{\circ}\text{C}$ ). Primary pyrolysis occurred from 20% mass loss to 80% mass loss in the GG coal sample (i.e. from  $\pm 424 - 571^{\circ}\text{C}$ ). The TSH coal sample showed signs of primary pyrolysis before the 20% mass loss sample, thus primary pyrolysis occurred from the start of pyrolysis up to the 80% mass loss sample i.e. at  $\pm 612^{\circ}\text{C}$ .

Secondary pyrolysis, Stage 3, is associated with additional  $\text{CH}_4$ ,  $\text{CO}$  and  $\text{H}_2$  evolution from ether links and ring condensation reactions. This stage occurs at the end of the primary pyrolysis, where almost all of the aliphatic hydrogen ( $\text{H}_{(\text{al})}$ ) is depleted. The TWD coal sample, the non-caking coal, underwent secondary pyrolysis from 80% mass loss, i.e. from  $\pm 657^{\circ}\text{C}$  up to  $900^{\circ}\text{C}$ . Secondary pyrolysis in the GG coal sample also occurred from 80% mass loss, i.e. from  $\pm 571^{\circ}\text{C}$ . Secondary pyrolysis was observed at approximately  $612^{\circ}\text{C}$  in the TSH coal sample, thus at 80% mass loss. The high concentration of minerals, present in the TSH coal sample, also contributes to the changes in the physical properties during pyrolysis.

These differences between the coal samples in the pyrolysis process can be assigned to the thermoplastic behaviour of the GG and the TSH coal samples. More changes in the structure were observed during the secondary pyrolysis stage for the GG and TSH coal samples, in comparison to the TWD non-caking coal. The most significant differences between non-caking and caking coals occurred mainly in two stages:

(1) Between 40 and 60% mass loss;

The re-solidification temperature for the GG and the TSH coal sample was within this stage and as a result more changes were observed for these two caking coals. The decrease in BET surface area, observed for the TSH coal sample as well as the decrease in the peak areas observed in the DRIFT spectra for the GG and TSH coal samples are some of the significant changes that occurred within the caking coals during this phase. These changes were not observed for the TWD non-caking coal.

(2) During the secondary pyrolysis stage, i.e. from 80 to 100% mass loss;

It is evident that the BET surface area decreased in the GG coal sample, thus a sign of caking behaviour. This caking behaviour was confirmed by the SEM images, where melting and swelling of particles were observed from 80% mass loss onwards for the GG coal sample. With regards to the TSH coal sample, the aromaticity started to increase again from

80% mass loss onwards, thus confirming the depletion of  $H_{(al)}$ . The decrease of  $H_{(al)}$  is an indication of the end of the plastic range and the start of the caking/swelling phase [Serio *et al.*, 1987]. The TWD non-caking coal only exhibited  $H_2$  evolution and showed an increase in BET surface area from 80 to 100% mass loss. There were no signs of thermoplastic behaviour for the TWD coal sample.

It can be concluded that, for caking coals, the metaplast occurs between 40 and 60% mass loss where hydrogen is removed from the hydro-aromatic systems and the pore structure decreases, leading to an increase in volatile matter evolution. This metaplast forms in the region of maximum fluidity, and the most significant changes occur just before the solidification temperature. Caking behaviour can be observed from 80 to 100% mass loss, thus at temperatures above 571°C, for the medium caking coal, explaining the slight decrease in BET surface area and the increase of oxygen and hydrogen evolution.

### • 7.8 Recommendations

The following recommendations are made for possible further investigations into the pyrolysis behaviour of South African caking coals:

- Conduct a thorough petrographic analysis of the coal-char samples in order to investigate the changes occurring in the macerals composition during pyrolysis.
- Determine the macerals chemical composition and decomposition using petrographic analyses and electron microprobe (EMP).
- Molecular modelling of the different coal samples and coal-derived chars will provide insight into the molecular structure of the samples as well as the changes to the structure during pyrolysis.
- Quantitative FTIR measurement will provide insight into the quantity of the decomposition of the functional groups.
- Quantitative analyses on the evolution of gaseous species including  $NH_3$ ,  $HCN$  and  $H_2S$ , using the MS, to determine when the evolution occurs as well as the amount of the species released.
- Advanced analytical techniques such as  $^{13}C$  NMR will be useful for the identification of various chemical-structural components within the organic material of the coal and coal-derived char samples.
- Determine the coal and ash mineralogy, during pyrolysis, using EMP, XRD, XRF and Qemscan techniques.

All of these recommendations will add to the understanding of the differences between caking and non-caking South African coals.

# Bibliography

- Allen. (1981). *Particle Size Measurement*. Chapman and Hall.
- Alonso, M., Borrego, A., Alvarez, D., & Menendez, R. (1999). Pyrolysis behaviour of pulverised coals at different temperatures. *Fuel*, Vol 78, 1501-1513.
- Arenillas, A., Pevida, C., Rubiera, F., Garcia, R., & Pis, J. (2004). Characterisation of model compounds and a synthetic coal by TG/MS/FTIR to represent the pyrolysis behaviour of coal. *Journal of Analytical Applied Pyrolysis*, Vol 71, 747-763.
- Azhagurajan, A., & Nagaraj, P. (2009). An experimental analysis of coal aluminium mixture in coal fired furnace. *Journal of Thermal analysis and Calorimetry*, Vol 98, 253-259.
- Barriocanal, C., Diez, M., Alvarez, R., & Casal, M. (2003). On the relationship between coal plasticity and thermogravimetric analysis. *Journal of Analytical and Applied Pyrolysis*, Vol 67, 23-40.
- Benfell, K. (2001). *Assessment of char morphology in high pressure pyrolysis and combustion*. P.h.D Thesis: Department of Geology, University of Newcastle.
- Berkowitz, N. (1985). *The Chemistry of Coal*. Amsterdam, New York: Elsevier.
- Borrego, A., Marban, G., Alonso, M., Alvarez, D., & Menendez, R. (2000). Maceral effects in the determination of proximate volatiles in coals. *Energy & Fuels*, 117-126.
- Cai, J., Wang, Y., Zhou, L., & Huang, Q. (2008). Thermogravimetric analysis and kinetics of coal/plastic blends during co-pyrolysis in nitrogen atmosphere. *Fuel Processing Technology*, 21-27.
- Campbell, Q., Bunt, J., & De Waal, F. (2010). Investigation of lump coal agglomeration in a non-pressurized reactor. *Journal of Analytical Applied Pyrolysis*, Vol 89, 271-277.
- Chermin, H., & Van Krevelen, D. (1957). Chemical structure and Properties of Coal XVII - A Mathematical Model of Coal Pyrolysis. *Fuel*, 84-104.

- Coetzee, S., Neomagus, H., Bunt, J., Strydom, C., & Schobert, H. (2014). The transient swelling behaviour of large (-20 +16 mm) South African coal particles during low-temperature devolatilisation. *Fuel*, Vol 136, 79-88.
- Collins, A. (2014). *The influence of potassium and calcium species on the swelling and reactivity of a high-swelling South African coal*. MSc Dissertation: University of the North-West Potchefstroom Campus.
- Elliott, M., & Yohe, G. (1981). The Coal Industry and Coal Research and Development Perspective. In M. Elliott, *Chemistry of Coal Utilization* (pp. 1-52). New York: Wiley-Interscience.
- Falcon, R. (1986). A Brief review of the origin, formation and distribution of coal in the Southern Africa. In C. Anhaeusser, *Mineral deposits of Southern Africa* (pp. 1879-1898). Johannesburg: Geological Society of South Africa.
- Falcon, R., & Snyman, C. (1986). *An introduction to coal petrography: Atlas of petrographic constituents in the bituminous coals of Southern Africa*. Johannesburg, RSA: The Geological Society of South Africa.
- Falcon, R., & Van der Riet, M. (2007). Effect of milling and coal quality on combustion. *International Pittsburgh Coal Conference*. Sandton: South Africa.
- Fangxian, L., Shizong, L., & Youzhi, C. (2009). Thermal Analysis study of the effect of coal-burning additives on the combustion of coals. *Journal of Thermal Analysis and Calorimetry*, 633-638.
- Fischer, F. (1925). The coking and swelling constituents of coal. *Industrial and Engineering Chemistry*, Vol 17, 707-711.
- Fletcher, T., Kerstein, A., Pugmire, R., Solum, M., & Grant, D. (1992). Chemical percolation model for devolatilization. 3. Direct use of carbon-13 NMR data to predict effects of coal type. *Energy & Fuels*, 414-431.
- Fu, Z., Guo, Z., Yuan, Z., & Wang, Z. (2007). Swelling and shrinkage behavior of raw and processed coals during pyrolysis. *Fuel*, Vol 86, 418-425.

- Fuller, M., & Griffiths, P. (1978). Diffuse reflectance measurements by infrared Fourier transform spectrometry. *Analytical Chemistry*, 1906-1910.
- Gao, H., Murata, S., Nomura, M., Ishigaki, M., Qu, M., & Tokuda, M. (1997). Experimental Observation and Image Analysis for Evaluation of Swelling and Fluidity of Single Coal Particles Heated with CO<sub>2</sub> Laser. *Energy Fuels*, Vol 11, 730-738.
- Gavalas, G. (1982). *Coal Pyrolysis*. Elsevier Scientific Publishing Company.
- Green, T. (1987). The macromolecular structure of coal. *Journal of Coal Quality*, 90-93.
- Gregg, S., & Sing, K. (1967). *Adsorption, surface area and porosity*. London: Academic express.
- Habermehl, D., Orywal, F., & Beyer, H. (1981). Plastic properties of coal. In M. Elliot, *Chemistry of Coal Utilization* (pp. 317-368). New York: Wiley-Interscience.
- Hambly, E. (1998). *The Chemical Structure of Coal Tar and Char During Devolatilization*. A Thesis Presented to the Department of Chemical Engineering: Brigham Young University.
- Hattingh, B. (2012). *Product evaluation and reaction modelling for the devolatilization of large coal particles*. PhD Thesis: North-West University.
- Heald, C. L., Krol, J. H., Jimenez, J. L., Docherty, K. S., DeCarlo, P. F., Aiken, A. C., et al. (2010). A simplified description of the evolution of organic aerosol composition in the atmosphere. *Geophys. Res. Lett.*, 37, American Geophysical Union.
- Heald, E., & Weiss, C. (1972). Kinetics and mechanism of the anatase/rutile transformation, as catalyzed by ferric oxide and reducing conditions. *Am. Mineral*, Vol 57, 10-23.
- Howard, J. (1981). Fundamentals of Coal Pyrolysis and Hydroxyrolysis . In M. Elliott, *Chemistry of Coal Utilization* (pp. 665-784). New York: Wiley-Interscience.
- Huang, H., Wang, K., Klein, M., & Calkins, W. (1980). *Determination of coal rank by thermogravimetric analysis*. Delaware: University of Delaware.
- Hurt, R., Sarofim, A., & Longwell, J. (1991). The role of microporous surface area in the gasification of chars from sub-bituminous coal. *Fuel*, Vol 70, 1079-1082.

- Hustad, J., & Barrio, M. (2000, October 17). *What is biomass?* Retrieved January 28, 2014, from IFRF Combustion Handbook: <http://www.handbook.ifrf.net/handbook/cf.html?id=23>
- Illingworth, S. R. (1922). Coal and its Carbonisation. *Fuel in Science and Practice*, 3-6.
- Ito, O. (1992). Diffuse reflectance spectra of coals in the UV-visible and near-IR regions. *Energy & Fuels*, 662-665.
- Ito, O., Seki, H., & Lino, M. (1988). Diffuse reflectance spectra in near-ir region of coals; a new index for degrees of coalification and carbonization. *Fuel*, 573-578.
- Jeffrey, L. (2005). Characterization of the coal resources of South Africa. *The Journal of The South African Institute of Mining and Metallurgy*, 95-102.
- Johnson, R., Sellers, G., & Fleming, S. (1989). *USGS Bulletin 1823, Methods for sampling and inorganic analysis of coal*. Retrieved October 22, 2013, from USGS Publications Warehouse: <http://www.pubs.usgs.gov/bul/b1823/05.htm>
- Kershaw, J., & Taylor, G. (1992). Properties of Gondwana coals with emphasis on the Permian coals of Australia and South Africa. *Fuel Processing Technology*, 127-168.
- Komaki, I., Itagaki, S., & Miura, T. (2005). *Structure and Thermoplasticity of Coal*. New York: Nova Science Publishers, Inc.
- Kugo, M. (1953). Chemical Changes of the Coal Constituents Occuring in the Temperature Range below the Plastic State. *The Caking of Bituminous Coal*, 383-427.
- Kuhn, J., William, F., & Shimp, N. (1975). X-ray Fluorescence analysis of whole coal. *Illinois State Geological Survey*, 72-77.
- Larsen, J., Hall, P., & Wernett, P. (1995). Pore Structure of the Argonne Premium Coals. *Energy & Fuels*, Vol 9, 324-330.
- Leonard III, J., & Hardinge, B. (1991). *Coal Preparation*. Littleton, Colo: Society of Mining, Metallurgy and Exploration: 780-930.
- Lowell, S., Shields, J., Thomas, M., & Thommes, T. (2004). Characterization of porous solids and powders: Surface area, pore size and density. *Dordrecht: Kluwer Academic Publishers*, 353.

- Machnikowska, H., Krzton, A., & Machnikowski, J. (2002). The characterization of coal macerals by diffuse reflectance infrared spectroscopy. *Fuel*, 245-252.
- Maloney, D., Jenkins, R., & Walker, P. (1982). Low-temperature air oxidation of caking coals. 2. Effect on swelling and softening properties. *Fuel*, 175-181.
- Malumbazo, N. (2011). *Chemical and physical structural studies on two inertinite-rich lump coals*. Johannesburg: School of Chemical and Metallurgical Engineering, University of the Witwatersrand.
- Maskew Miller Longman. (2013, April 8). Retrieved July 14, 2014, from Maskew Miller Longman: [http://www.mml.co.za/docs/FET\\_CAPS/Platinum-grade-12-activity.pdf](http://www.mml.co.za/docs/FET_CAPS/Platinum-grade-12-activity.pdf)
- Meyers, R. (1982). *Coal structure*. California: Academic Press, INC.
- Minkina, M., Oliveira, F., & Zymła, V. (2010). Coal lump devolatilization and the resulting char structure and properties. *Fuel Processing Technology*, Vol 91, 476-485.
- Moore, D., & Reynolds Jnr, R. (1997). *X-ray diffraction and the identification and analysis of clay minerals*. New York: Oxford University Press.
- Morga, R. (2010). Chemical structure of semifusinite and fusinite of steam and coking coal from the Upper Silesian Coal Basin (Poland) and its changes during heating as inferred from micro-FTIR analysis. *International Journal of Coal Geology*, Vol 84, 1-15.
- Nandi, S., & Walker, P. (1964). The diffusion of nitrogen and carbon dioxide from coals of various rank. *Fuel*, Vol 43, 358-393.
- Nel, M. (2010). *The influence of coal-associated trace elements on sintering and agglomeration of a model coal mineral mixture*. P.h.D thesis: North West University.
- Niksa, S. (1995). Predicting the Devolatilization Behavior of Any Coal from its Ultimate Analysis. *Combustion and Flame* , Vol 100, 384-394.
- Oboirien, B., Engelbrecht, AD, North, B., du Cann, V., Verryn, S., et al. (2011). Study on the structure and gasification characteristics of selected South African bituminous coals in fluidised bed gasification. *Fuel Processing Technology*, Vol 92, 735-742.



- Painter, P., Graf, J., & Coleman, M. (1990). Coal solubility and swelling. 3. A Model for coal swelling. *Energy & Fuels*, 393-397.
- Painter, P., Snyder, R., Starsinic, M., Coleman, M., Kuehn, D., & Davis, A. (1981). Concerning the application of FT-IR to the study of coal: a critical assessment of band assignments and the application of spectral analysis programs. *Applied Spectroscopy*, 475-485.
- Perkin Elmer. Inc. (2010). Thermogravimetric analysis TGA. Winter street, Waltham. Retrieved from Perkin Elmer: [http://www.perkinelmer.com/CMSResources/Images/44-74556GDE\\_TGABeginnersGuide.pdf](http://www.perkinelmer.com/CMSResources/Images/44-74556GDE_TGABeginnersGuide.pdf)
- Reifenstein, A., Kahraman, H., Coin, C., Calos, N., Miller, G., & Uwins, P. (1999). Behaviour of selected minerals in an improved ash fusion test: quartz, potassium feldspar, kaolinite, illite, calcite, dolomite, siderite, pyrite and apatite. *Fuel*, Vol 78, 1449-1461.
- Sakurovs, R., French, D., & Grigore, M. (2007). Quantification of mineral matter in commercial cokes and their parent coals. *International Journal of Coal Geology*, 81-88.
- Salmang, H. (1961). *Ceramics. Physical and chemical fundamentals*. Butterworths, London: Translated by Francis, M.
- Samaras, P., Diamadopoulou, E., & Sakellaropoulos, G. (1996). The effect of mineral matter and pyrolysis conditions on the gasification of Greek lignite by carbon dioxide. *Fuel*, Vol 75, 1108-1114.
- Saxena, S. (1990). Devolatilization and combustion characteristics of coal particles. *Progress in Energy and Combustion Science*, 55-94.
- Scaroni, A., Rashid Khan, M., Eser, S., & Radovic, L. (2005, January). *Coal Pyrolysis*. Retrieved July 14, 2014, from Solids Process Engineering & Particle Technology TUHH: [http://www.spe.tu-harburg.de/fileadmin/userfiles/SuperiorGraphite/SG052\\_Coal%20Pyrolysis\\_Ullmanns\\_2000.pdf](http://www.spe.tu-harburg.de/fileadmin/userfiles/SuperiorGraphite/SG052_Coal%20Pyrolysis_Ullmanns_2000.pdf)
- Schobert, H. H. (2013). *Chemistry of Fossil Fuels and Biofuels*. New York: Cambridge University Press.

- Schumann, R. (1952). *Metallurgical Engineering Volume I Engineering Principles*. Addison-Wesley.
- Serio, M., Hamblen, D., Markham, J., & Solomon, P. (1987). Kinetics of volatile product evolution in coal pyrolysis: experiment and theory. *Energy Fuels*, Vol 1, 138-152.
- Sheng, C., & Azevedo, J. (2000). Modeling the evolution of particle morphology during coal devolatilization. *Proceedings of the Combustion Institute*, (pp. 2225-2232, Vol 28).
- Sheng, C., & Azevedo, J. (2000). Modeling the evolution of particle morphology during coal devolatilization. *Proceedings of the Combustion Institute*, (pp. 2225-2232).
- Silverstein, R., Webster, F., & Kiemle, D. (2005). *Spectrometric Identification of Organic compounds*. John Wiley & Sons, Inc. pp 1-38.
- Skoog, D., Holler, F., & Crouch, S. (2007). *Principles of Instrumental Analysis 6th Edition*. Belmont, USA: BROOKS/COLE CENGAGE Learning.
- Skoog, D., Holler, F., & Nieman, T. (1998). *Principles of instrumental analysis*. USA: Harcourt Brace & Company.
- Smoot, L., & Pratt, D. (1979). *Pulverised coal combustion and gasification*. New York: Plenum Press.
- Sobkowiak, M., & Painter, P. (1995). A Comparison of Drift and KBr Pellet Methodologies for the Quantitative Analysis of Functional Groups in Coal by Infrared Spectroscopy. *Energy & Fuels*, 359-363.
- Sobolik, J., Ludlow, D., & Hessevick, W. (1992). Parametric sensitivity comparison of the BET and Dubinin-Radushkevich models for determining char surface area by CO<sub>2</sub> adsorption. *Fuel*, Vol 71, 1195-1202.
- Solomon, P., Fletcher, T., & Pugmire, R. (1993). Progress in coal pyrolysis. *Fuel*, Vol 72, 587-597.
- Solomon, P., Hamblen, D., Carangelo, R., Serio, M., & Deshpande, G. (1987). General model of coal devolatilization. *ACS Div Fuel Chem Prepr*, 32-83.

- Solomon, P., Hamblen, D., Carangelo, R., Serio, M., & Deshpande, G. (1988). General model of devolatilization. *Energy Fuels*, 405-422.
- Solomon, P., Serio, M., & Suuberg, E. (1992). Coal pyrolysis: Experiments, kinetic rates and mechanisms. *Progress in Energy and Combustion Science*, Vol 18, 133-220.
- Speight, J. (2005). *Handbook of Coal Analysis*. John Wiley & Sons. Inc.
- Speight, J. G. (1994). *The Chemistry and Technology of Coal*. New York: CRC Press.
- Swapp, S. (2012, July 23). *Geochemical Instrumentation and Analysis, SEM*. Retrieved May 31, 2013, from Integrating Research and Education:  
[http://serc.carleton.edu/research\\_education/geochemsheets/techniques/SEM.html](http://serc.carleton.edu/research_education/geochemsheets/techniques/SEM.html)
- TA instruments. (2010). *Thermal Analysis Application Brief*. Retrieved June 20, 2013, from TA instruments: [www.tainstruments.com/library\\_download.aspx?file=TA129.pdf](http://www.tainstruments.com/library_download.aspx?file=TA129.pdf)
- Takagi, H., Maruyama, K., Yoshizawa, N., Yamada, Y., & Sato, Y. (2004). XRD analysis of carbon stacking structure in coal during heat treatment. *Fuel*, Vol 83, 2427-2433.
- Tsai, C., & Scaroni, A. (1987). The structural changes of bituminous coal particles during the initial stages of pulverized-coal combustion. *Fuel*, Vol 66, 200-206.
- Ulloa, C., Gordon, A., & Garcia, X. (2004). Distribution of activation energy model applied to the rapid pyrolysis of coal blends. *Journal of Applied Pyrolysis*, Vol 71, 465-483.
- Van Krevelen, D., Huntjens, F., & Dormans, H. (1956). Chemical Structure and Properties of Coal XVI-Plastic Behaviour on Heating. *Fuel*, 462-475.
- Van Niekerk, D., Mitchell, G., & Mathews, J. (2009). Petrographic and reflectance analysis of solvent-swelled and solvent-extracted South African vitrinite-rich and inertinite-rich coals. *International Journal of Coal Geology*, 45-52.
- Van Niekerk, D., Pugmire, R., Solum, M., Painter, P., & Mathews, J. (2008). Structural characterization of vitrinite-rich and inertinite-rich Permian-aged South African bituminous coals. *International Journal of Coal Geology*, Vol 76, 290-300.
- Wang, J., Du, J., Chang, L., & Xie, K. (2010). Study on the structure and pyrolysis characteristics of Chinese western coals. *Fuel Processing Technology*, Vol 91, 430-433.

- Ward, C. (2002). Analysis and significance of mineral matter in coal seams. *International Journal of Coal Geology*, Vol 50, 135-168.
- Wu, X., Zang, Z., Piao, G., He, X., Chen, Y., Kobayashi, N., et al. (2009). Behavior of mineral matter in Chinese coal ash melting during char-CO<sub>2</sub>/H<sub>2</sub>O gasification reaction. *Energy Fuels*, 2420-2428.
- Xianglin, S., Ying, C., & Haibin, L. (1999). Research on the melting points of some Chinese coal ashes. In *Impact of Mineral Impurities in Solid Fuel Combustion*. New York: Kluwer Academic/Plenum Publishers.
- Xin, H., Wang, D., Qi, X., Qi, G., & Dou, G. (2014). Structural characteristics of coal functional groups using quantum chemistry for quantification of infrared spectra. *Fuel Processing Technology*, Vol 118, 287-295.
- Yoshizawa, N., Maruyama, K., Yamashita, T., & Akimoto, A. (2006). Dependence of microscopic structure and swelling property of DTF chars upon heat-treatment. *Fuel*, Vol 85, 2064-2070.
- Yu, J., J. L., Wall, T., Liu, G., & Sheng, C. (2004). Modeling the development of char structure during the rapid heating of pulverized coal. *Combustion and Flame*, Vol 136, 519-532.
- Yu, J., Lucas, J., & Wall, T. (2007). Formation of the structure of chars during devolatilization of pulverized coal and its thermoproperties: a review. *Progress in Energy and Combustion Science*, Vol 33, 135-170.
- Yu, J., Strezov, V., Lucas, J., & Wall, T. (2003). Swelling behaviour of individual coal particles in the single particle reactor. *Fuel*, Vol 82, 1977-1987.
- Zubkova, V. (2005). Some aspects of structural transformation taking place in organic mass of Ukrainian coals during heating. Part 1. Study of structural transformations when heating coals of different caking capacity. *Fuel*, Vol 84, 741-754.

# Appendix A

H/C ratios vs O/C ratio for the three coal samples.

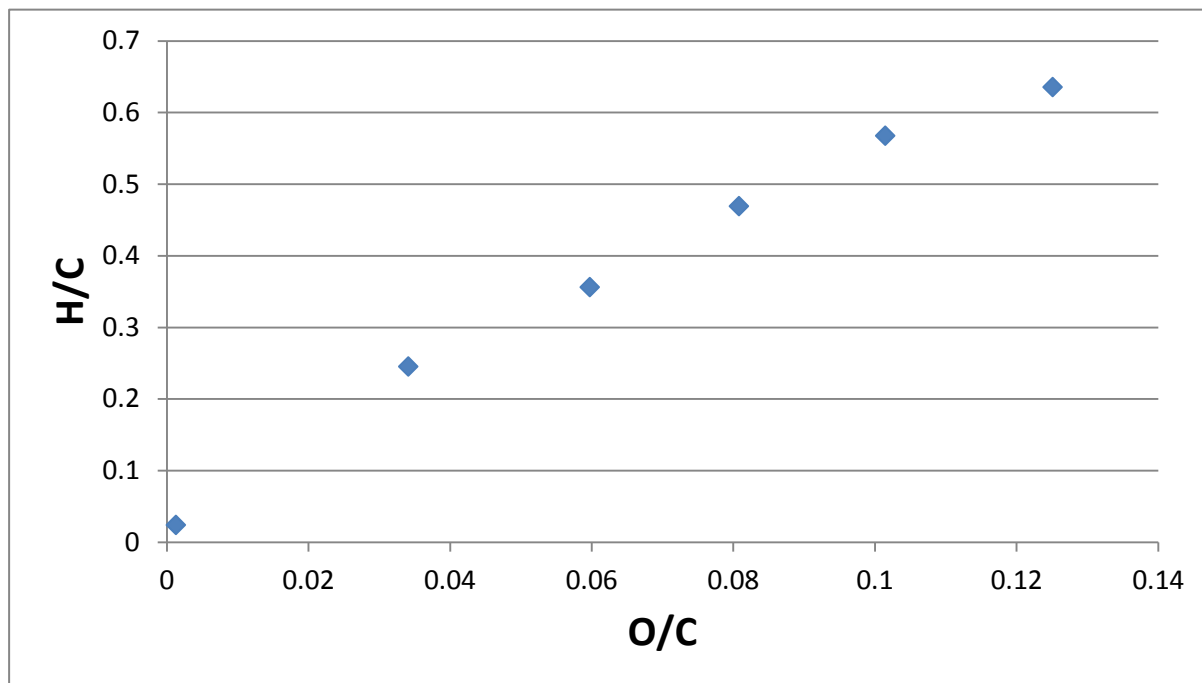


Figure A1: O/C and H/C atomic ratio for the TWD coal sample

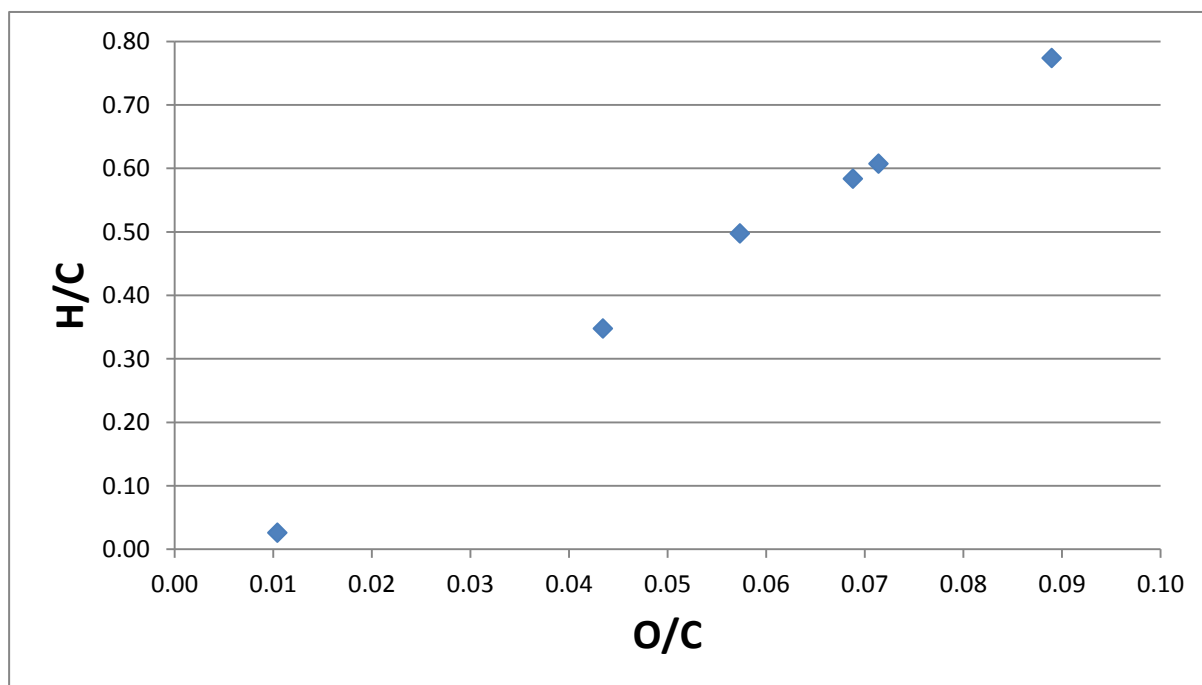


Figure A2: O/C and H/C atomic ratio for the GG coal sample

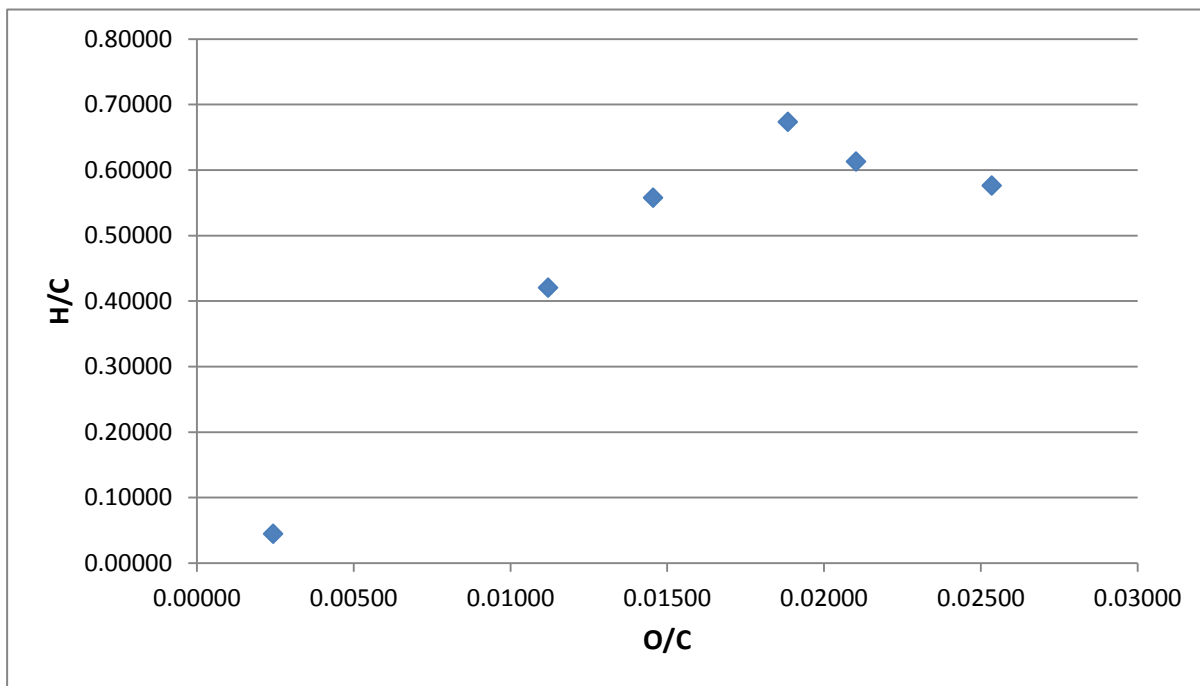


Figure A3: O/C and H/C atomic ratio for the TSH coal sample

# Appendix B

Repetition of the TG runs of each coal individually.

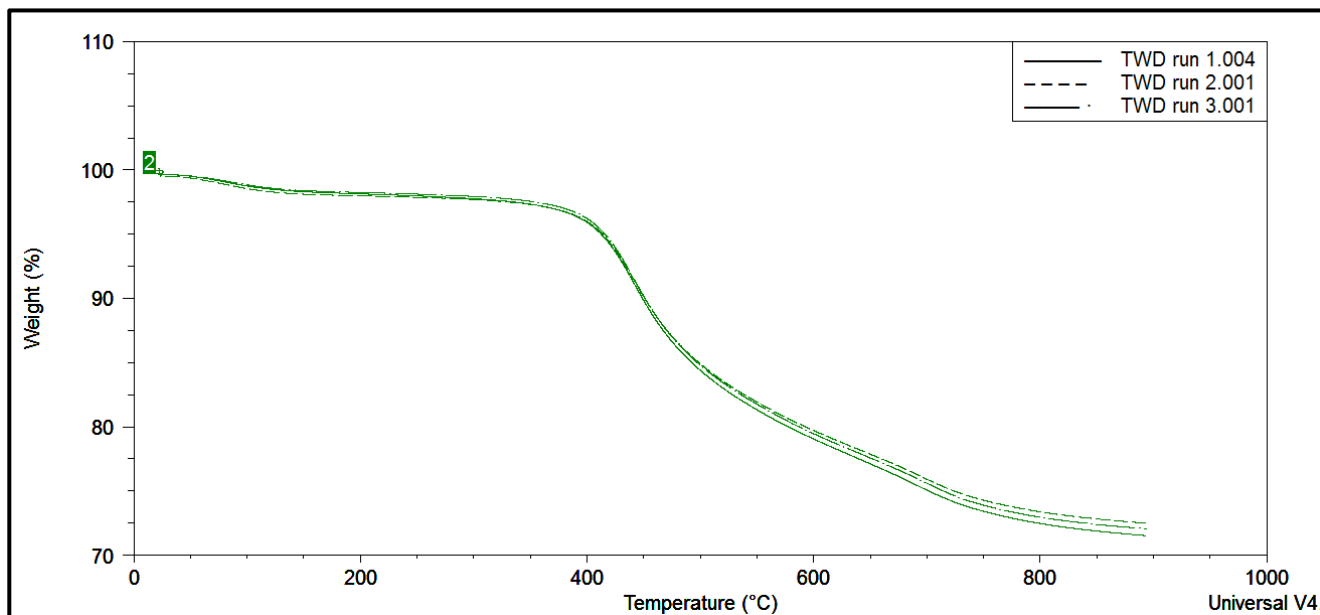


Figure B1: Three TGA curves for the TWD coal sample

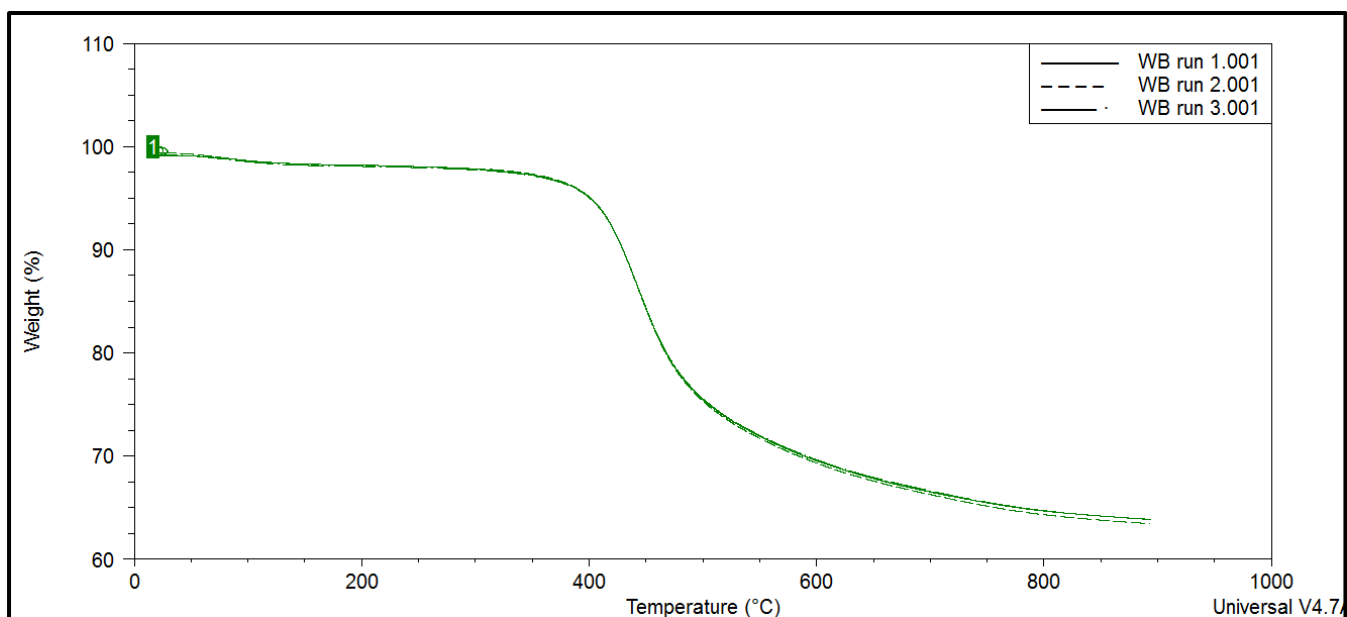


Figure B2: Three TGA curves for the GG coal sample

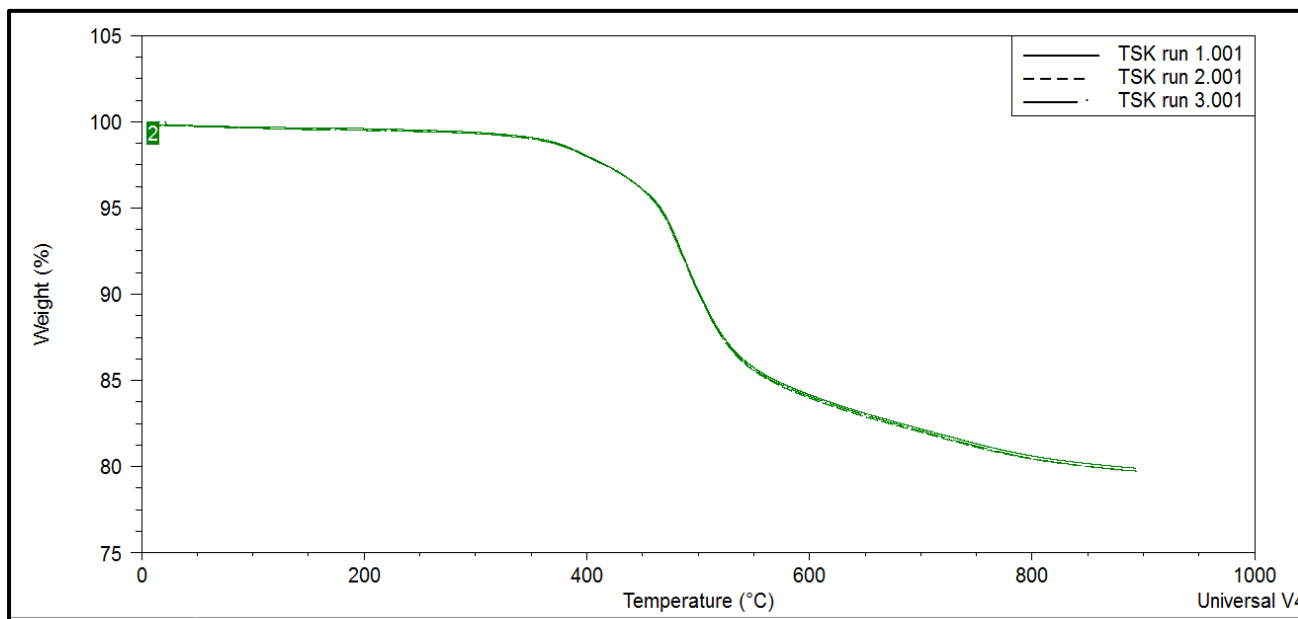


Figure B3: Three TGA curves for the TSH coal sample



# Appendix C

MS spectra of the evolution of CO and gaseous carbon.

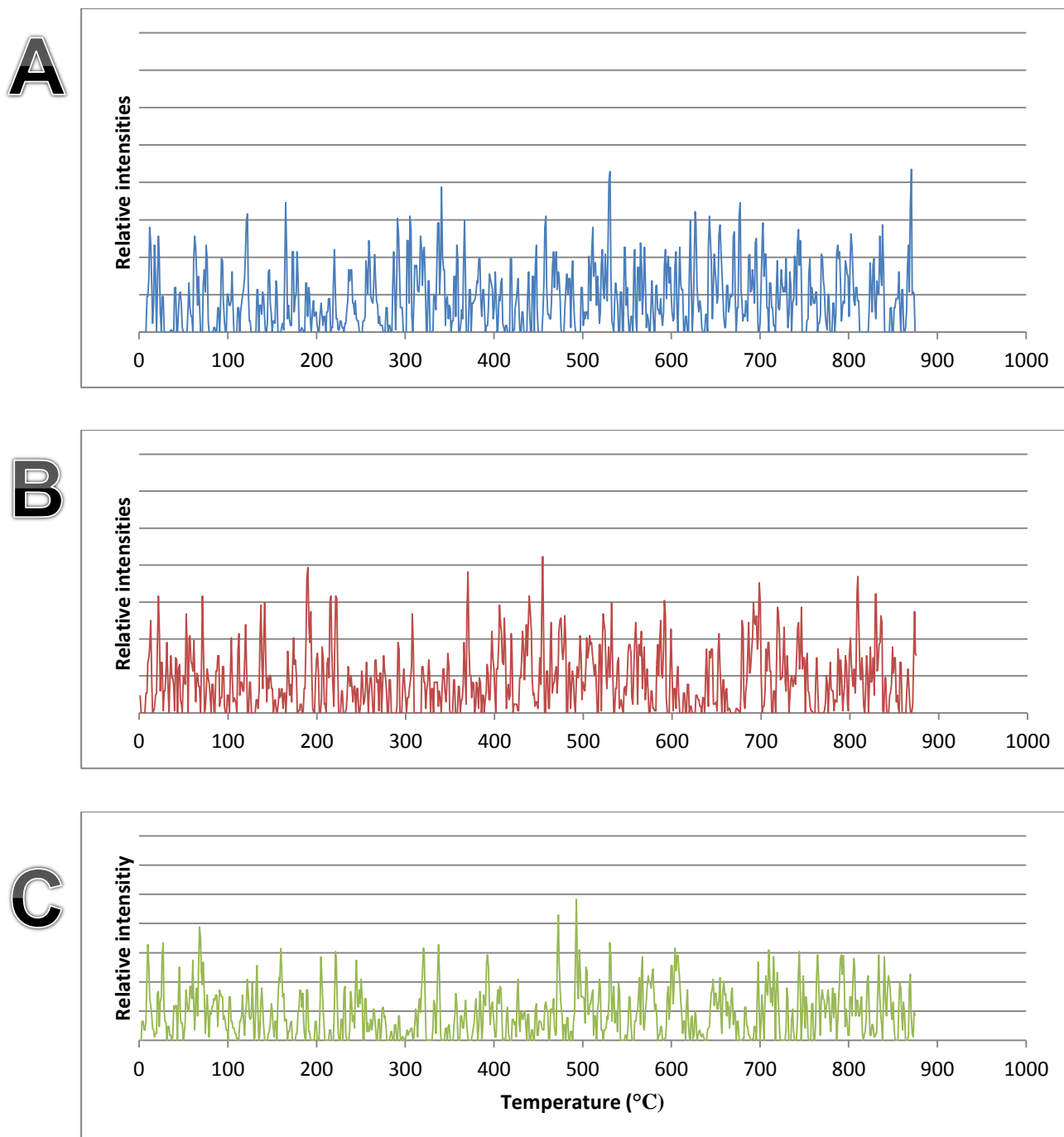


Figure C1: The evolution of gaseous carbon for (A) TWD, (B) GG, and (C) TSH

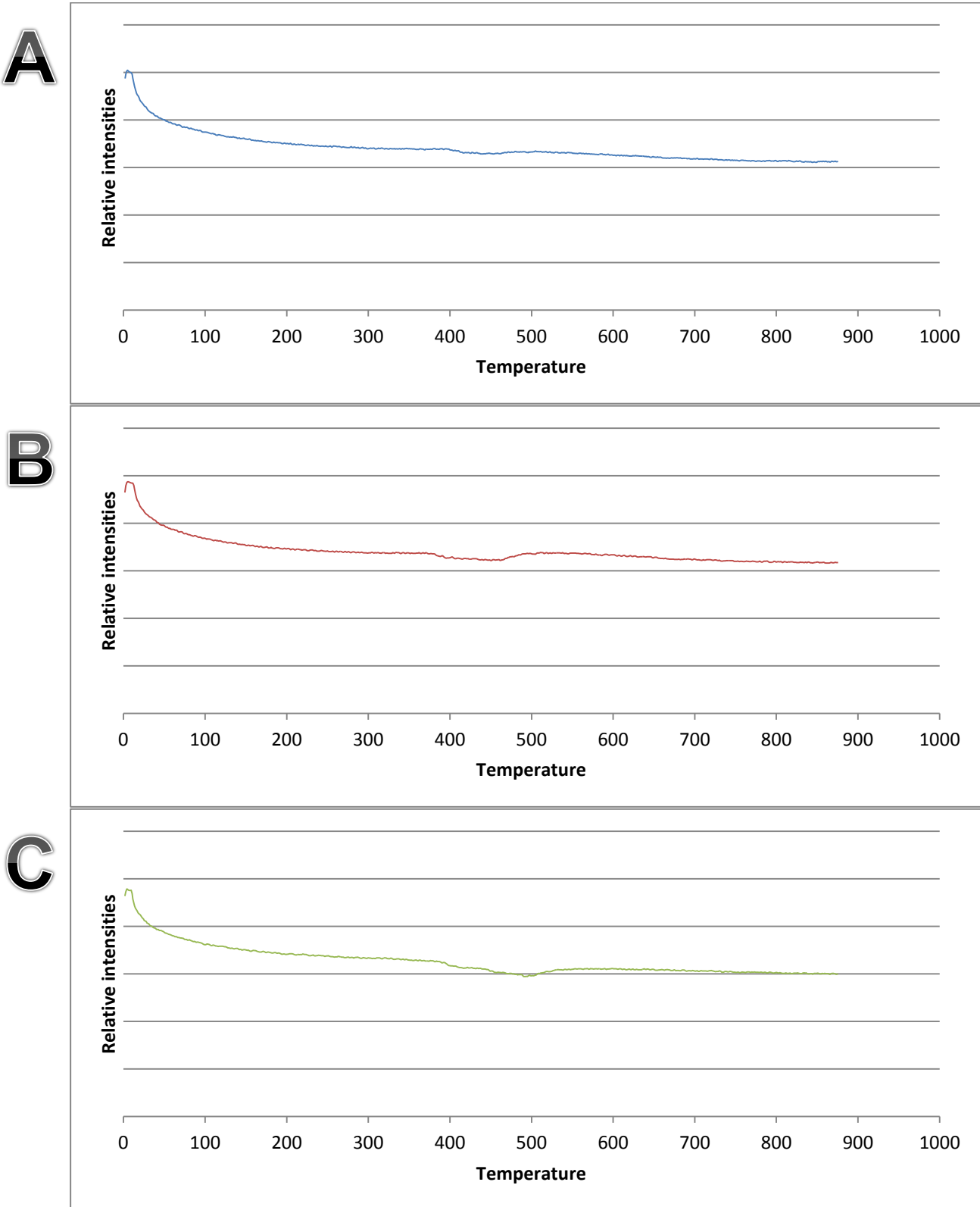


Figure C2: Evolution of CO in (A) TWD, (B) GG, and (C) TSH

# Appendix D

## Integration results from the DRIFT spectra

	cm <sup>-1</sup>	TWD 1	TWD 2	TWD 3	TWD 4	TWD 5	TWD 6
OH	3700 - 3100	0.038	0.022	0.017	0.004	0	0
Aliphatic CH	3000 - 2800	0.058	0.031	0.005	0	0	0
Aromatic CH	3100 - 3000	0.012	0.01	0.008	0.004	0.001	0
C=C	1790 - 1530	0.282	0.206	0.142	0.087	0.049	0
Si-O-Si	1200 - 960	0.386	0.208	0.165	0.086	0.037	0.002
C-O	850 - 720	0.095	0.076	0.069	0.059	0.042	0
Si-O-Si and Al-O-Al	660 - 509	0.336	0.191	0.158	0.055	0	0
CH <sub>ar</sub> /CH <sub>al</sub>		0.21	0.32	1.6	0	0	0
Char/C=C <sub>ar</sub>		0.04	0.05	0.06	0.05	0.02	0

	cm <sup>-1</sup>	GG 1	GG 2	GG 3	GG 4	GG 5	GG 6
OH	3700 - 3100	0.011	0.003	0.004	0	0	0
Aliphatic CH	3000 - 2800	0.002	0.002	0.002	0.001	0	0
Aromatic CH	3100 - 3000	0.05	0.018	0.019	0.001	0	0
C=C	1790 - 1530	0.098	0.094	0.157	0.025	0.009	0
CH <sub>2</sub> CH <sub>3</sub> stretch	1530 - 1400	0.046	0.039	0.061	0.008	0.002	0
C-O stretch	1300 - 1100	0.013	0.01	0.018	0.003	0.001	0
CH <sub>ar</sub> /CH <sub>al</sub>		25	9	9.5	1	0	0
CH <sub>ar</sub> /C=C <sub>ar</sub>		0.51	0.19	0.12	0.04	0	0

**Table D3: Integration results from the DRIFT spectroscopy for TSH coal**

	cm <sup>-1</sup>	TSH raw	TSH 20	TSH 40	TSH 60	TSH 80	TSH 100
OH	3700 - 3100	0.007	0	0	0	0	0
CH aro	3100 - 3000	0.032	0	0.004	0.004	0	0
CH <sub>2</sub> asym	3000 - 2800	0.127	0	0.008	0.002	0	0
C=C	1790 - 1530	0.269	0.002	0.175	0.172	0.01	0
CH <sub>2</sub> , CH <sub>3</sub>	1530 - 1400	0.188	0.002	0.107	0.087	0.004	0.001
Si-O-Si	1200 - 960	0.524	0.011	0.558	0.464	0.021	0.003
C-O	850 - 720	0.124	0.001	0.074	0.086	0.019	0
S-S	620 - 390	0.531	0.018	0.622	0.612	0.115	0.607
CHar/CHal		0.25	0	0.5	2	0	0
CHar/C=Car		0.12	0	0.02	0.02	0	0